Isotopic and trace element geochemistry of the Hyangsanni Dolomite and its implications on the evolution of the Okcheon Metamorphic Belt, Korean Peninsula

Youngji HA

Doctoral Program in Environmental Science and Technology
Graduate School of Science and Technology
Niigata University

September 21, 2021

Thesis Supervisor: Professor Madhusoodhan Satish-Kumar

TABLE OF CONTENTS

LIST OF FIGURES

LIST OF TABLES

LIST OF APPENDIXES

Abstract

The Okcheon Metamorphic Belt, located in the middle of the Korean Peninsula, is a key to understand the tectonic evolution of East Asia. This belt is mainly composed of the pelitic and psammitic schists, phyllites, and sparsely distributed meta-carbonate rocks. Despite its importance, the depositional timing of the protoliths of the Okcheon Metamorphic Belt has been debatable last few decades. Recently, U-Pb zircon age dating attempts have been made on various constituents of the Okcheon Metamorphic Belt. Such U-Pb zircon geochronology data facilitate a better understanding of the evolutionary history of the Okcheon Metamorphic Belt. However, it has been concentrated in clastic metasedimentary sequences. Because it is tough to find proper absolute dating methods applicable to carbonate rocks. This thesis aims to constrain the age of carbonate sequence, especially Hyangsanni Dolomite, by adopting chemostratigraphy.

The age-unknown Hyangsanni Dolomite is distributed in the northeastern part of the Okcheon Metamorphic Belt. It has been claimed as Early to Middle Cambrian because of the misidentified Archaeocyatha fossil in the past, but the time of sedimentation has not yet been confirmed. In order to clarify this, I performed elemental and isotopic analyses for the Hyangsanni Dolomite. Several geochemical parameters suggest that the Hyangsanni Dolomite was deposited in a rift basin connected to the ocean rather than in the passive continental margin, considering the occurrence of magmatism related to continental rifting within the Okcheon Metamorphic Belt. The isotope results concur with the proposal that Hyangsanni Formation is not the Phanerozoic strata but Neoproterozoic strata. The consistent high $\delta^{13}C$ values (mostly > 5‰) and minimum value of $^{87}Sr/^{86}Sr$ ratio (present value, 0.7074) obtained from the Hyangsanni Formation refer to Neoproterozoic. The shale-normalized REE+Y signatures for the Hyangsanni Dolomite are generally flat and negative cerium anomaly is commonly negligible to the extent that it display solely weakly in some samples. Y/Ho ratios ranges from 29 to 43, which is quite lower than that of typical modern seawater. It indicates that the Hyangsanni Dolomite might have been influenced by terrigenous materials. All metacarbonate samples from the Hyangsanni Dolomite were analyzed for carbon and oxygen isotopic compositions. To avoid recrystallized calcite, the analysis was carried out on dolomite powders scraped off from polished surfaces which are unstrained with Alizarin-Red-S. The Hyangsanni Dolomite has $\delta^{13}C_{(V\text{-}PDB)}$ and $\delta^{18}O_{(V\text{-}SMOW)}$ values ranging from +2.9‰ to + 6.2‰ and from +11.3‰ to + 24.5‰, respectively. These $\delta^{13}C$ values are

significantly higher than those in the Cambro-Ordovician, and it is coinciding of the Neoproterozoic values. The minimum $^{87}Sr/^{86}Sr$ ratio acquired from the Hyangsanni Dolomite pertain to Neoproterozoic, not Phanerozoic as well.

Taken together, I suggest that the Hyangsanni Dolomite is the Neoproterozoic sedimentary sequence in accordance with other sedimentary sequences of the northeastern Okcheon Metamorphic Belt. Thus, the isotope results concur with the proposal that Hyangsanni Formation is not the Phanerozoic strata but Neoproterozoic strata. The consistently high $\delta^{13}C$ values (mostly > 5‰) and minimum value of $^{87}Sr/^{86}Sr$ ratio obtained from the Hyangsanni Formation refer to Neoproterozoic.

In addition, this thesis reports the zircon U-Pb data of other constituents, metasedimentary sequences, of the Okcheon Metamorphic Belt as well. These include the Daehyangsan Quartzite, Bugnori Formation, Hwanggangni Formation, Seochangni Formation, and Changni Formations. Daehyangsan Quartzite has largely occurred in association with the Hyangsanni Dolomite along Lake Chungju. The stratigraphic relationship between this formation and Hyangsanni Dolomite has been suggested to be conformable, but, still debatable. Because recently reported reliable zircon U-Pb age of the Daehyangsan Quartzite is Paleozoic (ca. 420 Ma). This study also identified that the Daehyangsan Quartzite belongs to the Paleozoic. The Bugnori and Hwanggangni Formations, pebble-bearing phyllitic sequences, are considered as composing of glaciogenic sediments. The detrital zircon age of Hwanggangni Formation it is dominated by ca. 1870 Ma and 750 Ma even though differs from region to region. While in the case of Bugnori Formation, the Mesoproterozoic component is predominant. The Seochangni and Changni Formations, phyllitic sequences, are considered equivalent to each other. However, opinions differ on this matter depending on the researcher. The ages of Late Paleoproterozoic to Mesoproterozoic are dominant and reveal the age component of Neoproterozoic as well. The geochronology data from these two formations are similar, and such results lend weight to the possibility for correlation of these two strata.

The presence of Mesoproterozoic detrital zircons found in the metasedimentary sequences of the Okcheon Metamorphic Belt is also the same as the Neoproterozoic sedimentary sequences in the southern margin of North China Craton. Taken together, I suggest that the correlation of the Okcheon Metamorphic Belt, at least in part, with the southern margin of the North China Craton, provides important clues in interpreting crustal evolution and tectonics on the Korean Peninsula.

CHAPTER 1

Introduction

Recent studies in East Asia have focused on the crustal and tectonic evolution from the late Paleoproterozoic to the Neoproterozoic, particularly on the Korean Peninsula, due to the controversy over its correlation with cratons in China (Chough et al., 2000; Kim et al., 2020; Oh et al., 2019).

This period represent the disruption of the Paleoproterozoic supercontinent Colombia, and amalgamation of supercontinent Rodinia and its subsequent disruption (Li et al., 2008; Zhao et al., 2003). The igneous activities during this period also were conserved as estimative age distribution pattern in detrital zircons from the Neoproterozoic sedimentary rocks in the region. Especially, the commonly appearing age distribution patterns, primarily from the late Paleozoic to the late Mesoproterozoic, was used as a criterion for regional correlation (Hu et al., 2012, 2016; Kim et al., 2019, 2020). As a consequence, the Neoproterozoic sedimentary sequences distributed in the western Gyeonggi Massif and Okcheon Metamorphic Belt in South Korea were ascertained that it was connected to Sangwon Supergroup in the southern North Korea and those distributed in the southern margin of the North China Craton (Kim et al., 2019. 2020).

The Okcheon Metamorphic Belt, located in the middle of the Korean Peninsula, is distributed between Paleoproterozoic Gyeonggi and Yeongnam massifs. There is still much debate about when this belt was made, the stratigraphy of its constituent units, and its relationship to Gyeonggi and Yeongnam massifs. The traditional view is that both Gyeonggi and Yeongnam Massifs are part of a Sino-Korean Craton connected to the North China Craton. In this case, the Okcheon Metamorphic Belt is also part of the Sino-Korean Craton. However, there is a suggestion that the boundary between Gyeonggi massif and Yeongnam massif, respectively correlated to South China Craton and North China Craton, passes along the southern margin of the Okcheon Metamorphic Belt (Chough et al., 2000; Cho et al., 2013).

Okcheon Metamorphic Belt is also important in understanding the tectonic environment during Neoproterozoic because they show the A1-type intra-plate magmatisms of about 860 Ma and 760 Ma, respectively, that may be associated with break-up of Neoproterozoic supercontinent Rodinia.

Neoproterozoic period is also drawing attention for the global glaciations episodes that result in the deposition of diamictites and cap carbonates couplet, that has been reported in East Asia as well (Zhang et al., 2005; Zhou et al., 2004). Zhou et al. (2020) reported a modified Neoproterozoic seawater $^{87}Sr/^{86}Sr$ evolution curve based on a detailed a study of the Tonian Huaibei Group in the Huaibei area

located in the southern part of the North China Craton (Figure. 1-2).

The consensus is that there were multiple severe glaciations in the Neoproterozoic: i.e. Sturtian (ca. 715 Ma, early Cryogenian), Marinoan (ca. 635 Ma, late Cryogenian) and questionable Gaskiers (ca. 580 Ma, Ediacaran) glaciations. These three major glaciations, as well as terminal Ediacaran glaciogenic deposits (i.e. younger than the Gaskiers glaciations), have occurred in the southwestern and northwestern flanks of the North China Craton (Liu et al., 2018).

In addition, there is also research on the Ediacaran glaciation, which has not been well known in the North China Craton (Yang et al., 2019), notwithstanding the Ediacaran-Cambrian glaciation event was recorded in the Luoquan Formation in the southern margin of the North China Craton (Le Heron et al., 2018). With the Luoquan Formation in southern North China Craton, the Pirangdong Formation has found in North Korea (Hu et al., 2016). Luoquan Formation and Pirangdong Formation were composed of Neoproterozoic glaciogenic sediments, and had similar detrital zircon age distributions, suggesting that they shared the same provenance. The Rungri Formation overlying the Pirangdong Formation displayed negative drifting of $\delta^{13}C$ values, which was matched up with the negative excursion at the end of the Ediacaran, not during the Ediacaran Gaskiers glaciation (Kim et al., 2016).

Several studies on the Neoproterozoic paleoenvironment and seawater evolution relevant studies from the North China Craton and some parts of North Korea has been reported, but comparable studies on the South Korea are dearth. Recently, several sedimentary sequences in South Korean have also been known to correlate with the Neoproterozoic sedimentary sequences in the southern margin of the North China Craton with the Sangwon Supergroup in North Korea (Kim et al., 2020; Kim et al., 2021). However, only few studies on Neoproterozoic carbonate rocks in South Korea have been reported.

Furthermore, there have been reports on the occurrence of glacial deposits in South Korea as well. Hwanggangni Formation in the Okcheon Metamorphic Belt has been claimed to be a glacial diamictite deposition (Ha, 2021; Ryu and Ahn, 2016), but the timing of deposition is not yet clear.

The age-unknown Hyangsanni Dolomite is distributed in the northeast Okcheon Metamorphic Belt where the Neoproterozoic sedimentary sequences are equivalent to the North China Craton (Kim et al., 2020; Kim et al., 2021). However, because of the limited means of precisely determining the age of Hyangsanni Dolomite, I intend to constrain the depositional age more precisely by adopting

chemostratigraphy to the Hyangsanni Dolomite, which was presumed to be Neoproterozoic by several researchers (e.g., Choi and Woo, 2012; Kim, 1968). This method could limit the age of Hyangsanni Dolomite to a degree useful enough to advance the discussion of the formation and evolution of the Okcheon Metamorphic Belt. This will in turn have important implication on our understanding of the crustal evolution of the Korean Peninsula and East Asia.

To achieve this, I conducted a detailed geochemical examination of the Hyangsanni Dolomite, including trace and rare earth element abundances, carbon and oxygen stable isotope composition, and strontium isotope composition. The study of the Hyangsanni Dolomite is helpful for proper understanding paleoenvironment during the Neoproterozoic, as well as the restoration of Paleogeography through the regional correlation of the Neoproterozoic carbonate rocks in East Asia.

Based on carbon, oxygen, and strontium isotopic compositions, this thesis discusses the possibility and significance of the deposition of Hyangsanni Formation and adjacent Hwanggangni Formation in the northeastern Okcheon Metamorphic Belt associated with the period of glaciation of Neoproterozoic. The clear presence of glaciation of Neoproterozoic is not yet known in South Korea, and the research on paleoenvironment of Late Neoproterozoic, which is attracting much attention, is not active.

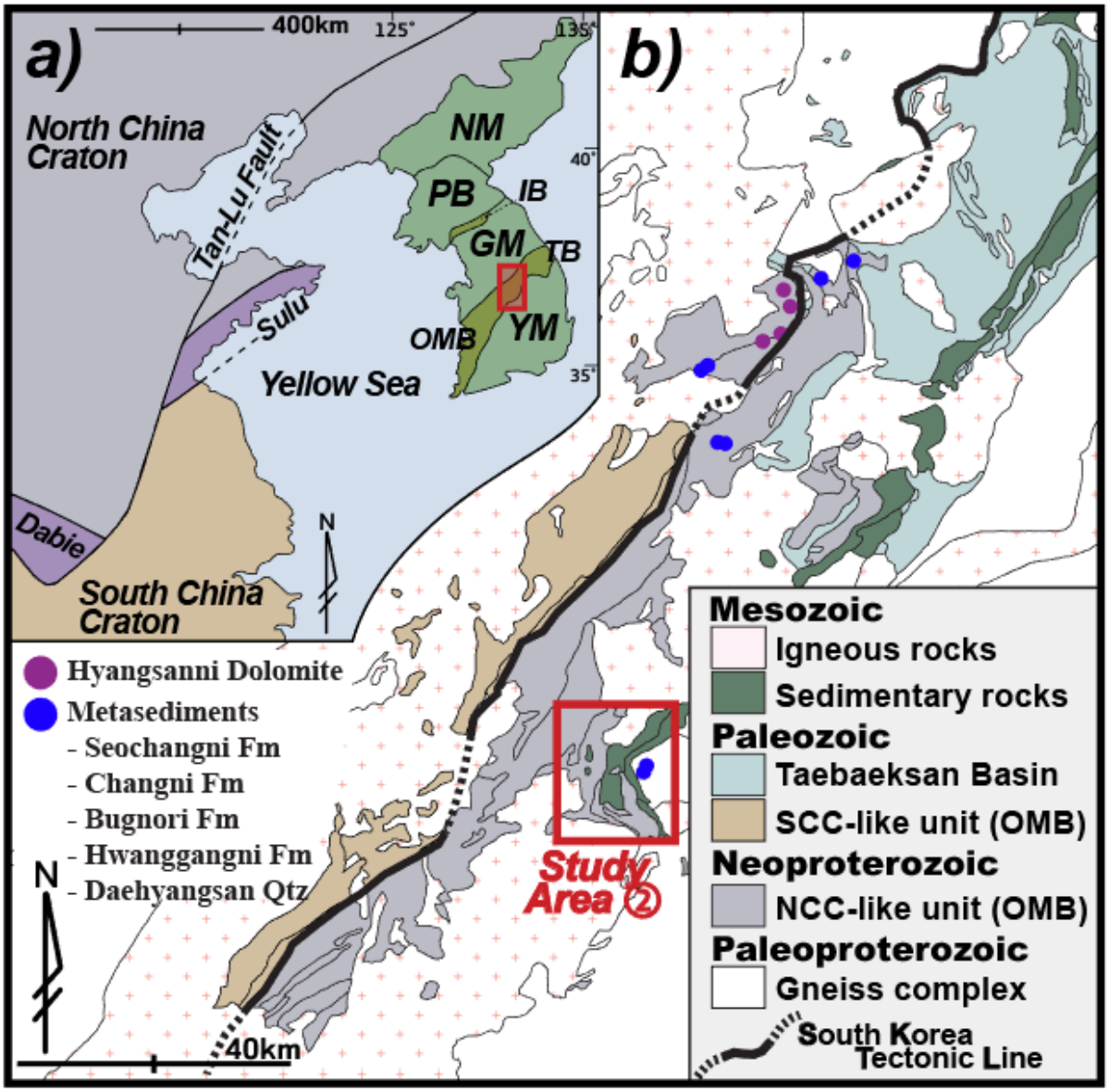

Figure 1-1. a) A map showing the Korean Peninsula with parts of the North China Craton and the South China Craton. The continental collision belts of the Dabie and Sulu regions are also shown. The tectonic units of the Korean Peninsula are marked with abbreviations. NM: Nangrim massif, PB: Pyongnam basin, IB: Imjingang belt, GM: Gyeonggi massif, OMB: Okcheon metamorphic belt, TB: Taebaeksan basin, and YM: Yeongnam massif. b) A map showing the Okcheon metamorphic belt distributed over the south-central Korean Peninsula. The Okcheon metamorphic belt was divided into two, NCC (North China Craton)-like and SCC (South China Craton)-like, modified after Cho et al. (2013). Purple and blue circles represent the location of the sites where isotope data and detrital zircon age data are reviewed in this study.

① Chungju-Jecheon area (Figure 2-1). ②Okcheon-Boeun area (Figure 2-2).

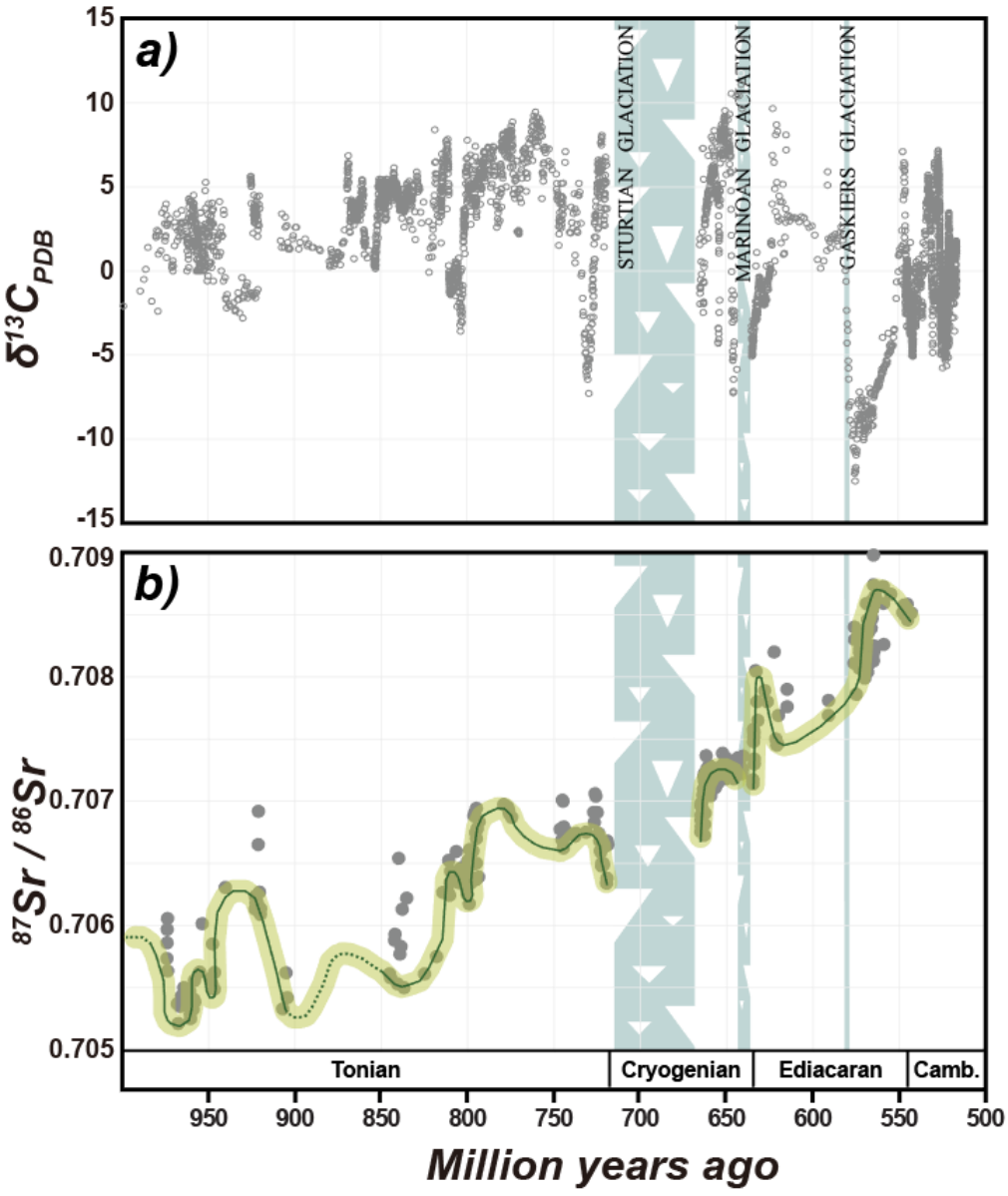

Figure 1-2. Composite $\delta^{13}C$ records for the Neoproterozoic from marine carbonate rocks with Cambrian data (modified from Zhou et al., 2020).

CHAPTER 2

General Geology

2.1 Historical background

The geology of Korea is a very complex system with various rock types from Precambrian to Quaternary. From the north to south, the basement rocks are named the Nangrim (Nangnim) Massif, the Gyeonggi Massif, and the Yeongnam Massif (Figure 1-1). The basement rocks exposed over more than half the area of the Korean peninsula mainly consist of early to middle Paleoproterozoic (2.0-1.8 Ga) high-grade gneiss complexes (Kim, 2012; Oh et al., 2019; Zhao et al., 2006), with much older late Archean to early Paleoproterozoic (~2.5 Ga) rocks in the Nangrim Massif (Zhao et al., 2006) and western Gyeonggi Massif (Cho et al., 2008).

Two sedimentary basins, Pyeongnam Basin and E-W trending Imjingang Belt, are in between the Nangrim Massif and Gyeonggi Massif, and they are separated by Imjingang Belt. The Pyeongnam Basin (Figure 1-1) is sedimentary basin composed of Mesoproterozoic to Paleozoic sedimentary rocks overlying the Nangrim Massif (Hu et al., 2012; Zhai et al., 2019). The sedimentary characteristics of the Pyeongnam Basin are analogous to those of the Taebaeksan Basin of the Okcheon Belt. Lower to south, there is an orogenic belt named Imjingang Belt containing Devonian sedimentary rocks with fossils (Ree et al., 1996; Kwon et al., 2009; Kim et al., 2020), and it is unclear whether this belt is distributed across the Korean Peninsula or not.

The Gyeonggi Massif and Yeongnam Massif are separated by the Okcheon Belt. The Okcheon Belt is a typical Phanerozoic mobile belt with Imjingang Belt. Both belts are worth considering the structural evolution of East Asia and the Korean Peninsula, as either or both may be candidates for an eastern continuation of the Qinling-Dabie-Sulu collision belt (Cluzel et al., 1990; Yin and Nie 1993; Ernst and Liou, 1995; Cheong et al., 2006; Cho et al., 2017) (Figure 1-1).

Sedimentary and volcanic rocks of Paleozoic and Mesozoic were distributed on those basements accompanied with tectonic movements. As for tectonic framework of the peninsula is based on lithological characteristics, geologic time rather than tectonic distinction.

It is noted that the northern part of the Korean Peninsula has evolved with the adjacent North China Craton since at least Paleoproterozoic (Zhai et al., 2019). However, various contrasting hypotheses have been proposed regarding the structural evolution of the southern part of the Korean Peninsula. The most notable thing that has drawn the attention in the meantime is whether the Early Triassic continental collision belt, which developed east-west between the North China Craton and the South China Craton, extends to the Korean Peninsula (Li, 1993; Ree et al., 1996). It has long been controversial that the

position of the collision belt on the Korean Peninsula is either the Imjingang Belt (Ree et al., 1996) or the belt connecting Hongseong and Odaesan in the Gyeonggi Massif (Oh et al., 2006, 2007).

According to these concepts, most of the Gyeonggi Massif and the Okcheon Metamorphic Belt should be correlated to the South China Craton, and the other Gyeonggi Massif and Okcheon Metamorphic Belt, Taebaeksan Basin, and Yeongnam Massif of South Korea with Pyeongnam Basin of North Korea should be correlated to North China Craton. However, such arguments have been challenged in recent years. For example, some parts of the Gyeonggi Massif and Okcheon Metamorphic Belt were turned out to be correlated with the North China Craton, based on recently reported detrital zircon age data.

The northeastern part of the Okcheon Metamorphic Belt is in contact with the Cambro-Ordovician sediments of the Taebaeksan Basin. According to the researcher, various opinions have been proposed about this boundary as conformity, unconformity, or fault contact (Kihm et al., 1996, 1999; Chough et al., 2000, 2006; Kim et al., 2017). Particularly, Chough et al. (2000) suggested this boundary as an accretion or collision boundary between continental blocks with different evolutionary histories and named it the South Korean Tectonic Line (SKTL). The so-called South Korean Tectonic Line (SKTL) was demarcated along the west side of the Yeongnam Massif and the Taebaeksan Basin along the border with the Okcheon Metamorphic Belt. Because the southerly Yeongnam Massif should correlate with the North China Craton, when following the indentation model (Chough et al., 2000).

The Korean Peninsula has strong interconnection with the Cratons in China, but relativity between both was in a lot of trouble because of a consequence of insufficiency of geochronological data from North Korea. By the way, studies on North Korean geology over the last decade (eg, Hu et al., 2012; Wu et al., 2007; Zhao et al., 2006) have been very helpful and useful in understanding East Asian crustal evolution. Studies on the Archean to Paleoproterozoic basement of North China Craton had been brought to bear on the Eastern and Western Blocks and the Trans-Orogenic Belt in between (e.g., Liu et al., 2012; Zhao et al., 2003). Recently, however, research has been extended further east to the Nangrim Massif in North Korea and the Jiao-Liao-Ji belt in between (Meng et al., 2014; Tam et al., 2012; Zhai et al., 2019). Besides, studies on the Neoproterozoic sedimentary rocks at the southern margin of North China Craton and southern North Korea revealed the late Paleoproterozoic to Mesoproterozoic detrital zircon age distributions, suggesting a correlation between the two regions. (Hu et al., 2012).

The Okcheon Belt, which is bounded to the north-west by the Gyeonggi Massif and to the southeast by the Yeongnam Massif, is composed of the non-metamorphosed Taebaeksan Basin in the northeast and the metamorphosed zone in the southwest. (Figure 1-1). The Taebaeksan Basin in the northeast consists of the Lower Paleozoic (Cambro-Ordovician) Joseon Supergroup and the Upper Paleozoic (Carboniferous-Permian) Pyeongan Supergroup, which are correlated with the Paleozoic strata of the Pyongnambasin in North Korea (Chough et al., 2000). Their stratigraphy is well established because of their rich fossil yields and well-preserved sedimentary structures (Chough et al., 2000).

On the other hand, the Okcheon Metamorphic Belt in the southwest is composed of high temperature low-pressure type metavolcanic and metasedimentary rocks ranging from greenschist facies to amphibolite facies, from Neoproterozoic (Kim et al., 2020; Lee et al., 1998a) to Permian (Lim et al., 2005) periods. It is not easy to observe sedimentary structures and fossils due to repeated metamorphism and deformation (Kim et al., 2005; Oh et al., 2004). Therefore, despite many researchers working for decades, the definite timing and stratigraphic relationship of the Okcheon Metamorphic Belt has not been established.

Cho et al. (2013) divided the Okcheon Metamorphic Belt into two narrow and long regions based on their detrital zircon U-Pb age similarity. They are compatible with North China Craton and South China Craton, and are called NCC-like and SCC-like, respectively (Figure 1-1). These two regions display contrasting U-Pb age distribution of detrital zircons and fossil occurrences.

In the SCC-like region, the detrital zircon ages reveal the wide range the oldest are few of the Paleoproterozoic and the youngest include the Paleozoic age. Namely, Neoproterozoic and Paleozoic ages are predominant, while the Paleoproterozoic age of about 1870 Ma which is a prominent feature of basement rocks of Korean peninsula (Lee and Cho, 2012; and references therein) is absent. The areas where Lim et al. (2005, 2006, 2007) have found Carboniferous to Permian plant fossils from metasedimentary rocks are included in the SCC-like area, indicating that they were deposited during Upper Paleozoic.

On the other hand, in the NCC-like region, Paleoproterozoic detrital zircon ages (ca. 1870 Ma) are noticeable with youngest age is about 750 Ma and a weak Mesoproterozoic age component (Cho et al., 2013; S.W. Kim et al., 2020; M.J. Kim et al., 2021), however, the Daehyangsan Quartzite exceptively appears to be the northeast extension of the SCC-like unit. Unlike the SCC-like unit, Paleozoic plant fossils have not been discovered.

The northeastern region of the Okcheon Metamorphic Belt (Figure 1-1) is considered to have a North China Craton affinity and is where the Hyangsanni Dolomite occurs, which is the subject of this study. The age obtained for metavolcanics in the Munjuri Formation is ca 750 Ma, which is commonly appearing in South China. For that reason, Cho et al. (2013) classified Munjuri Formation in considered as SCC-like. However, since this age is often included as a characteristic detrital zircon age component of the NCC-like region, and also surrounded by other formations having NCC-affinities. Thus, it is more appropriate to classify the Munjuri Formation as NCC-like.

Neoproterozoic metavolcanics are distributed in the Gyemyeongsan Formation and the Munjuri Formation in the study area, which has known to have erupted at about 860 Ma and about 750 Ma, respectively (Kim et al., 2006, 2020; Lee et al., 1998a). Both formations have A-1 type characteristics (Cho et al., 2004; Kim et al., 2006, 2011; Ko et al., 2005; Lee et al., 1998). The U-Pb age distribution of detrital zircons in metasedimentary rocks in the study area can be broadly divided into two types; one type has mainly late Paleoproterozoic to Mesoproterozoic age component, and another type has Paleoproterozoic age (ca 1870 Ma) and Neoproterozoic age (ca. 750 Ma) as major age components (Cho et al., 2013; Kim et al., 2020; Kim et al., 2021). The former is characterized by the Seochangni Formation and the Myeongori Formation, which are mainly composed of phyllites and intercalated thin layers of quartzite. Since the youngest detrital zircon age in these formations is about 750 Ma, it has been suggested that these formations may have been deposited in Neoproterozoic (Kim et al., 2020).

The Chungju area, from where the samples were collected for this study, is located in the northeastern part of the Okcheon Metamorphic Belt and is in direct contact with the Taebaeksan basin (the Great Limestone; Fig. 1c). For some of the Okcheon Metamorphic Belt formations in Chungju, the timing of sedimentation was relatively firmly determined.

An important evidence for the tectonic environment associated with the development of the Okcheon Metamorphic Belt is A-1 type magmatism indicating continental rifting (Eby, 1992). As mentioned before, U-Pb zircon ages of about 860 and 750 Ma were reported from A-1 type metavolcanics included in Gyemyeongsan (Kim et al., 2006, 2011; Ko et al., 2005) and Munjuri formations (Kim et al., 2006; Lee et al., 1998a), respectively. These magmatic activities refer to two Neoproterozoic continental rifting events that seems to have led to the deposition of sedimentary basins in the Okcheon Metamorphic Belt.

Gyemyeongsan Formation, unconformably overlained by Hyangsanni Dolomite, is known to have metavolcanics of about 860 Ma as the main rock type. This Gyemyeongsan metavolcanics has A-1 type magma characteristics, and igneous rocks of this nature are found mainly in tectonic environments such as within-plate rifts, which are often associated with continental fragmentation (Kim et al., 2006, 2011; Ko et al., 2005).

The detrital zircons of the Daehyangsan Quartzite, distributed between Hyangsanni Dolomite and Munjuri Formation, exhibit U-Pb ages of about 410 Ma with distinct Neoproterozoic ages (Park et al., 2011). Therefore, the oldest estimation of Daehyangsan Quartzite deposition can be constrained to 410 Ma.

The Hyangsanni Dolomite is distributed as a narrow-elongated layer parallel to the Gyemyeongsan Formation and the Daehyangsan Quartzite. The Daehyangsan Quartzite is the only sedimentary layer with Paleozoic detrital zircon ages within the NCC-like unit of the Okcheon Metamorphic Belt. Although the Daehyangsan Quartzite is distributed between the Hyangsanni Dolomite and the Munjuri Formation, the relationship between these layers has not yet been unambiguously understood despite several studies (e.g., Ihm et al., 1991; Ryu and Kim, 2009).

Farther east than the Munjuri Formation, sedimentary layers mainly composed of diamictites (the Hwanggangni and the Bungnori Formation) and the layers mainly composed of phyllites (the Myeongori Formation and the Seochangni Formations) are alternately distributed.

There have been several reports of fossil discovered from the Hyangsanni Dolomite. Lee et al. (1972) reported a single Archaeocyatha fossil from the Hyangsanni Dolomite, suggesting that this was a marine formation of Early to Middle Cambrian. However, some researchers have raised questions about the Archaeocyatha fossils discovered by Lee et al. (1972) in Hyangsanni Dolomite. Recently, Ree et al. (2016) reexamined the actual specimen, suggesting that this is a structural form that differs from the typical shape of Archaeocyatha and may be a result of deformation and metamorphism followed by radial cracking caused by a volume-increasing reaction and crack filling. However, Yang et al. (2017) refuted the opinion of Ree et al. (2016) that it was formed by metamorphism and deformation, and argued that this is a definite fossil. While the findings of Lee et al (1972) do not completely rule out fossils, the evidence from this study suggests that they are not fossils of at least the Cambridge period.

The Sr isotope composition of Hyangsanni Dolomite has also been reported by Park and Cheong (1998) and Shin and Lee (2008). These data are discussed later with the data analyzed in this study.

Lee et al. (1998b) suggested that the Hwanggangni Formation was composed of glaciogenic diamictite and inferred sedimentation time to Late Paleozoic because of the discovery of Cambro-Ordovician conodont fossils from limestone clasts of this formation (Lee et al., 1989). However, the discovery of conodonts in this formation has not been confirmed since then and needs to be verified. Yi et al. (2000) analyzed the Sr isotope composition of carbonate pebbles in the Hwanggangni Formation and suggested that the sedimentation of this formation was post-Ordovician.

Suzuki et al. (2006) found that Paleoproterozoic granitic gneiss clasts had xenotime grains with a metamorphic rim of about 370 Ma, suggesting that sedimentation of the Hwanggangni Formation was thereafter. Yi et al. (2000) analyzed the Strontium isotope composition of carbonate pebbles in the Hwanggangni Formation and suggested that the sedimentation of this formation was post-Ordovician. However, this age estimation method assumes that the analyzed Sr isotope values are the same as those at the time of deposition. Therefore, further verification is needed given that carbonate rocks often tend to change towards higher values than the seawater at the time of deposition for various reasons. Lee et al. (1998), who suggested that Hwanggangni Formation was composed of glaciogenic diamictite, inferred sedimentation time to Late Paleozoic because of the discovery of Cambro-Ordovician conodont fossils from limestone clasts of this formation (Lee et al., 1989). In contrast, Choi and Woo (2012) suggests that this formation and overlying Geumgang Limestone are glaciogenic diamictite-cap carbonate couplet deposited during the Neoproterozoic Snowball Earth event based on correlation with stratigraphy of Nanhua Basin in South China Craton. But nothing do provide definitive evidence. The detrital zircons of the Hwanggangni Formation features age groups of ca. 750 Ma and ca. 1870 Ma, that implies their deposition was later than 750 Ma (Cho et al., 2013).

U-Pb age determination and Hf isotope analysis of detrital zircons were carried out on the Seochangni Formation among the layers more east than the Hwanggangni Formation (Kim et al., 2021). The detrital zircons of the Seochangni Formation manifest a conspicuous Mesoproterozoic age distribution. The youngest zircon age suggest that the Seochangni Formation also consist of Neoproterozoic sedimentary layers (Kim et al., 2020; Kim et al., 2021). Judging from Neoproterozoic sedimentary deposits with Mesoproterozoic detrital zircon age components, they correlate to the

southern margin of North China Craton together with the Sangwon Supergroup of North Korea (Hu et al., 2012).

Though numbers of the U-Pb age determinations for detrital zircons from the siliciclastic sequences have conducted (Cho et al., 2013; Kim et al., 2020), the precise depositional timing of the remaining sedimentary sequences is still pending.

In the case of carbonate rocks, in particular, that do not have detrital zircon, it is more difficult to limit the depositional time because proper dating means are limited. However, a recent chemostratigraphy study based on carbon and strontium isotopic composition suggested that the Hyangsanni Dolomite was deposited in Neoproterozoic (Ha et al., 2021 and this study). This study demonstrates geochronology for carbonates which has been age debatable in the Okcheon Metamorphic Belt by adopting chemostratigraphy.

2.2 Studied area

This study was conducted on the central-western (Boeun-Okcheon area, Figure 2-1) and the northeastern (Chungju-Jecheon area, Figure 2-2) Okcheon Metamorphic Belt bordering the Taebaeksan Basin to the east (Figure 1-2). In the legend (Figure 2), the arrangement of metasedimentary formations of the Okcheon Metamorphic Belt does not imply stratigraphic order. The constituents of the studied area in the Okcheon Metamorphic Belt are as follows.

Gyemyeongsan Formation

The Gyemyeongsan Formation is the lowest unit of sequence distributed around lake-Chungju, in the central western part of study area. The Gyemyeongsan Formation is chiefly composed of pelitic and psammitic phyllites/schist derived from bimodal volcanic rocks (Na et al., 1982; Cluzel, 1992; Kang and Ryoo, 1997; Park et al., 2003; Koh et al., 2005; Park et al., 2005; Kim et al., 2006a; Kim et al., 2011; Kang et al., 2012) based on geochemical studies suggesting that this formation was related to the intracratonic rifting of the paleocontinents. (Koh et al., 2005; Park et al., 2005; Kim et al., 2006). Afterwards, the volcanic rock was transformed into metamorphic rock by over twice of greenschist-

amphibolite facies metamorphism in Mesozoic. Recently reported zircon U-Pb age of ca. 870-860 Ma (Kim et al., 2011) is interpreted to timing of initial rift stage correlating to Nanhua Basin, South China (Choi et al., 2012 and referenced therein).

This formation is conformably underlain by the Hyangsanni Dolomite (Choi et al., 2012). While Ryu et al., (2009) suggested that a thrust fault has developed in boundary between the Gyemyeongsan Formation and Hyangsanni Dolomite. In this respect, Gyemyeongsan and Munjuri Formation are considered as and equivalent one based on their lithologic and geochronologic features. However, Munjuri Formations has much younger age than Gyemyeongsan Formation, about 100 Ma.

Hyangsanni Dolomite (Figure 3-1)

The Hyangsanni Dolomite is well exposed in association with the Gyemyeongsan Formation. The Hyangsanni Dolomite was originally established by Kim and Lee (1965) as the Hyangsanni Dolomitic Limestone. This formation makes a feature of massive dolomitic limestone with intercalation of quartzite layer. Additionally, the rocks of this formation are country rock of the talc deposits (Hwanggangni quadrangle).

Reliable geologic age information has not been available yet, but it is supposed to be Neoproterozoic on a basis of stratigraphic position between the Neoproterozoic Formations which are Gyemyeongsan Formation (ca. 870-860 Ma, Kim et al., 2011; Kang et al., 2012) and Munjuri Formation (ca. 760-740 Ma, Cheong et al., 2014). The conflicting Cambrian age with the finding of Archaeocyatha fossil is suggested (Lee et al., 1972), but questionable. Ree et al. (2016) has raised the question of palaeontological evidence for Archaeocyatha concluding that it is not Archaeocyatha but metamorphosed structure. Besides, the presence of fossil has not been reconfirmed by other researchers.

Daehyangsan Quartzite (Figure 3-4)

The Daehyangsan Quartzite was named by Kim and Lee (1965). The Daehyangsan Quartzite is primarily distributed in association with the Hyangsanni Dolomite alongside the Lake Chungju. The stratigraphic relation between the Daehyangsan Quartzite and Hyangsanni Dolomite is suggested to be

conformable (Ryu et al., 2009). But stratigraphic relation between both is also still pending. This rock is made up of recrystallized equigranular quartz (e.g. Hwanggangni quadrangle).

Recently reliable zircon U-Pb age is reported from this formation (ca. 420 Ma, Park et al., 2012). It is difficult to interpret stratigraphically because stratigraphy has still been vague.

Munjuri Formation (Figure 3-6)

The Munjuri Formation was originally proposed by 1:50,000-scale Chungju quadrangle (Kim and Lee, 1965). This Formation is disconformable overlying the Daehyangsan Quartzite.

This formation exhibits a very wide distribution among the various constituents of the Okcheon Metamorphic Belt. Most of the 10 quadrangles (1:50,000 scale; Ganggyeong (Lee et al., 1980), Goesan (Lee et al., 1972), Geumsan (KIGAM, 1978), Mokgye (Park and Yeo, 1971), Miwon (Lee et al., 1980), Boeun (Kim et al., 1977), Okcheon (KIGAM, 1978), Yongyuri (KIGAM, 1973), Jecheon (Kim et al., 1967), and Hwanggangni (Lee and Park, 1965) quadrangles) which cited the stratigraphic name of Munjuri Formation, described the main rocks as the age-unknown or Paleozoic metapellite.

The Munjuri Formation is predominantly composed of bimodal metavolcanic rocks and metasedimentary rocks, mostly schist. The Neoproterozoic U-Pb age, ca. 760-750 Ma, from the A-1 type metavolcanics of this formation is reported (Lee et al., 1998; Cho et al., 2004; Kim et al., 2006a). Choi et al. (2012) interpreted that it can be equivalent to the second rift stage of the Nanhua Basin in South China Craton. In accordance with this interpretation, it is suggested that the Hyangsanni Dolomite and Daehyangsan Quartzite might be deposited in normal marine setting between these two rifting stages. Ryu et al. (2009) suggested bedding parallel faults have been developed in the boundary between two formations. It however should be carefully reconsidered.

The A-1 type metavolcanics are only recognized in the Chungju area, and not unknown in the Munjuri Formation, which is distributed in the southern part of the Okcheon Metamorphic Belt. However, so far, such A-1 type metavolcanics have not been known in the Munjuri Formation, which is distributed in the southern part of the Okcheon Metamorphic Belt, suggesting the possibility of being a sedimentary layer that is not correlated with the Munjuri Formation in Chungju.

Hwanggangni Formation (Figure 3-2) and Bugnori Formation (Figure 3-3)

The Hwanggangni Formation and the Bugnori Formation were first named in the 1:50,000-scale Hwanggangni quadrangle (Lee and Park, 1965). The Hwanggangni Formation is distributed over a wide area in the mid-southern part of the Okcheon Metamorphic Belt. This formation is also recognized close to the left of the South Korean Tectonic Line in northeastern Okcheon Metamorphic Bel, but on the other, it is mapped as the Bugnori Formation by Lee and Park (1965).

In the northeastern Okcheon Metamorphic Belt, these two formations do not come into direct contact, and the Myeongori Formation, mainly composed of phyllite, exists between the two. According to the Hwanggangni quadrangle, the Chungju area, there is a relatively thin, continuous carbonate layer with a thickness of about 15-20 meters between the Myeongori Formation and the Bugnori Formation.

These Formations feature pebble-bearing phyllitic rocks. The pebbles are different sizes and shapes of limestone, granite, gneiss and quartzite and such.

These formations were originally considered to be distinct from each other by Lee and Park (1965). What is interesting, this formation has been suggested to be correlated with the diamictites of Neoproterozoic snowball Earth episode, equivalent to the Nanhua Basin even though no reliable age is much enough at present (Choi et al., 2012). Such a proposal was suggested by Reedman et al. (1973) at first. Since then, Lee et al., (1998) also interpreted Hwanggangni Formation as glaciogenic sediments but assumed that it might be Permo-Carboniferous glacial deposits of Gondwana.

With regard to lithology of Hwanggangni Formation concerned as diamictite, there was another interpretation, submarine debris flows derived by slope failure of semi-consolidated sediments (Chough and Bahk, 1992).

The depositional timing has also been incompatible as previous stated, the Precambrian or Post-Cambrian. The conodont fossils from limestone clasts (Lee et al., 1989) and granitic gneiss clast (Suzuki et al., 2006) advocate the latter, post-Ordovician and late Devonian respectively. Recently reported U-Pb age information (Cho et al., 2013; Kim et al., 2020; this study) put weight on the theory that the Hwanggangni Formation was deposited in Neoproterozoic. Thus, further studies are necessary for estimating the depositional age of the Hwanggangni Formation and particularly for linkage with the snowball Earth hypothesis.

Some author (Choi et al., 2012; Ha, 2021) treated the Hwanggangni and Bugnori formations as a single formation, based on the recognition of thin limestone layer, named Geumgang Limestone. Ha

(2021) suggests that diamictite deposit with the limestone layer developed at the boundary is called Bugnori Formation, otherwise it is called Hwanggangni Formation.

Seochangni Formation, Changni Formation (Figure 3-5), and Myeongori Formation

The pelitic rocks are classified into the Seochangni, Myeongori, and Munjuri formations in the 1:50,000-scale Hwanggangni quadrangle (Lee and Park, 1965). These formations are sedimentary layers composed mainly of pelitic rocks such as phyllite, slate, or shale distributed in the northeastern part of the Okcheon Metamorphic Belt. The Myeongori Formation is only in contact with the carbonate layer.

The Seochangni Formation, which consists mainly of pelitic rocks with alternating quartzose sandstones and calcareous units, is distributed in the northeastern part of the Okcheon Metamorphic Belt. The detrital zircon U-Pb ages from the Seochangni Formation displays from late Paleoproterozoic to the latest Mesoproterozoic. An intercalated limestone layer shows 0.70587 of the $^{87}Sr/^{86}Sr$ ratio. This value suggests that it was deposited at ca. 850 Ma.

However, in the 1:50,000-scale of the Okcheon (Kim et al., 1978) and Boeun (Kim et al., 1977) quadrangles, such pelitic rocks are rather simply treated. The sedimentary layers distributed in the southern region of the Okcheon Metamorphic Belt are largely composed of pelitic rocks. Such pelitic rocks that were investigated and named later than these, are typically Munjuri Formation and Changni Formation. During geological surveys in Boeun and Okcheon areas for the preparation of 1:50,000 scale quadrangle, sedimentary layers composed of mostly green phyllitic rocks were classified as Munjuri Formation, and those composed of dark gray phyllitic rocks were named as Changni Formation (Kim et al., 1977, 1978).

The lithologies of the Changni Formation are similar to the Seochangni Formation or the Myeongori Formation, which are distributed in the northeastern part of the Okcheon Metamorphic Belt but do not come into direct contact with them, and there is no definite evidence for correlation, so different formation names are maintained.

There is no significant difference between the Munjuri Formation and the Changni Formation

except for the general color, and even this may be difficult to distinguish in some outcrops.

Geumgang Limestone

The Geumgang Limestone was originally established in 1:50,000 Okcheon quadrangle (Kim et al., 1978) and was traced into the Lake Chungju area (Lee, 1995).

The Geumgang Limestone are locally recognized in part of northwestern Okcheon Metamorphic Belt, central Korea. And it has a thickness of about 10 meters and extends from Chungju to Boeun-Okcheon area. It is uncommonly intercalated between pebble-bearing phyllitic and phyllitic metasedimentary rocks.

It has a possibility of post-glaciogenic cap carbonates. In this context, the underlying pebble-bearing phyllitic rock, Hwanggangni Formation, has been interpreted as glaciogenic diamictite (Lee et al., 1998; Choi et al., 2012; Ryu and Ahn, 2016; Ha, 2021). Therefore, the Geumgang Limestone is a key stratum helpful in understanding the Neoproterozoic Snowball Earth event in the Korean peninsula and establishing the stratigraphy of the Okcheon Metamorphic Belt. Because the post-glacial cap carbonates can help to limit its geological time. Recent studies based on carbon isotopes (Ryu and Ahn, 2016; Ha, 2021) suggests that the Geumgang Limestone was deposited after the Neozoic Ice Age, although they do not know exactly when.

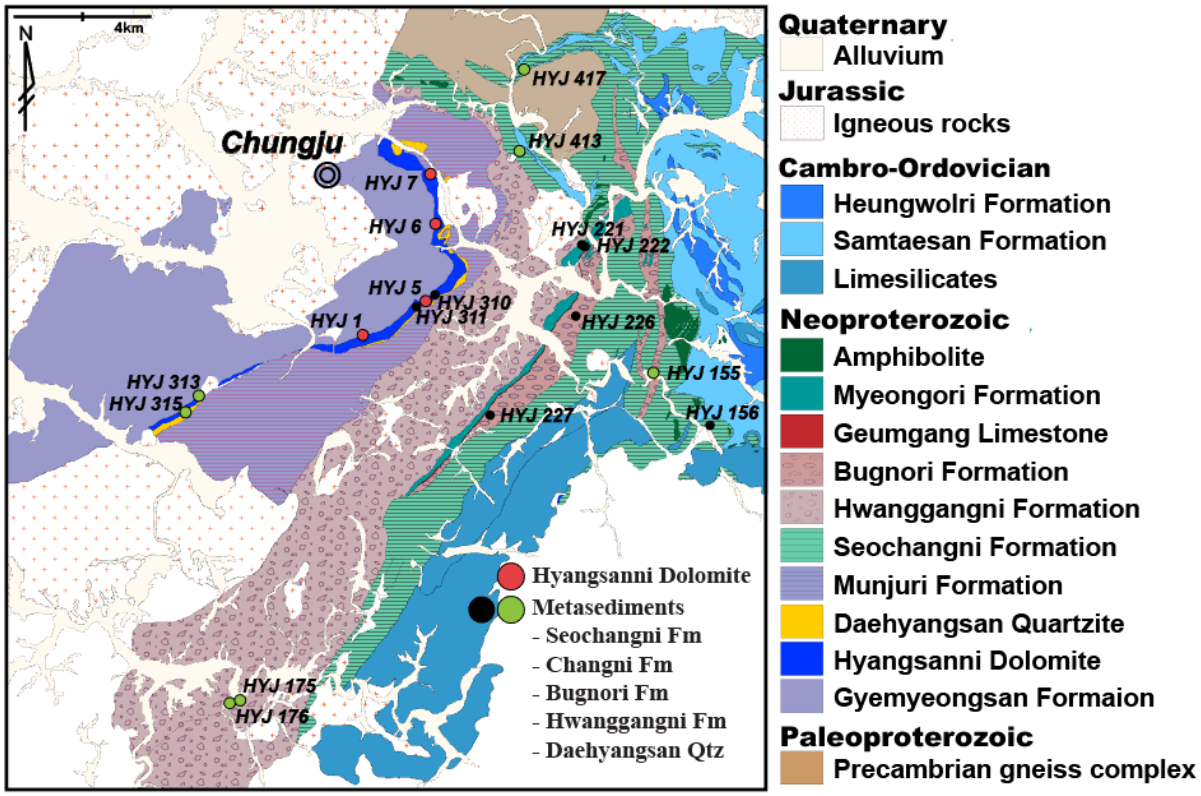

Figure 2-1. Geological map of the northeastern Okcheon Metamorphic Belt and the western Taebaeksan basin modified after Kim et al., (1967), Lee et al., (1965), Geological Society of Korea (1962) and Won et al. (1967). Sampling locations are shown along with outcrop numbers. Red circles represent the Hyangsanni Dolomite samples. Green and Black circles represent the metasediment sequences; Green one is used for zircon U-Pb age dating.

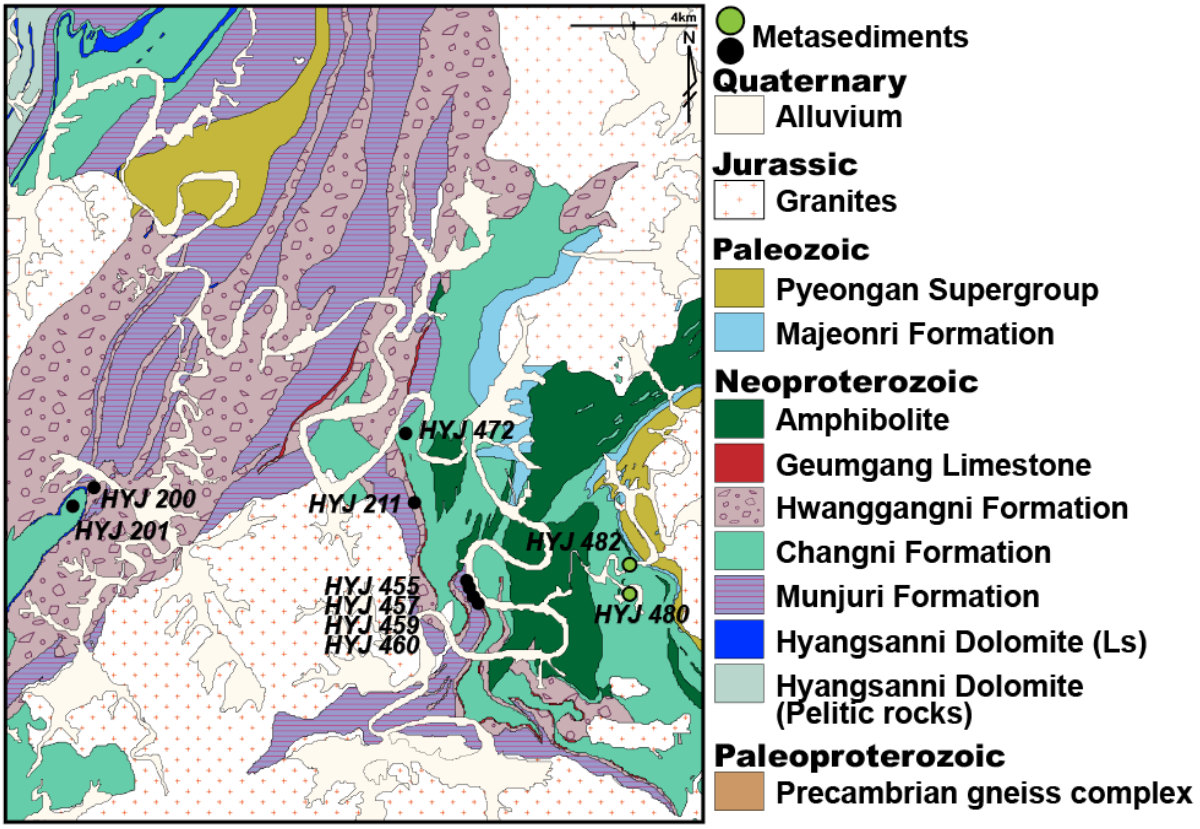

Figure 2-2. Geological map of the Okcheon-Boeun area, modified after Kim et al. (1978) and Kim et al. (1977). Sampling locations are shown with outcrop numbers. Green and Black circles represent the metasediment sequences; Green one is used for zircon U-Pb age dating.

CHAPTER 3

Sampling and analytical methods

3.1 Field observation and sampling

The studied areas are near the lake Chunju area (Figure 2-1) and Okcheon-Boeun area (Figure 2-2). For this study, I carried out the field observation and sampling from the meta-carbonate and metasedimentary sequences in the northwestern Okcheon Metamorphic Belt in central Korea.

The Hyangsanni Dolomite samples were measured carbon, oxygen, and strontium for chemostratigrphic age dating. Metasedimentary samples were collected from several outcrops for U-Pb age determination of detrital zircons. Metasedimentary samples for this study were collected from Hwanggangni Formation (HYJ 175 and HYJ 176, Figure 3-2), Bugnori Formation (HYJ 155, Figure 3-3), Daehyangsan Quartzite (HYJ 313 and HYJ 315, Figure 3-4), Seochangni Formation (HYJ 413 and HYJ 417, Figure 3-5), and Changni Formation (HYJ 480 and HYJ 482, Figure 3-5). Their stratigraphic names, exposed quadrangles and GPS coordinates are summarized in Table 3-1.

Table 3-1. Quadrangles and Stratigraphy names, with GPS coordinates for sampling localities of the studied samples.

Sample #	Quadrangle	Stratigraphy name	GPS coordinate	Remark for analysis	Figure #
HYJ 1	Chungju	Hyangsanni Dolomite	N36 55.951 E127 57.396	C-O isotope anaylsis Sr isotope analysis	2-1
HYJ 5			N36 56.834 E127 59.447		2-1
HYJ 6			N36 58.826 E127 59.730		2-1
HYJ 7			N37 00.090 E127 59.585		2-1
HYJ 155	Hwanggangni	Bugnori Formation	N36 54.863 E128 06.746	zircon U-Pb analysis	2-1
HYJ 221			N36 58.118 E128 04.389		2-1
HYJ 222			N36 58.140 E128 04.595		2-1
HYJ 226			N36 56.315 E128 04.165		2-1
HYJ 227			N36 53.884 E128 01.360		2-1
HYJ 175	Goesan	Hwanggangni Formation	N36 46.558 E127 53.147	zircon U-Pb analysis (matrix)	2-1
HYJ 176			N36 46.553 E127 53.135	zircon U-Pb analysis (granite pebble)	2-1
HYJ 200	Okcheon		N36 19.716 E127 31.953		2-2
HYJ 201			N36 19.484 E127 31.398		2-2
HYJ 211			N36 19.458 E127 38.597		2-2
HYJ 472	Boeun		N36 20.527 E127 38.386		2-2
HYJ 310	Chungju	Daehyangsan Quartzite	N36 56.843 E127 59.463		2-1
HYJ 311			N36 56.791 E127 59.144		2-1
HYJ 313			N36 54.233 E127 51.923	zircon U-Pb analysis	2-1
HYJ 315			N36 53.913 E127 51.613	zircon U-Pb analysis	2-1
HYJ 156	Hwanggangni	Seochangni Formation	N36 53.577 E128 08.465		2-1
HYJ 413	Jecheon		N37 00.647 E128 02.549	zircon U-Pb analysis	2-1
HYJ 417			N37 03.040 E128 06.446	zircon U-Pb analysis	2-1
HYJ 14-3	Daejeon	Changni Formation	N36 12.033 E127 26.988		-
HYJ 480	Okcheon		N36 17.848 E127 43.284	zircon U-Pb analysis	2-2
HYJ 482			N36 18.209 E127 43.205	zircon U-Pb analysis	2-2
HYJ 429	Miwon	Munjuri Formation	N36 32.163 E127 41.843		-
HYJ 455	Okcheon		N36 18.041 E127 39.796		2-2
HYJ 457			N36 17.997 E127 39.811		2-2
HYJ 459			N36 17.952 E127 39.820		2-2
HYJ 460			N36 17.946 E127 39.817		2-2

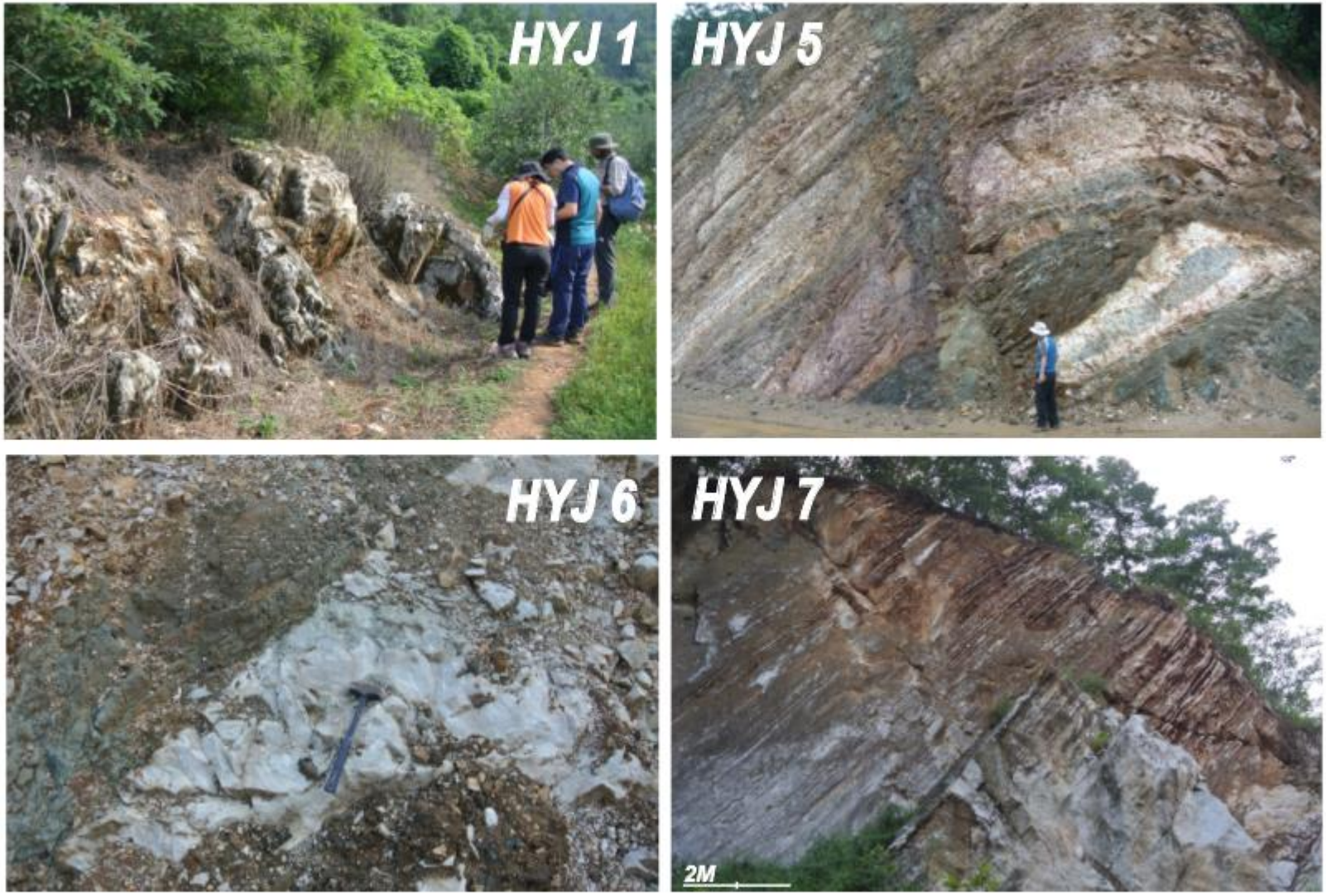

Figure 3-1. Outcrop photographs of the Hyangsanni Dolomite.

Figure 3-2. Outcrop photographs of the Bugnori Formation.

Figure 3-3. Outcrop photographs of the Hwanggangni Formation.

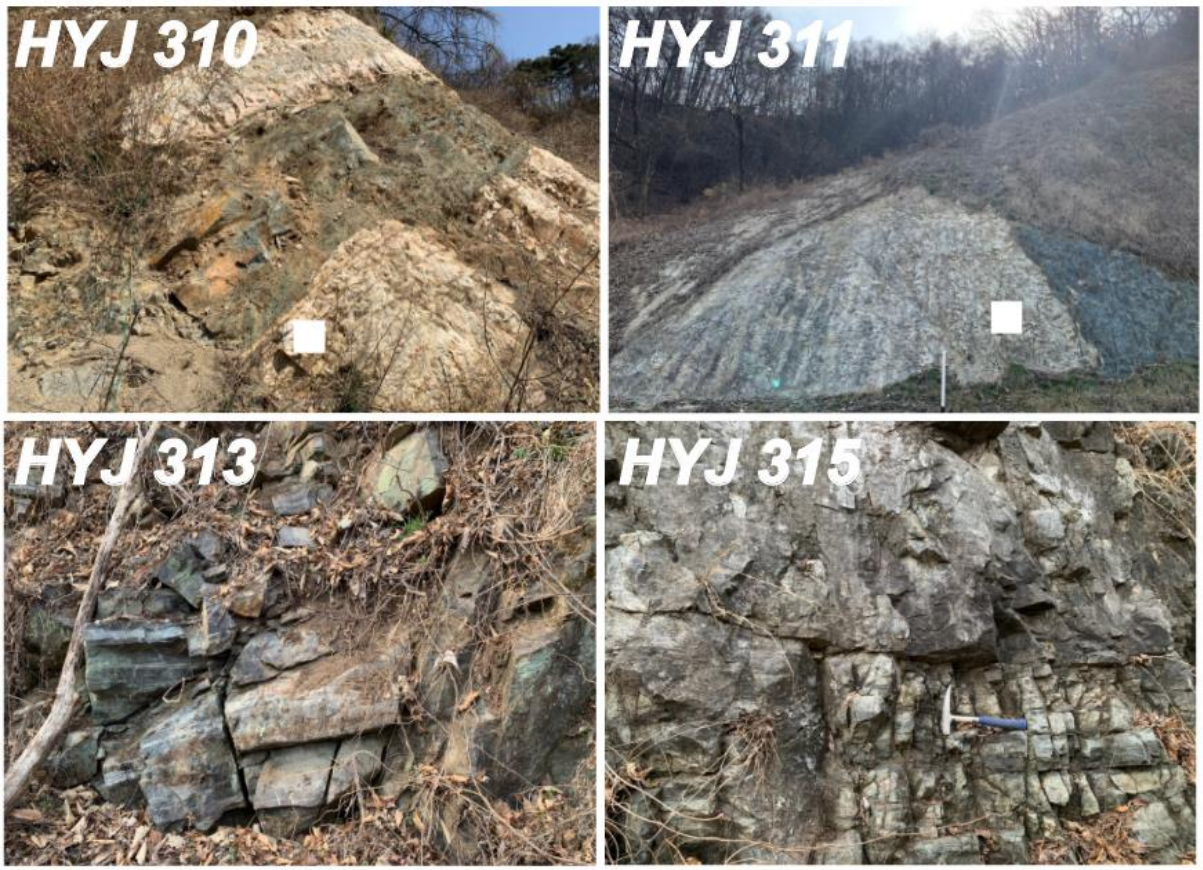

Figure 3-4. Outcrop photographs of the Daehyangsan Quartzite. White squares represent the sampling location.

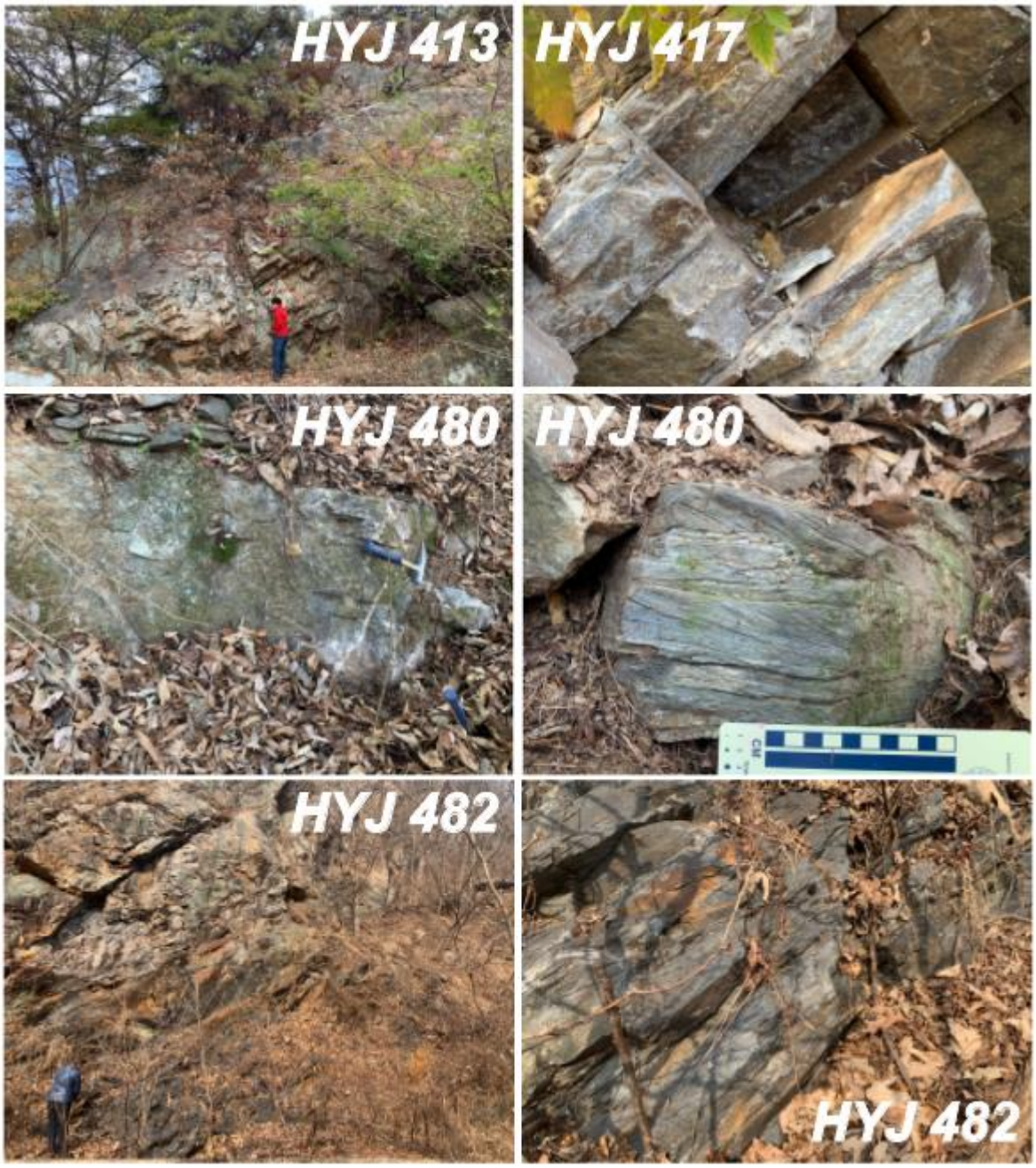

Figure 3-5 Outcrop photographs of the Seochangni Formation (HYJ 413 and HYJ 417) and Changni Formation (HYJ 480 and HYJ 482).

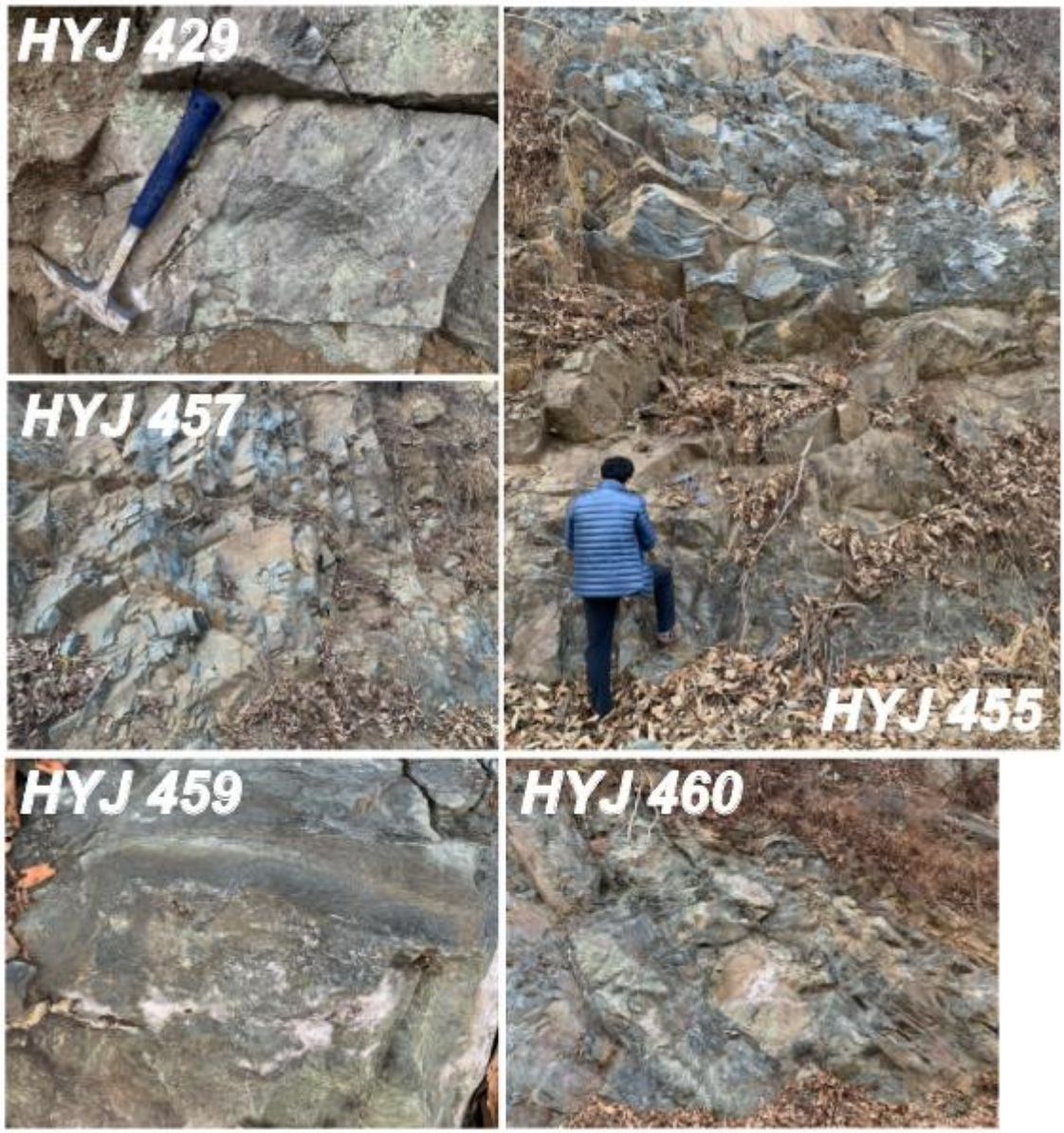

Figure 3-6. Outcrop photographs of the Munjuri Formation.

3.2 Trace element geochemistry

For geochemical analysis, samples were chipped using a hand press. The crushed rock chips were pulverized in an agate mortar. After putting it in a porcelain crucible and drying it in an oven for half a day, it was more finely powdered with an agate mortar. An aliquot of 50 mg of the powdered sample, suitable standards (BHVO-2, W-2a, JB-2) and several blanks were dissolved in acetic acid spiked with Indium solutions as standard for measurements. After dissolution the vial was centrifuged and the supernatant was separated and dried. After drying, a mixed acid (nitric acid, hydrochloric acid, and hydrofluoric acid) was used to dissolve the dried residue and dried repeatedly three times. The solution was diluted to 10,000 times when measuring REE, and 50,000 times when measuring for Mn.

Isotope dilution methods follow the protocol described in detail by Neo et al. (2006). Trace elements including REE, Rb and Sr compositions of the samples were measured using ICP-MS (Agilent 7500a) at Niigata University, Japan.

3.3 C-O isotopes

Rock slabs were prepared for the analysis of carbon and oxygen isotopes. Polished surfaces of the rock slabs were stained with Alizarin-Red-S solution to distinguish between calcite and dolomite and sample only primary dolomite, avoiding areas recrystallized with calcite (Figure 3-7). Staining of Alizarin red-S does not influence the C and O isotope ratio (Wada et al., 1983). The dolomite powders scraped off the stained surface with a knife were further crushed under the stereomicroscope and transferred to a small stainless steel cup. Slab chip samples were also prepared for comparison with those scraped from selected spots of slabs. Chip samples were made into powder using agate. A stainless steel cup was dropped into a vacuum pot containing 100 °C phosphoric acid and reacted with dolomite powder to generate CO_2 gas for analysis. The liberated CO_2 gas was then purified cryogenically for analysis.

The carbon and oxygen isotope composition were acquired simultaneously on Finnigan MAT 251 Mass Spectrometer installed at the Niigata University. The results are expressed as per mil (‰) values and reported in conventional δ notation relative to the V-PDB standard for carbon and V-SMOW

standard for oxygen. Machine standards calibrated to NBS-20 standard, and the precision of $\delta^{13}C$ and $\delta^{18}O$ for the laboratory standard CO2 gas were 0.03‰ and 0.05‰, respectively (Otsuji et al., 2013).

3.4 Strontium isotope

Strontium isotopes were measured from the same powder samples used for the analysis of trace elements including rare earth elements (REE). Carbonate samples were firstly decomposed in a mixed solution of distilled water and CH_3COOH in a Teflon® vessel. Only carbonate minerals will dissolve in acetic acid, which restricts the effect of minor silicate minerals, especially detrital components, on strontium isotopes. After dissolution the vial was centrifuged and the supernatant was separated. Distilled water was added once again to the residue and supernatant was collected. The collected supernatant liquid was evaporated to dryness and nitric acid was added. Ca–Rb–Sr and REE were separated by 1st column separation (BioRad, AG50W-X8 cation-exchange resin). Sr purification was done through a 2nd column separation (Eichrom resin for Sr). The Rb-Sr isotope analyses were carried out following the procedures of Miyazaki and Shuto (1998) using a Thermal Ionization Mass Spectrometry on a Finnigan MAT 262 mass spectrometer at Niigata University, Japan. A Ta (sample) and Re (ionization) filament combination is used. The NIST 987 standard was analyzed before and after each analytical session. Repeated measured $^{87}Sr/^{86}Sr$ ratios were normalized to $^{86}Sr/^{88}Sr=0.1194$ to calibrate the instrumental mass fractionation. Repeated measurements of the Sr isotope composition for the NIST 987 standard agree well with the known values, (averaging $^{87}Sr/^{86}Sr=0.710237\pm0.000014$, 2σ, n=20).

3.5 Zircon U-Pb age dating

U-Pb age determination of detrital zircons was conducted using a Sensitive High- Resolution Ion Microprobe (SHRIMP IIe/MC) and Laser Ablation–Multiple Collector–Inductively Coupled Plasma Mass Spectrometer (LA–MC–ICPMS) installed at the Korea Basic Science Institute (KBSI).

Zircon grains were hand-picked under the stereomicroscope after separation from crushed and

Figure 3-7. Representative slab photographs of carbonate rocks of the Hyangsanni Dolomite. The spot number and the carbo (left) and oxygen isotope (right) values are shown together.

pulverized rock samples by water-based panning. Hand-picked zircon grains were mounted with chips of the FC 1 (Duluth gabbro of 1099 Ma; Paces and Miller, 1993) and SL 13 (Sri Lankan gem zircon) reference zircons in epoxy resin. To observe the internal texture of the zircons, the epoxy mounts were grounded until half the thickness of the zircon grains was exposed. Before analyses, the internal texture of the zircon grains was examined using cathodoluminescence (CL) and backscatter electron (BSE) images obtained using a scanning electron microscope (JEOL 6610LV) at the KBSI. The locations of the analysis spots were selected by checking the presence or absence of remarkable cracks, inclusions of other minerals, inherited zircon, or metamorphic overgrowth by referring to CL and BSE images. In the U-Pb age determination of zircon grains using SHRIMP or LA-MC-ICPMS, we tried to randomly select the grains analyzed without any systematic discrimination as much as possible after scanning such CL and BSE images.

The analytic conditions and data acquisition procedures using SHRIMP were similar to those of previous studies (Williams, 1998; Lee et al., 2018). A 3–4 nA mass filtered negative ion oxygen (O_2^-) primary beam was focused to a spot (ca. 25μm diameter) on the polished zircon surface with 10 kV accelerating voltage. Each spot was analyzed five cycles through the mass range. For the U-Pb age determination, the collector slit was fixed at 100μm in width, achieving a mass resolution of about 5000 at 1% peak height. The FC 1 (1099 Ma, Paces and Miller, 1993) and SL 13 (238 ppm, Claoue-Long et al., 1995) zircons were used for Pb/U calibration and U concentration, respectively.

Data processing was conducted using SQUID 2.5 (Ludwig, 2008) and Isoplot 3.75 (Ludwig, 2012) programs. To construct concordia diagrams, probability density diagrams, and age histograms, the ^{207}Pb and ^{204}Pb correction method was applied to the apparent $^{206}Pb/^{238}U$ zircon ages less than 1000 Ma, and the apparent $^{207}Pb/^{206}Pb$ zircon ages greater than 1000 Ma, respectively. Weighted mean ages of age clusters were calculated using ^{204}Pb-corrected $^{206}Pb/^{238}U$ ratios, and they are reported at 95% confidence levels. I used only concordant or almost concordant (<10% discordancy) ages for the following discussions.

Additional U-Pb age determination of detrital zircons was performed using an LA-MC-ICP-MS (Nu Plasma II multi-collector inductively coupled plasma mass spectrometer equipped with a New Wave Research 193-nm ArF excimer laser ablation system). The analytic conditions and data acquisition procedures using the LA-MC-ICP-MS were similar to those of previous studies (e.g., Lee

et al., 2018). The Nu Plasma II mass spectrometer contains fixed collectors of sixteen Faraday detectors and five ion-counting electron multipliers. For the U-Pb age determination, the collectors were set for simultaneous detections in the following array: ^{208}Pb (IC 0), ^{207}Pb (IC 1), ^{206}Pb (IC 2), ^{204}(Hg+Pb) (IC 3), ^{202}Hg (IC 4), ^{232}Th (high 7) and ^{238}U (high 9) for background correction of ^{204}Pb + ^{204}Hg. ^{235}U was calculated from ^{238}U using a natural ^{238}U/^{235}U ratio of 137.88. Mass number 204 was used as a monitor for common ^{204}Pb after discarding the ^{204}Hg background. The U-Pb age determination reported in this study was obtained using spot sized of about 15μm in diameter, 5 Hz repetition rate, and an energy density of 5 J/cm^2. Helium (600ml/min) was used as the carrier gas. Background intensities, dwell time, wash out time were measured 35s, 30s and 20s, respectively. Signal intensities for each collector were collected every 0.2s which is integration time.

Raw data were corrected for the background, mass discrimination, laser-induced elemental fractionation, and drift in ion counter gains. U–Pb isotope ratios were calibrated using reference zircon 91500 (1,065 Ma; Wiedenbeck et al., 1995) analyzed at the beginning and end of each analytical session and also during the session at regular intervals. All ages were calculated with 2σ errors, and data reduction was conducted using the software programs Iolite 2.5 (Paton et al., 2011) and Isoplot 3.75 (Ludwig, 2012). U–Pb zircon ages with less than 10 % discordance were used in the discussion. I used ^{206}Pb/^{238}U ages for zircons younger than 1000 Ma and ^{207}Pb/^{206}Pb ages for those older than 1000 Ma.

CHAPTER 4

Results

4.1 Petrography

In this study, the representative age unknown meta-carbonate rock, the Hyangsanni Dolomite, was studied in detail. In addition, neighboring metasedimentary sequences were studied as well. The petrography of the studied sample is as follows.

4.1.1 Meta-carbonate rock

Hyangsanni Dolomite

The Hyangsanni Dolomite mainly consists of milky white to gray or light gray to dark gray massive dolomite and in part pinkish crystalline massive limestone. An intercalated thin quartzite is also observed. The samples were collected from Hyangsanni Dolomite near the Chungju Lake in the northeastern part of the Okcheon Metamorphic Belt (HYJ 1, 5, 6, and 7; Figure 2-1, Figure. 3-1).

HYJ 1 outcrop is relatively small scale (Figure 3-1), in fact. Most HYJ 1 samples are very pure and white in color. Their grain size is the most smallest (10-20 μm) among the Hyangsanni Dolomite samples and similar to each other with anhedral grain boundary. A few amphibolite and quartz were examined as an accessory mineral (Figure 4-1). HYJ 5 outcrop is considered that affected by amphibolite and dyke (Figure 3-1). And limestone layer is also quite thin and little altered compared than other samples. I collected several samples such as original one, altered one, dyke and amphibolite and used most pure one for geochemical analysis. They show the different mineral size, smallest one of about 10 μm and largest on of about 40 μm) with anheral grain boundaries. Calcite and relatively large quartzite and small amount of mica were also examined as an accessory mineral (Figure 4-2). HYJ 6 sample is generally homogeneous and fresh with white color (Figure 3-1 and 4-3). Their mineral size depends on the samples, the smallest one is 10-15 μm and the largest one is over 300 μm. A few of calcite showing clear twin is observed. HYJ 7 outcrop (Figure 3-1) displays that dolomite well alternates with quartzite. The protolith of quartzite is considered to be originally chert and then experienced metamorphism. HYJ 7 samples seem to be similar to HYJ 1 samples, but grain size is little larger than those of HYJ 1 samples.

Among the rock samples collected from each outcrop, fine-grained and non-recrystallized specimens were selected, and several slabs were made from them, crushed into chips, or the powder was scraped off the slab surface for analysis. The selected slab samples used for the analysis have a

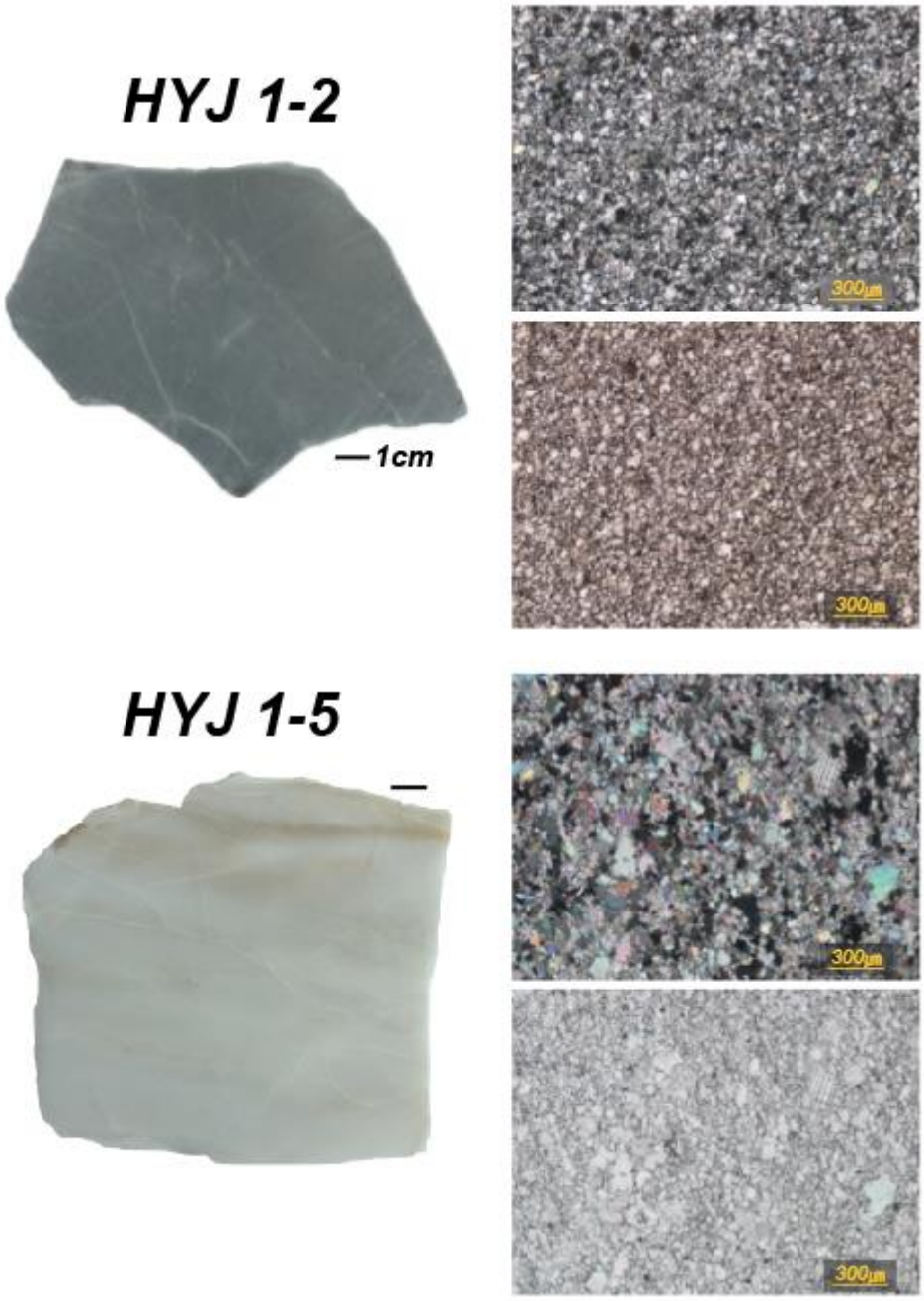

Figure 4-1. Photographs for the slab and photomicrographs for the thin section from the Hyangsanni Dolomite (HYJ 1).

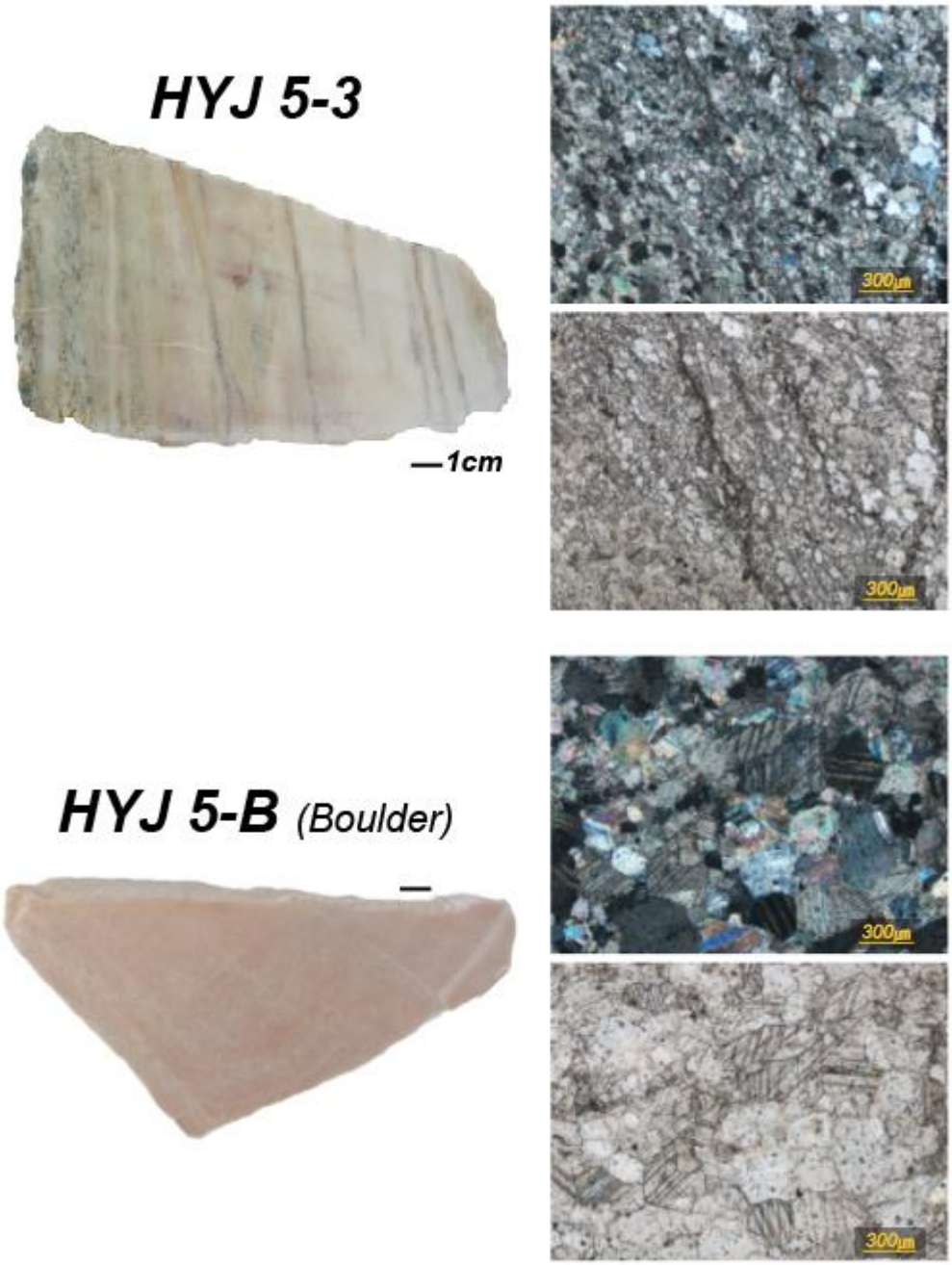

Figure 4-2. Photographs for the slab and photomicrographs for the thin section from the Hyangsanni Dolomite (HYJ 5).

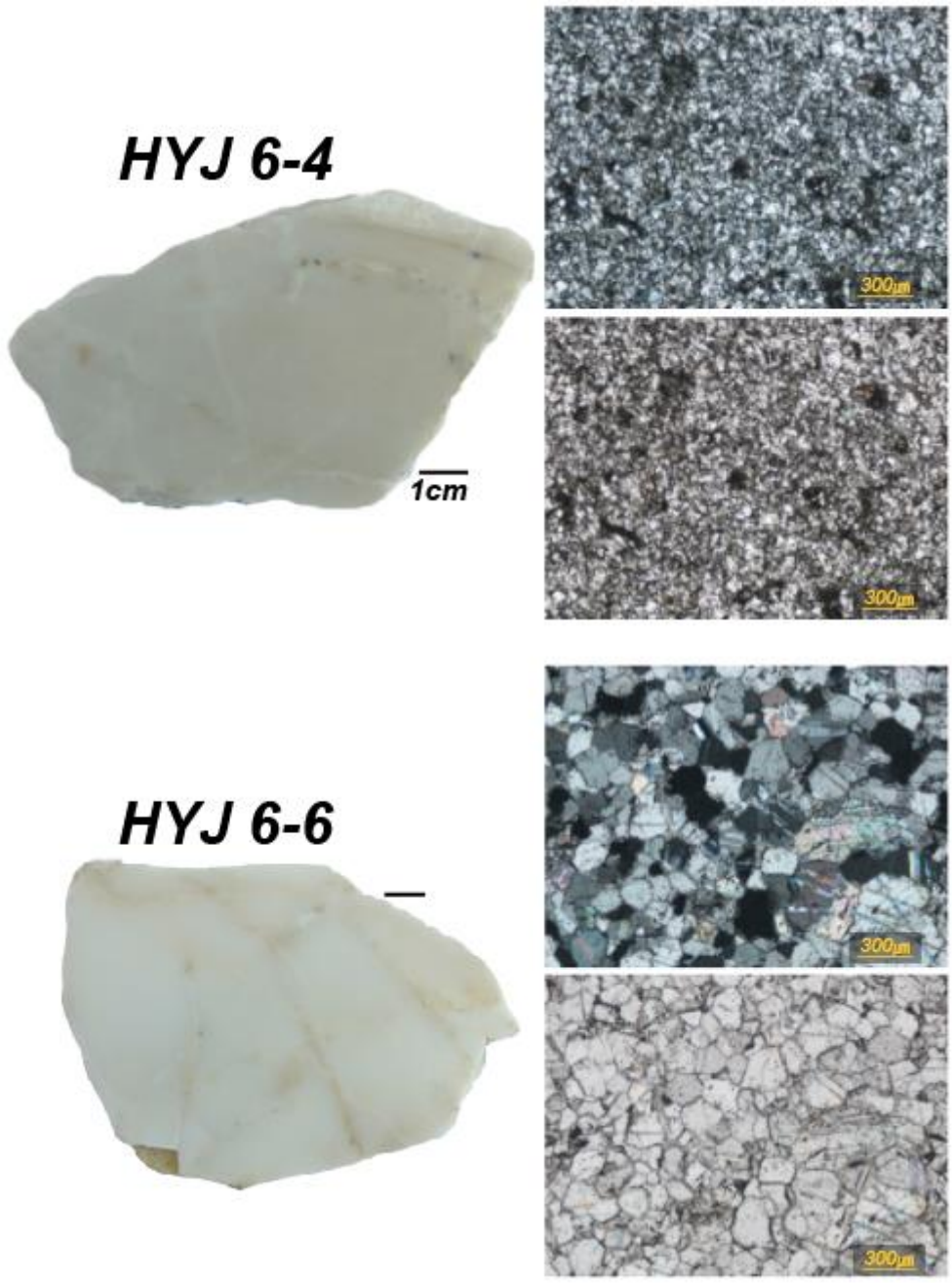

Figure 4-3. Photographs for the slab and photomicrographs for the thin section from the Hyangsanni Dolomite (HYJ 6).

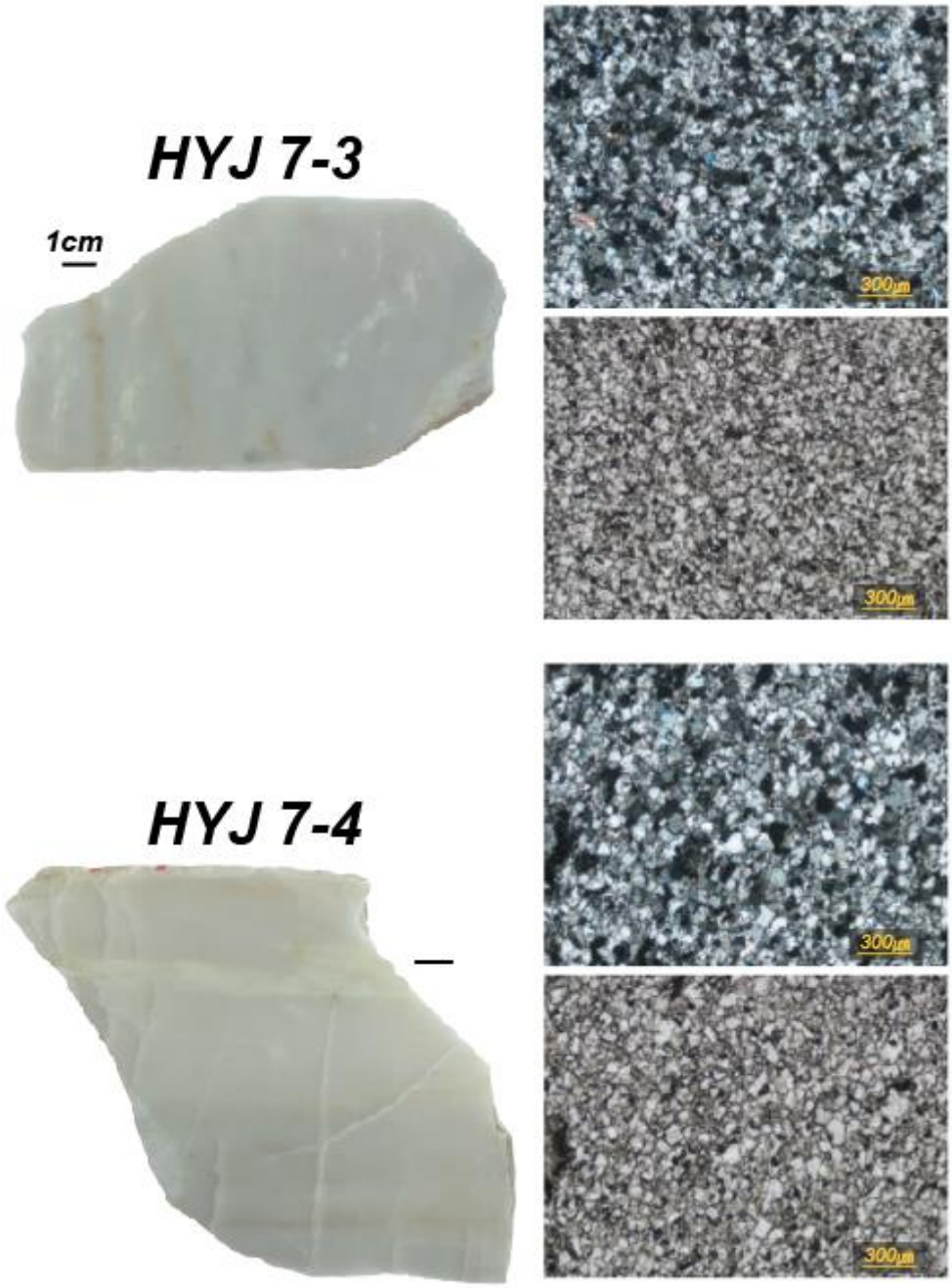

Figure 4-4. Photographs for the slab and photomicrographs for the thin section from the Hyangsanni Dolomite (HYJ 7).

dolomite grain size of about 10–50 μm, and in some cases, a grain size of about 180 μm is also observed.

4.1.2 Metasedimentary rocks

Pebble-bearing phyllitic rocks: Bugnori and Hwanggangni Formations

The pebble bearing phyllitic rocks distributed in the study areas are named the Bugnori Formation and Hwanggangni Formation. These two formations are the main constituents occupying an area of 60% of the Okcheon Metamorphic Belt and have been suggested to glaciogenic sedimentary sequences (Lee et al., 1998; Choi et al., 2012; Ryu and Ahn, 2016; Ha, 2021). However, it is controversial issue since no distinct glacial sedimentological feature has been observed in both these formations.

Lee and park (1965) suggested that Bugnori Formation and Hwanggangni Formation are different layers based on pebble size and characteristics of the matrix. They described that the Hwanggangni Formation has a calcareous matrix and more than 15 cm of the pebbles while the Bugnori Formation has commonly sandy matrix with smaller and uniform size of pebbles.

In order to confirm the features of diamictite from both formations and the similarities between them, I conducted several field observations (Figure 3-2 and 3-3) and made thin sections (Figure 4-5 and 4-6) as well. In fact, it is not easy to fine the glacial features such as dropstones, striated clasts and such as. Nevertheless, there is imperative to consider the particular characteristics of the Okcheon Metamorphic Belt which has undergone greenschist-amphibolite facies metamorphism. Because the glacial features might be overprinted or misidentified with structures caused by deformation and metamorphic reaction.

In addition, when I conducted field observation, the lithology of Bugnori Formation is almost similar in appearance for those of Hwanggangni Formation. The kinds of pebbles of the both formations are limestone, quartzite and quartz grains. Fresh parts of the rock display reaction to HCl indicate that it contains the carbonate mineral as a component mineral. Compared to Bugnori Formation, Hwanggangni Formation is only more phyllitic in its matrix and contains pebbles larger in quantity and size, but is varies in different localities.

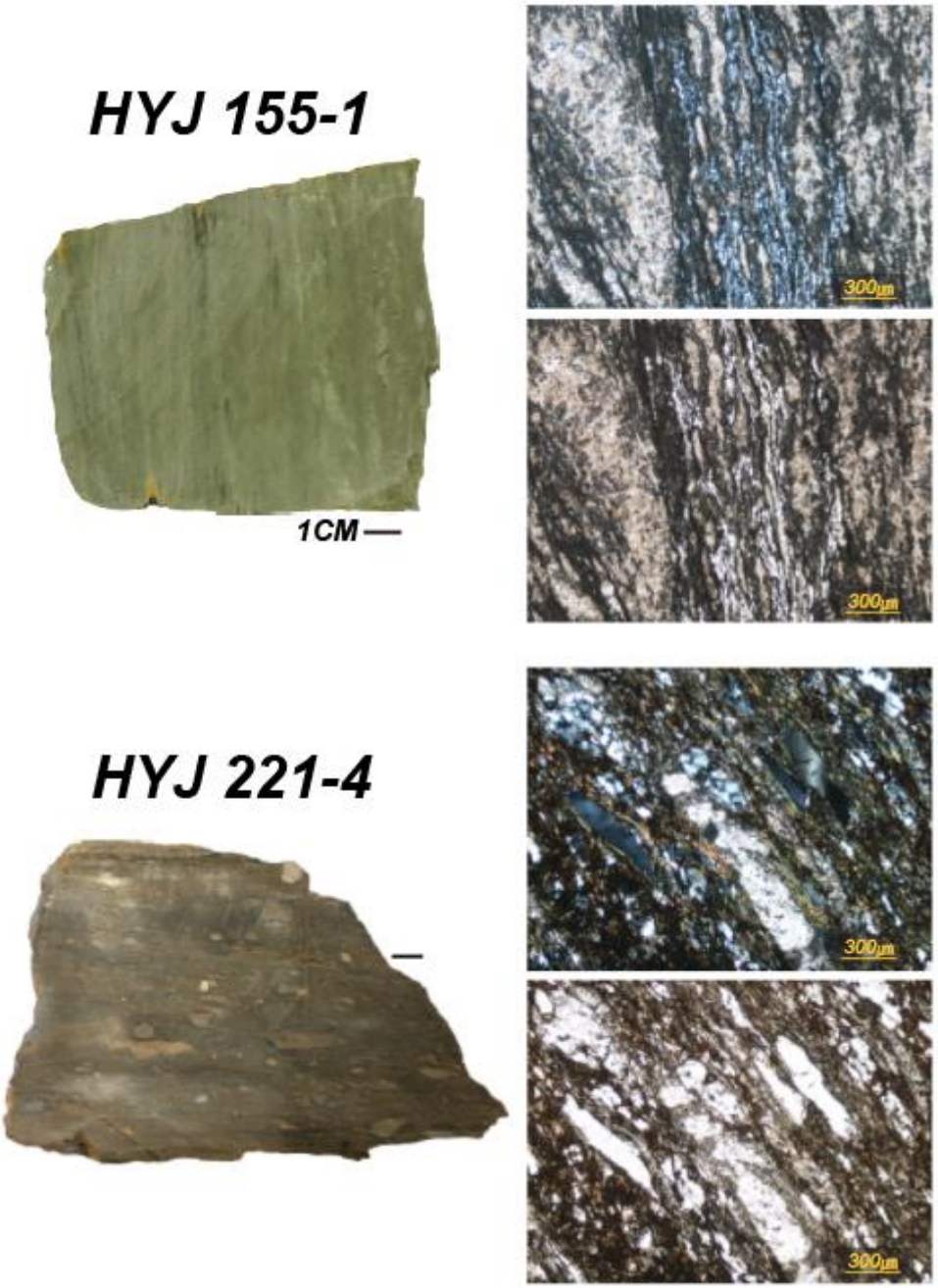

Figure 4-5. Photographs for the slab and photomicrographs for the thin section from Bugnori Formation.

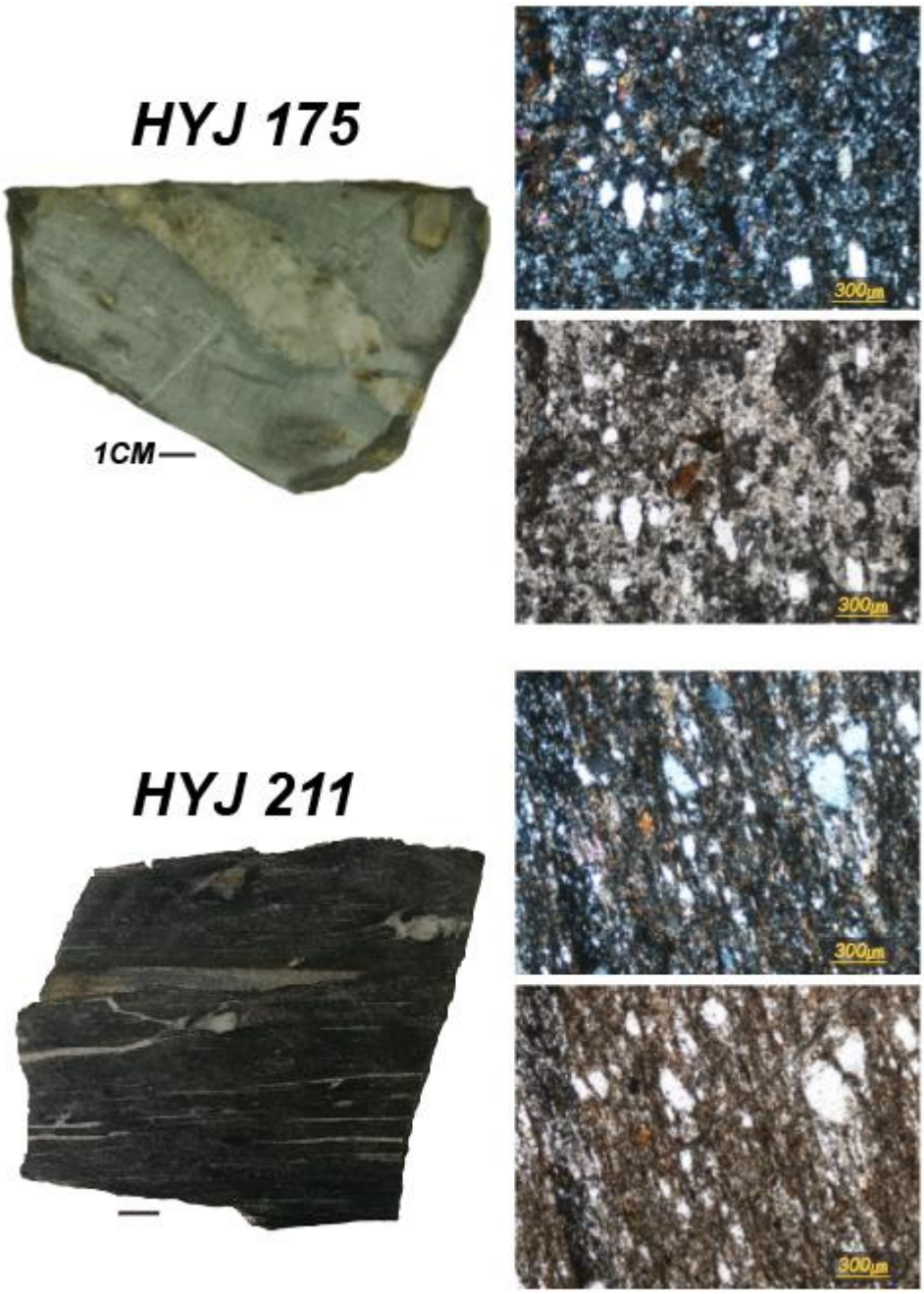

Figure 4-6. Photographs for the slab and photomicrographs for the thin section from Hwanggangni Formation.

Daehyangsan Quartzite

Daehyangsan Quartizite is quite weird layer. Because the Paleozoic layer is sandwiched in between the two Neoproterozoic layers. In order to make sure the geochronology, I conducted field observation and zircon U-Pb analysis. The U-Pb age determination results were detailed in Chapter 5.

Especially, Daehyangsan Quartzite samples were collected from where the previous study area for Daehyangsan Quartzite (HYJ 313 and HYJ 315) and near the Hyangsanni Dolomite sampling locations (HYJ 310 and HYJ 311) (Figure 2-1, 3-4 and 4-7).

The outcrop, where I collected the samples of HYJ 310 and HYJ 311, look like more purer and whitey than the other Daehyangsan quartzite samples for zircon U-Pb analysis. The Daehyangsan Quartzite has been well known to be associated with the Hyangsanni Dolomite. During the field work, it observed as bedded layer between Hyangsanni Dolomite.

Whereas the outcrop (HYJ 313 and HYJ 315) where the previous studies characterized light gray massive quartzite. But it seems to be lithologically heterogeneous and more psammitic. Overall, the leucocratic and melanocratic domains appeared differently. The leucocratic domains might be the predominant silicic components whereas melanocratic domains predominant pelitic components.

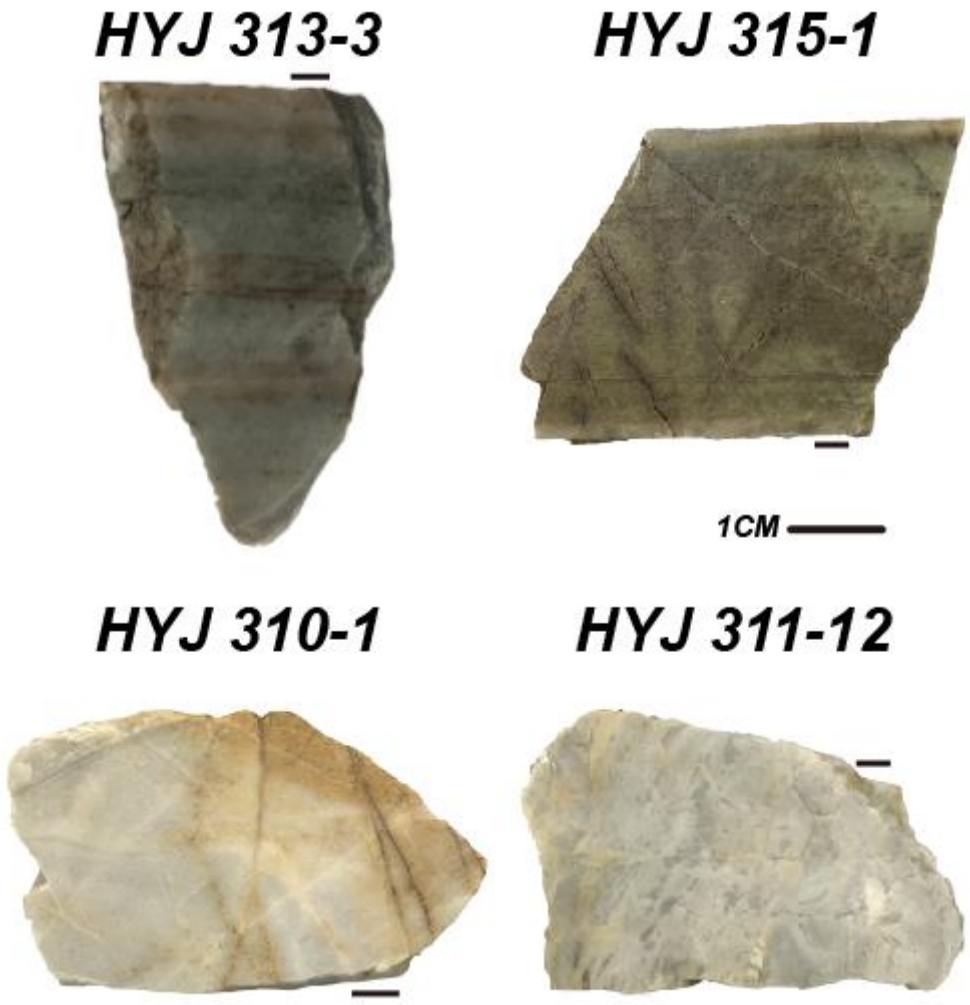

Figure 4-7. Photographs for the slab samples from the Daehyangsan Quartzite.

Pelitic rocks: Seochangni Formation and Changni Formation

The pelitic rocks are classified into the Seochangni, Myeongori, and Munjuri Formations in the Chungju area (containing 1:50000 scale Hwanggangni quadrangle, Lee and Park, 1965). In the Okcheon-Boeun area, 1:50000 scale of the Okcheon (Kim et al., 1978) and Boeun (Kim et al., 1977) quadrangles, pelitic rocks are rather simply classified to Changni and Munjuri Formations. In other words, they have lithological similarity. Amphibolite intrusion is common between the Seochangni and Changni Formation (Figure 2-1 and 2-2).

The Seochangni Formation of the study area mainly consists of phyllite and includes thin quartzite layers and carbonate intercalations. Quartzite samples (HYJ 413 and 417) were collected from two outcrops of the Seochangni Formation for U–Pb age determination (Figure 3-5 and 4-8). According to microscopic observation it contains quartz and sericite. Biotite and chlorite are also observed as minor components. Because the thin sections were made from samples in the Seochangni Formation alteration zone, which is stated on Hwanggangni quadrangle, more altered minerals such as sericite have been observed than Changni Formation.

The Changni Formation is commonly composed of thick monotonous black to dark gray slate and phyllite. Microscopy reveals that it contains quartz and a few sericites and hornblende (Figure 4-9).

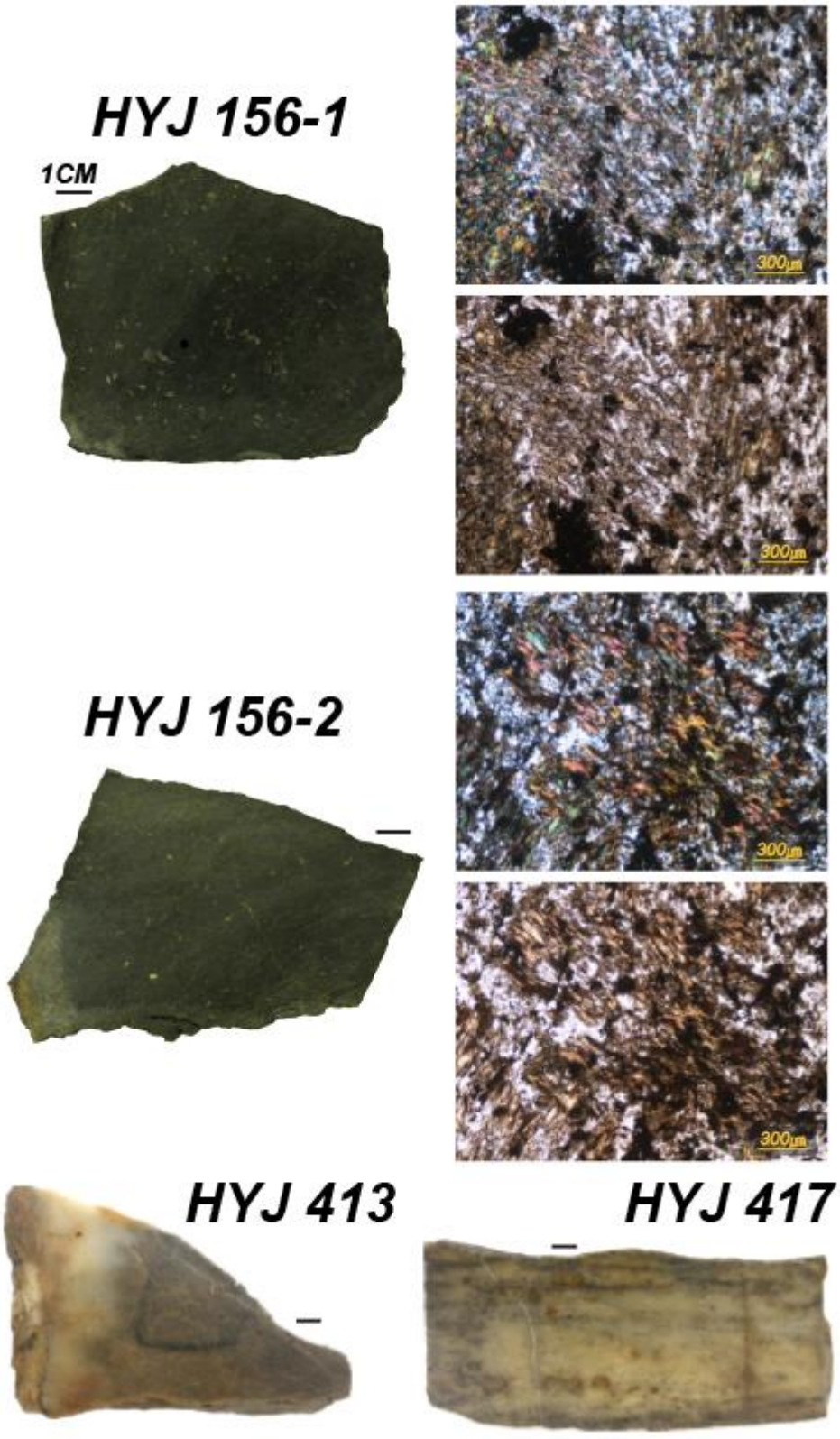

Figure 4-8. Photographs for the slab and photomicrographs for the thin section from Seochangni Formation. HYJ 413 and HYJ 417 samples are quartzite intercalations and used for zircon U-Pb age determination.

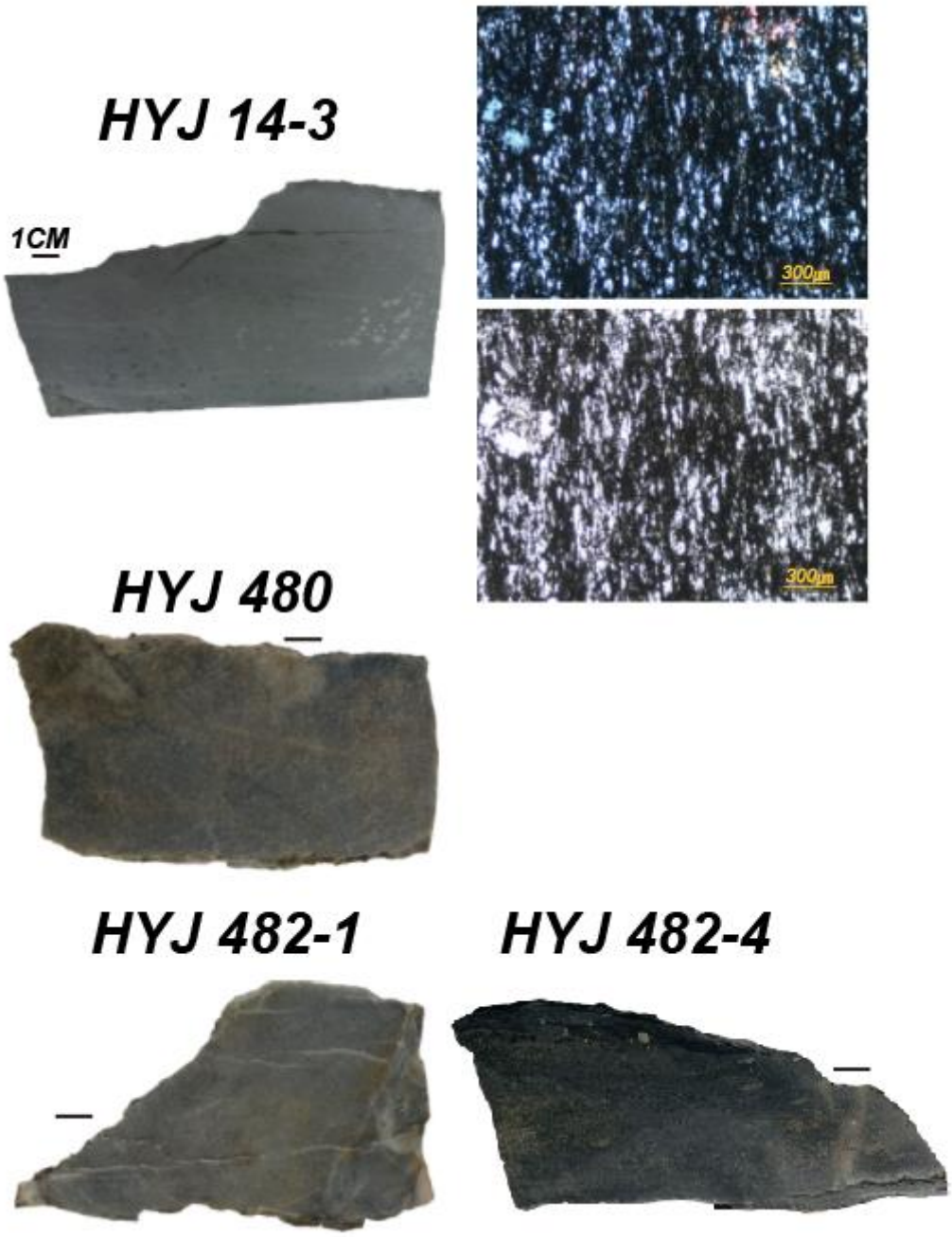

Figure 4-9. Photographs for the slab and photomicrographs for the thin section from Changni Formation. HYJ 480 and HYJ 482 samples are used for zircon U-Pb age determination.

4.2 Meta-carbonate geochemistry

The concentrations of trace and rare earth elements (REE) in the Hyangsanni Dolomite are presented in Table 4-1 and 4-2.

For the REE data, anomalies were calculated as below:

$(Ce/Ce^*)_N = 2*Ce_N/(La_N + Pr_N)$: Bau and Dulski (1996)

$(Eu/Eu^*)_N = 2*Eu_N(Sm_N + Gd_N)$: Kamber and Webb (2001)

$(Pr/Pr^*)_N = 2*Pr_N(Ce_N+Nd_N)$: Bau and Dulski (1996)

To construct REE + Y patterns (Figure 4-10), the concentration of each element was normalized to its concentration in the Post-Archean Australian Shale (PAAS) (Taylor and McLennan, 1985), as indicated by the subscript "$_N$".

The Hyangsanni Dolomite has relatively constant total concentration of REEs, from 3.49 to 33.21. With the exception of two samples, HYJ 1-3 and HYJ 5-2, the others have a value of less than 10.

The REE + Y patterns of the samples of the Hyangsanni Dolomite are generally similar, but there are some differences between the different outcrops. Although it is generally flat, HYJ 7 display a pattern of slightly depleted light rare earth elements, and HYJ 6 display a pattern of relatively low abundance of heavy rare earth elements Yb and Lu. In case of HYJ 5 has a comparatively high total REE content compared to other samples. Unlike other samples, HYJ 1–3 display a light rare earth element enriched pattern. This may reflect the accidental involvement of the crustal material, although no distinct detrital fragments are observed. Eu positive anomalies can be recognized in all samples except HYJ 1, and the extent is most pronounced in HYJ 6. Ce negative anomaly is generally negligible to the extent that it appears only weakly in some analysis values of HYJ 5 and HYJ 7.

Weak but recognizable Y positive anomaly is present in almost all samples and is most distinct in HYJ 7. Yttrium (Y) and Holmium (Ho) have similar ionic radii and charges. Therefore, they can be freely replaced with each other. Ho is removed from seawater at a faster pace than Y due to the different surface complexing behavior (Bau et al., 1999; Filho et al., 2018). The Y/Ho ratio is one of the useful indicators for assessing the purity of marine carbonate (e.g. Nance and Taylor, 1976) because the Y/Ho ratio in seawater changes easily with terrestrial materials (Yang et al., 2019). Modern seawater has substantially higher Y/Ho ratio (from 60 to 90; Lawrence and Kamber, 2006) than the upper continental crust (~26; Kamber et al., 2005). Throughout history of the Earth, the Y/Ho ratio of pure marine precipitates has remained practically the same since the beginning of formation of marine chemical

sediments, suggesting that seawater has always been characterized by positive Y anomalies (e.g., Bau and Dulski, 1996). The Y/Ho ratios for the Hyangsanni Dolomite range from 29 to 43, which is fairly lower than typical Y/Ho ratio of seawater. These values imply that the Hyangsanni Dolomite may have been affected by terrigenous input. Considering that diagenesis such as dolomitization can commonly reduce the Y/Ho ratio, dolomitization as well as terrestrial input is thought be the factors that lead to a decrease in the Y/Ho ratio of the Hyangsanni Dolomite. The Rb concentrations are in the range of 0.03–5.5 ppm except for one sample that is 11.3 ppm, and the Sr concentrations are in the range of 50–331 ppm. The Rb/Sr ratios show a variation between 0.0002 and 0.0967.

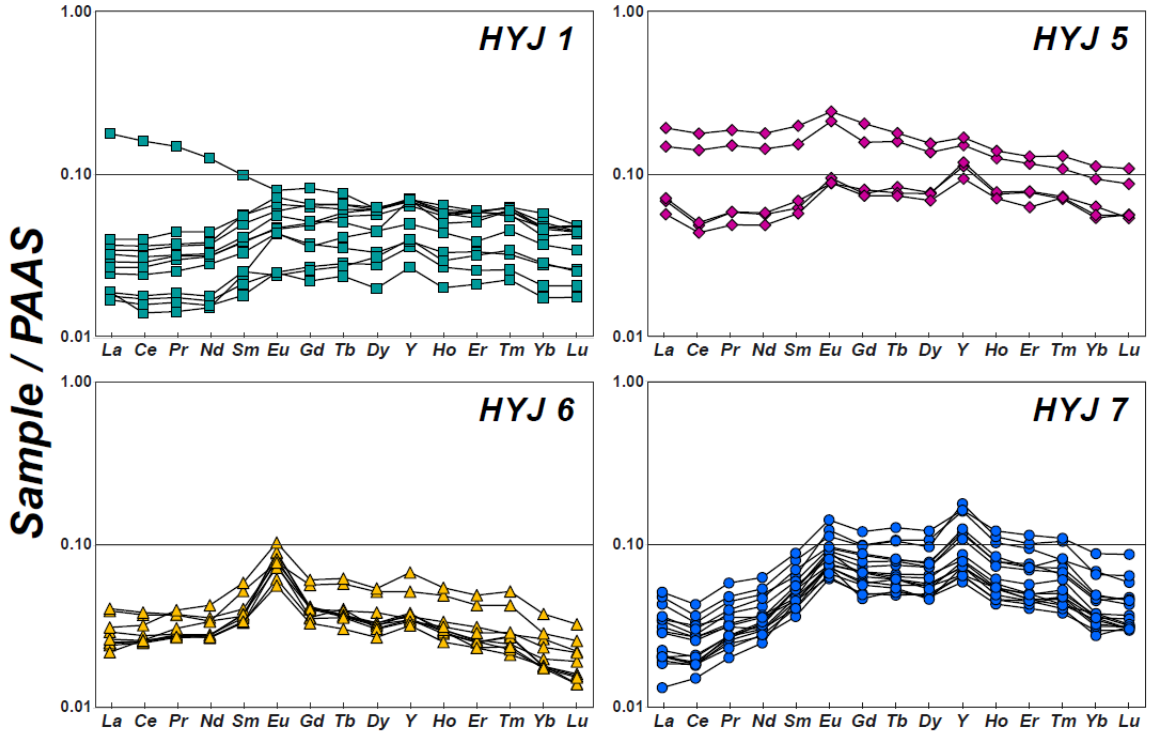

Fig. 4-10. PAAS-normalized REE+ Y patterns of the Hyangsanni Dolomite, PAAS data is from McLennan (1989). See discussions in the text.

Table 4-1. Ce, Pr, and Eu anomalies calculated by using PAAS-normalized values and trace element concentrations of the Hyangsanni Dolomite. $(La/Yb)_N$ values are also calculated by PAAS-normalized values

Sample #	Mn	Rb	Sr	Ba	Zr	Mn/Sr	$(Ce/Ce^*)_N$	$(Pr/Pr^*)_N$	$(Eu/Eu^*)_N$	$(La/Yb)_N$	$^{87}Sr/^{86}Sr$ (measred)	2σ
HYJ 1-1 a	185	0.38	70.4	1.66	5.83	2.6	0.97	0.97	1.28	0.88	0.708367	0.000014
HYJ 1-1 b	310	0.07	60.8	0.74	5.54	5.1	0.95	1.03	1.04	0.47	0.708959	0.000018
HYJ 1-1 c		0.07	65.9	0.62	2.24		0.95	1.05	1.05	0.63		
HYJ 1-2 a	610	2.01	124.2	9.18	3.45	4.9	0.97	1.00	1.13	0.72	0.707836	0.000015
HYJ 1-2 b	169	5.51	131.7	19.70	2.88	1.3	0.98	1.00	1.26	0.88	0.708198	0.000014
HYJ 1-2 c		5.14	122.5	19.09	1.53		0.97	1.02	1.09	0.82		
HYJ 1-3 a	148	4.57	73.6	19.83	6.29	2.0	0.95	1.05	1.23	0.83	0.709371	0.000015
HYJ 1-3 b		3.51	74.6	11.57	2.27		0.98	1.04	0.87	3.75		
HYJ 1-4 a	165	0.04	266.2	5.34	0.71	0.6	0.84	0.98	1.46	0.41	0.715355	0.000015
HYJ 1-5 a	170	0.24	68.0	0.85	1.39	2.5	0.96	1.04	0.93	0.66	0.707395	0.000015
HYJ 1-5 b	635	0.72	64.5	1.81	1.22	9.8	0.95	1.04	1.25	0.97	0.707974	0.000014
HYJ 1-5 c		0.23	61.8	0.88	0.85		0.97	1.03	1.06	0.87		
HYJ 5-1 a	270	0.96	330.7	4.99	2.46	0.8	0.78	1.08	1.23	1.12	0.708472	0.000014
HYJ 5-1 b		0.85	304.2	4.87	0.81		0.76	1.11	1.37	1.27		
HYJ 5-2 a	794	11.31	117.0	55.27	17.40	6.8	6.79	1.05	1.26	1.72	0.709433	0.000014
HYJ 5-2 b		11.22	118.4	53.01	0.94		0.94	1.06	1.37	1.58		
HYJ 5-B a	735	0.49	274.9	7.02	3.30	2.7	0.83	1.06	1.41	1.01	0.708446	0.000015
HYJ 6-1 a	261	0.19	118.0	0.68	3.85	2.2	0.99	1.01	2.01	1.54	0.708538	0.000049
HYJ 6-1 b		0.19	108.8	0.66	1.93		0.97	1.04	2.43	1.97		
HYJ 6-2 a	292	0.06	110.6	0.38	1.32	2.6	0.96	1.04	1.95	1.40	0.710996	0.000014
HYJ 6-2 b		0.05	99.7	0.35	0.81		0.98	1.04	2.14	1.35		
HYJ 6-3 a	284	0.05	115.1	0.37	1.13	2.5	0.97	1.03	2.21	1.43		

Table 4-1. *(Continued)*

Sample #	Mn	Rb	Sr	Ba	Zr	Mn/Sr	$(Ce/Ce^*)_N$	$(Pr/Pr^*)_N$	$(Eu/Eu^*)_N$	$(La/Yb)_N$	$^{87}Sr/^{86}Sr$ (measred)	2σ
HYJ 6-3 b		0.05	107.9	0.33	0.69		0.96	1.05	2.45	1.39		
HYJ 6-4 a	304	0.12	127.7	0.60	2.99	2.4	0.96	1.04	1.80	1.24	0.710613	0.000014
HYJ 6-5 a	273	0.11	79.8	0.55	3.13	3.4	0.98	1.03	1.44	0.77		
HYJ 6-6 a	361	0.04	110.9	0.35	1.51	3.3	0.91	1.06	1.73	0.83	0.711495	0.000014
HYJ 6-7 a	246	0.03	93.2	0.37	0.77	2.6	0.96	1.03	1.71	1.50	0.710669	0.000015
HYJ 7-2 a	345	0.81	100.5	3.75	4.62	3.4	0.91	1.01	1.49	0.36		
HYJ 7-2 b	246	1.76	84.9	8.47	9.69	2.9	0.88	1.07	1.40	0.54		
HYJ 7-3 a	237	0.07	89.2	0.77	4.50	2.7	0.90	1.05	1.35	0.98	0.708371	0.000014
HYJ 7-3 b		0.06	81.2	0.85	1.67		0.89	1.09	1.64	0.99		
HYJ 7-4 a	194	0.05	69.5	0.37	0.97	2.8	0.81	1.02	1.43	0.42		
HYJ 7-4 b	159	0.11	61.2	0.42	1.18	2.6	0.80	1.09	1.48	0.40		
HYJ 7-5 a	211	1.10		3.10	1.09		0.77	1.06	1.27	0.73	0.708912	0.000014
HYJ 7-5 b		1.13	69.4	3.73	0.57		0.76	1.08	1.57	0.63		
HYJ 7-6 a	273	4.08	57.0	12.32	7.63	4.8	0.79	1.10	1.40	0.58	0.709528	0.000014
HYJ 7-7 a	218	0.91	53.5	2.65	1.75	4.1	0.80	1.03	1.31	0.74	0.708791	0.000015
HYJ 7-7 b		0.85	51.0	2.61	1.18		0.78	1.09	1.43	0.75		
HYJ 7-8 a	220	2.43	55.5	6.79	2.32	4.0	0.82	1.02	1.33	0.60	0.708820	0.000015
HYJ 7-8 b		2.42	50.4	6.83	1.48		0.80	1.08	1.46	0.57		
HYJ 7-9 a	217	0.50	57.1	2.71	1.82	3.8	0.84	1.00	1.47	0.63	0.708273	0.000015
HYJ 7-9 b		0.45	50.7	2.21	1.04		0.81	1.07	1.53	0.76		
HYJ 7-10 a	192	0.46	65.8	1.88	2.38	2.9	0.85	1.03	1.41	0.81	0.708643	0.000014
HYJ 7-10 b		0.38	59.5	1.71	1.64		0.85	1.02	1.74	0.99		

Table 4-2. Rare earth elements plus Yttrium concentrations of the Hyangsanni Dolomite. The data are presented in parts per million (ppm).

Sample #	Y	*La*	*Ce*	*Pr*	*Nd*	*Sm*	*Eu*	*Gd*	*Tb*	*Dy*	*Ho*	*Er*	*Tm*	*Yb*	*Lu*	∑REE	Y/Ho
HYJ 1-1 a	1.06	*0.95*	*1.94*	*0.23*	*0.96*	*0.18*	*0.047*	*0.18*	*0.03*	*0.16*	*0.033*	*0.10*	*0.013*	*0.08*	*0.011*	4.91	32
HYJ 1-1 b	1.75	*1.04*	*2.16*	*0.27*	*1.07*	*0.22*	*0.050*	*0.23*	*0.04*	*0.27*	*0.055*	*0.17*	*0.026*	*0.16*	*0.021*	5.77	32
HYJ 1-1 c	1.93	*1.12*	*2.31*	*0.28*	*1.08*	*0.21*	*0.051*	*0.24*	*0.05*	*0.29*	*0.058*	*0.17*	*0.026*	*0.13*	*0.021*	6.04	33
HYJ 1-2 a	1.35	*1.25*	*2.50*	*0.28*	*1.11*	*0.23*	*0.061*	*0.24*	*0.04*	*0.21*	*0.044*	*0.11*	*0.019*	*0.11*	*0.015*	6.23	31
HYJ 1-2 b	1.91	*1.41*	*2.92*	*0.33*	*1.31*	*0.31*	*0.071*	*0.30*	*0.05*	*0.28*	*0.064*	*0.17*	*0.025*	*0.14*	*0.020*	7.41	30
HYJ 1-2 c	1.86	*1.32*	*2.74*	*0.32*	*1.27*	*0.28*	*0.065*	*0.30*	*0.05*	*0.29*	*0.058*	*0.17*	*0.023*	*0.12*	*0.019*	7.02	32
HYJ 1-3 a	1.86	*1.54*	*3.21*	*0.40*	*1.52*	*0.31*	*0.079*	*0.31*	*0.05*	*0.30*	*0.058*	*0.15*	*0.025*	*0.14*	*0.019*	8.10	32
HYJ 1-3 b	1.92	*6.84*	*12.85*	*1.32*	*4.28*	*0.55*	*0.087*	*0.39*	*0.06*	*0.29*	*0.060*	*0.17*	*0.023*	*0.13*	*0.021*	27.07	32
HYJ 1-4 a	1.90	*0.74*	*1.14*	*0.13*	*0.52*	*0.14*	*0.048*	*0.17*	*0.03*	*0.21*	*0.050*	*0.15*	*0.025*	*0.13*	*0.019*	3.49	38
HYJ 1-5 a	1.09	*0.73*	*1.44*	*0.17*	*0.61*	*0.14*	*0.026*	*0.12*	*0.02*	*0.15*	*0.029*	*0.09*	*0.014*	*0.08*	*0.011*	3.63	37
HYJ 1-5 b	0.73	*0.66*	*1.27*	*0.15*	*0.54*	*0.10*	*0.027*	*0.10*	*0.02*	*0.09*	*0.020*	*0.06*	*0.009*	*0.05*	*0.008*	3.11	36
HYJ 1-5 c	0.98	*0.69*	*1.38*	*0.16*	*0.57*	*0.12*	*0.027*	*0.13*	*0.02*	*0.13*	*0.027*	*0.07*	*0.011*	*0.06*	*0.009*	3.41	36
HYJ 5-1 a	3.19	*2.72*	*4.02*	*0.52*	*1.96*	*0.38*	*0.095*	*0.37*	*0.06*	*0.36*	*0.077*	*0.22*	*0.030*	*0.18*	*0.023*	11.01	41
HYJ 5-1 b	3.02	*2.61*	*3.86*	*0.52*	*1.92*	*0.34*	*0.102*	*0.35*	*0.06*	*0.36*	*0.075*	*0.22*	*0.029*	*0.15*	*0.024*	10.64	40
HYJ 5-2 a	4.52	*7.32*	*14.12*	*1.65*	*6.04*	*1.10*	*0.261*	*0.95*	*0.14*	*0.72*	*0.138*	*0.37*	*0.052*	*0.31*	*0.047*	33.21	33
HYJ 5-2 b	4.06	*5.64*	*11.16*	*1.33*	*4.84*	*0.85*	*0.228*	*0.73*	*0.12*	*0.64*	*0.124*	*0.33*	*0.044*	*0.26*	*0.038*	26.33	33
HYJ 5-B a	2.53	*2.17*	*3.49*	*0.43*	*1.65*	*0.32*	*0.095*	*0.34*	*0.06*	*0.32*	*0.070*	*0.18*	*0.029*	*0.16*	*0.024*	9.33	36
HYJ 6-1 a	0.99	*1.56*	*3.08*	*0.33*	*1.22*	*0.23*	*0.086*	*0.20*	*0.03*	*0.16*	*0.034*	*0.09*	*0.012*	*0.08*	*0.010*	7.11	29
HYJ 6-1 b	0.94	*1.51*	*2.98*	*0.33*	*1.16*	*0.20*	*0.097*	*0.20*	*0.03*	*0.15*	*0.030*	*0.08*	*0.010*	*0.06*	*0.008*	6.84	32
HYJ 6-2 a	1.04	*0.96*	*2.04*	*0.25*	*0.95*	*0.21*	*0.079*	*0.19*	*0.03*	*0.16*	*0.029*	*0.07*	*0.011*	*0.05*	*0.007*	5.04	36
HYJ 6-2 b	0.95	*0.93*	*2.00*	*0.24*	*0.93*	*0.19*	*0.083*	*0.17*	*0.03*	*0.14*	*0.028*	*0.07*	*0.011*	*0.05*	*0.007*	4.89	33
HYJ 6-3 a	1.02	*0.96*	*2.03*	*0.24*	*0.95*	*0.21*	*0.089*	*0.19*	*0.03*	*0.15*	*0.030*	*0.07*	*0.009*	*0.05*	*0.006*	5.03	34

Table 4-2. *(Continued)*

Sample #	Y	*La*	*Ce*	*Pr*	*Nd*	*Sm*	*Eu*	*Gd*	*Tb*	*Dy*	*Ho*	*Er*	*Tm*	*Yb*	*Lu*	∑REE	Y/Ho
HYJ 6-3 b	0.95	*0.97*	*2.05*	*0.25*	*0.96*	*0.20*	*0.098*	*0.19*	*0.03*	*0.18*	*0.029*	*0.07*	*0.009*	*0.05*	*0.006*	5.09	32
HYJ 6-4 a	0.92	*1.12*	*2.22*	*0.25*	*0.92*	*0.19*	*0.067*	*0.17*	*0.03*	*0.14*	*0.031*	*0.08*	*0.012*	*0.07*	*0.010*	5.31	29
HYJ 6-5 a	1.40	*0.85*	*2.08*	*0.27*	*1.15*	*0.29*	*0.085*	*0.27*	*0.04*	*0.24*	*0.049*	*0.12*	*0.017*	*0.08*	*0.011*	5.56	29
HYJ 6-6 a	1.84	*1.20*	*2.57*	*0.35*	*1.45*	*0.33*	*0.112*	*0.29*	*0.05*	*0.25*	*0.054*	*0.14*	*0.021*	*0.11*	*0.014*	6.95	34
HYJ 6-7 a	0.87	*1.01*	*2.07*	*0.24*	*0.93*	*0.19*	*0.061*	*0.16*	*0.02*	*0.13*	*0.025*	*0.07*	*0.010*	*0.05*	*0.007*	4.97	34
HYJ 7-2 a	1.97	*0.50*	*1.20*	*0.18*	*0.84*	*0.25*	*0.078*	*0.28*	*0.04*	*0.26*	*0.053*	*0.14*	*0.020*	*0.10*	*0.014*	3.96	37
HYJ 7-2 b	1.75	*0.77*	*1.66*	*0.24*	*1.02*	*0.26*	*0.078*	*0.27*	*0.05*	*0.26*	*0.053*	*0.13*	*0.017*	*0.11*	*0.016*	4.93	33
HYJ 7-3 a	1.73	*1.32*	*2.52*	*0.31*	*1.21*	*0.25*	*0.068*	*0.23*	*0.04*	*0.23*	*0.045*	*0.12*	*0.019*	*0.10*	*0.015*	6.48	38
HYJ 7-3 b	1.58	*1.12*	*2.15*	*0.27*	*1.02*	*0.23*	*0.079*	*0.22*	*0.04*	*0.22*	*0.043*	*0.11*	*0.015*	*0.08*	*0.013*	5.61	37
HYJ 7-4 a	3.11	*0.78*	*1.51*	*0.23*	*1.11*	*0.30*	*0.093*	*0.34*	*0.06*	*0.34*	*0.078*	*0.21*	*0.029*	*0.14*	*0.020*	5.22	40
HYJ 7-4 b	2.90	*0.71*	*1.46*	*0.24*	*1.08*	*0.29*	*0.098*	*0.36*	*0.06*	*0.34*	*0.073*	*0.20*	*0.027*	*0.13*	*0.018*	5.09	40
HYJ 7-5 a	4.78	*1.81*	*2.90*	*0.42*	*1.81*	*0.44*	*0.121*	*0.45*	*0.08*	*0.45*	*0.110*	*0.29*	*0.042*	*0.18*	*0.028*	9.14	43
HYJ 7-5 b	4.30	*1.64*	*2.63*	*0.39*	*1.67*	*0.35*	*0.132*	*0.46*	*0.08*	*0.50*	*0.101*	*0.27*	*0.032*	*0.19*	*0.025*	8.47	43
HYJ 7-6 a	4.37	*1.94*	*3.40*	*0.51*	*2.12*	*0.49*	*0.152*	*0.56*	*0.10*	*0.56*	*0.120*	*0.32*	*0.044*	*0.25*	*0.037*	10.60	37
HYJ 7-7 a	3.35	*1.38*	*2.40*	*0.35*	*1.58*	*0.39*	*0.104*	*0.41*	*0.06*	*0.35*	*0.083*	*0.20*	*0.033*	*0.14*	*0.020*	7.50	40
HYJ 7-7 b	3.19	*1.29*	*2.22*	*0.33*	*1.41*	*0.33*	*0.102*	*0.40*	*0.06*	*0.36*	*0.077*	*0.22*	*0.026*	*0.13*	*0.020*	6.97	41
HYJ 7-8 a	2.33	*0.85*	*1.62*	*0.24*	*1.13*	*0.29*	*0.080*	*0.31*	*0.05*	*0.29*	*0.061*	*0.16*	*0.025*	*0.11*	*0.014*	5.24	38
HYJ 7-8 b	2.16	*0.74*	*1.44*	*0.23*	*1.00*	*0.25*	*0.081*	*0.32*	*0.05*	*0.30*	*0.057*	*0.14*	*0.017*	*0.10*	*0.013*	4.73	38
HYJ 7-9 a	1.97	*0.78*	*1.46*	*0.20*	*0.94*	*0.22*	*0.071*	*0.26*	*0.04*	*0.21*	*0.048*	*0.13*	*0.019*	*0.09*	*0.013*	4.50	41
HYJ 7-9 b	1.74	*0.80*	*1.47*	*0.22*	*0.92*	*0.20*	*0.066*	*0.23*	*0.04*	*0.23*	*0.045*	*0.13*	*0.016*	*0.08*	*0.013*	4.45	38
HYJ 7-10 a	2.12	*1.09*	*2.04*	*0.28*	*1.20*	*0.31*	*0.088*	*0.31*	*0.05*	*0.25*	*0.054*	*0.14*	*0.021*	*0.10*	*0.013*	5.95	39
HYJ 7-10 b	1.95	*1.19*	*2.14*	*0.29*	*1.25*	*0.26*	*0.097*	*0.29*	*0.05*	*0.27*	*0.053*	*0.13*	*0.019*	*0.09*	*0.013*	6.13	37

4.3 C and Sr isotope chemostratigraphy

4.3.1 Carbon isotope composition

The results of the stable isotope analysis were reported in conventional delta (δ) notation using the V-PDB standard for carbon, and the V-PDB and V-SMOW standards for oxygen and are presented in Table 4-3. The carbon and oxygen isotope composition for the Hyangsanni Dolomite was analyzed from a total of 31 spots in polished slabs and 5 whole rock powders from 4 outcrops.

The Hyangsanni Dolomite has $\delta^{13}C$ values between +2.9‰ and + 6.2‰, and $\delta^{18}O$ values between +11.3‰ and +24.5‰ (Table 4-3 and Figure 4-11). Except for two spot analysis showing low values of 2.9‰ (HYJ 5–3-2) and 3.1‰ (HYJ 5–3-1), the $\delta^{13}C$ values are concentrated in the range of 3.7–6.2‰. In this study, in the Hyangsanni Dolomite, any systematic variation of the composition of carbon and oxygen isotope according to the stratigraphic position was not recognized.

The maximum and minimum values of the carbon isotope results of the slab spots analyzed in each outcrop are in the range of 1.0–1.2‰, except for HYJ 5, which is 2.2‰. When two or more spots were analyzed in one slab, the difference in carbon isotope values was usually less than 0.7‰. In slab HYJ 5–3, which includes the lowest value, this difference reaches 1.3‰. In the case of outcrops other than HYJ 5, the $\delta^{13}C$ values are similar to each other and only a relatively narrow range of variation is interpreted as a result of retaining the original values better. On the other hand, the fact that HYJ 5 has relatively low $\delta^{13}C$ values with greater heterogeneity (Figure 4-11) seems to be the result of alteration rather than the original value. Factors that may have contributed to a change in carbon isotope values include dolomitization, regional metamorphism, contact metamorphism, and low-temperature chemical alteration.

The oxygen isotope values also show a similar trend as for the carbon isotope (Figure 4-11). When two or more spots were analyzed in one slab, the difference in oxygen isotope values was usually less than 0.8‰. However, the two slabs of outcrop HYJ 5, HYJ 5–1 and HYJ 5–3, show significantly larger differences of 3.1‰ and 3.8‰, respectively. This suggests that HYJ 5 has undergone significant post-sedimentary alteration of the oxygen isotope value. Outcrop HYJ 5 has an average of 13.1‰ of spot analyzes and 13.6‰ with chip analysis. In contrast, other outcrops show much higher and uniform values, with both spot and chip analysis combined, with the highest 24.5‰ and the lowest 21.1‰. What

factors caused outcrop HYJ 5 to have a low oxygen isotope value? Since meteoric water has a much lower $\delta^{18}O$ value than the seawater that was in equilibrium when the carbonate rocks were formed, it can act as a factor that causes a change toward a lower value during a low-temperature alteration process or hydrothermal activity associated with metamorphism. Stocks of Jurassic granite of various sizes are intruded throughout the Chungju area, and one of them may have influenced the more severe alteration of carbon and oxygen isotope values in HYJ 5.

Park et al. (1995) and Shin and Lee (2005) analyzed the carbon and oxygen isotope composition of the Hyangsanni Dolomite to determine the genesis of talc deposits that occur therein. Among these analysis values, those with low $\delta^{13}C$ values tend to also have low $\delta^{18}O$ values. The most pronounced trend of change in the values they reported is the change with depth within the talc mine. There is no noticeable change in the $\delta^{13}C$ values, but the average of $\delta^{18}O$ values gradually decreases with depth from 20.1‰ at the +170 m level, 18.2‰ at the −212 m level, and 16.1‰ at the −538 m level. These isotopic variations suggest that magmatic water with low $\delta^{18}O$ from deeper zone of the ore body was involved to the decarbonation reaction of dolomite for the talc mineralization (Shin and Lee, 2005). However, this decarbonation reaction of dolomite during the talc mineralization appears to have little effect on the $\delta^{13}C$ values.

4.3.2 Strontium isotope composition

The Sr isotope composition was analyzed in 23 samples for 4 outcrops of the Hyangsanni Dolomite, and as a result, the present day $^{87}Sr/^{86}Sr$ ratios ranged from 0.70740–0.71536. A similarly wide range of $^{87}Sr/^{86}Sr$ values (0.70828–0.71088) have been reported in previous studies for the Hyangsanni Dolomite (Park and Cheong, 1998). In the case of sample HYJ 1–4, which shows the highest $^{87}Sr/^{86}Sr$ ratio of about 0.7154, the carbon and oxygen isotope values are lower than most of the other samples (Figure 4-12). It is believed that the events that influenced the carbon and oxygen isotope composition of this sample also changed the strontium isotope composition. However, sample HYJ 5–1, whose oxygen isotope value was deviated toward a significantly lower value than other samples, showed a present day $^{87}Sr/^{86}Sr$ ratio of about 0.70847, which is not significantly different from other samples (Figure 4-12b). It is believed that this event, which greatly influenced the oxygen isotope value, did not significantly affect the strontium isotope composition. Looking at the correlation diagram between Y/Ho ratios and strontium isotopic composition, no distinct trend is recognized (Figure 4-13).

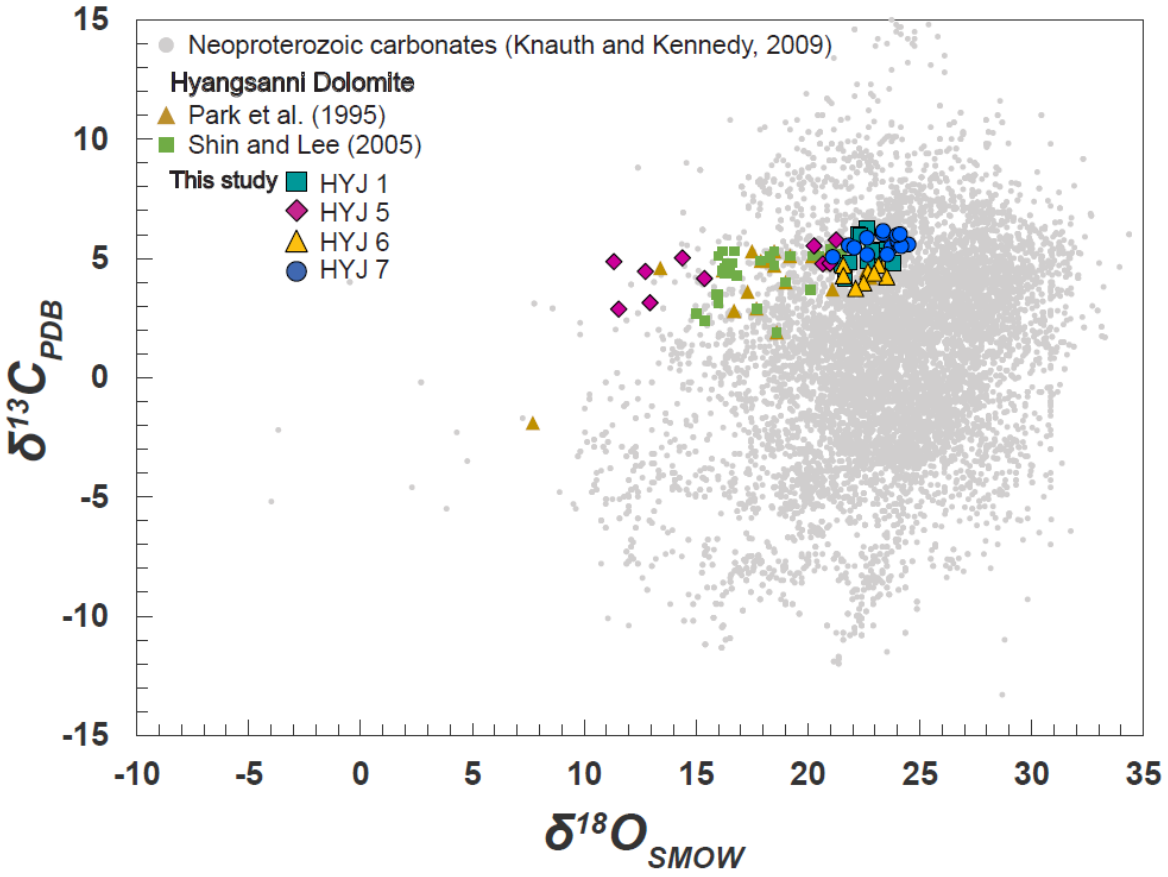

Figure. 4-11. Carbon vs oxygen cross-plot for the Hyangsanni Dolomite. Carbon and oxygen isotopic compositions analyzed from the talc mine in the Hyangsanni Dolomite (Park et al., 1995; Shin and Lee, 2005) and compiled data for the Neoproterozoic carbonate rocks (Knauth and Kennedy, 2009) are shown together. HYJ 5 shows a carbon and oxygen isotope composition that deviates from the values of other outcrops. HYJ 5 exhibits a carbon and oxygen isotope composition that deviates from the values of other outcrops, possibly due to some alteration events after sedimentation. The compiled data of carbon and oxygen isotope composition for Neoproterozoic carbonate rocks are from Knauth and Kennedy (2009).

Table 4-3. Carbon and oxygen isotopic composition of the Hyangsanni Dolomite.

Sample #	$\delta^{13}C_{PDB}$	$\delta^{18}O_{SMOW}$	$\delta^{18}O_{PDB}$
HYJ 1-1	5.37	23.31	-8.56
	4.80	23.81	-8.07
HYJ 1-2	6.03	22.44	-9.40
	6.27	22.63	-9.22
HYJ 1-3	6.04	22.22	-9.61
	5.99	22.34	-9.50
HYJ 1-4	4.74	21.51	-10.30
	4.84	21.88	-9.94
	4.17	21.67	-10.15
HYJ 1-5	5.10	22.96	-8.89
	5.31	22.87	-8.99
	4.90	22.65	-9.20
HYJ 5-1	4.86	11.33	-20.18
	4.45	12.74	-18.81
	5.02	14.39	-17.21
HYJ 5-2	5.77	21.26	-10.54
	5.53	20.28	-11.49
HYJ 5-3	3.14	12.94	-18.61
	2.87	11.55	-19.97
	4.16	15.38	-16.25
HYJ 5-B	4.77	20.66	-11.12
	4.79	20.99	-10.76
HYJ 6-1	4.71	21.59	-10.22
HYJ 6-2	4.27	21.59	-10.23
HYJ 6-5	4.71	23.16	-8.72
	4.23	23.52	-8.35
	4.46	22.68	-9.16
HYJ 6-6	3.97	22.49	-9.35
	3.75	22.14	-9.70
	4.39	22.97	-8.89
HYJ 7-2	5.55	21.82	-10.00
	5.06	21.11	-10.69
HYJ 7-3	5.45	22.07	-9.76
	5.16	22.64	-9.21

Table 4-3. *(Continued)*

Sample #	$\delta^{13}C_{PDB}$	$\delta^{18}O_{SMOW}$	$\delta^{18}O_{PDB}$
HYJ 7-4	6.03	23.35	-8.52
HYJ 7-5	6.16	23.35	-8.51
	5.87	22.63	-9.21
HYJ 7-6	5.47	23.72	-8.16
	5.17	23.54	-8.33
HYJ 7-7	5.59	24.49	-7.42
HYJ 7-8	5.66	24.02	-7.86
HYJ 7-9	5.75	24.01	-7.87
	5.52	24.17	-7.47
HYJ 7-10	5.97	23.97	-7.91
	6.02	24.11	-7.78

The group with the lower $^{87}Sr/^{86}Sr$ ratios has somewhat high Y/Ho ratios. Since these Y/Ho values are also somewhat lower than typical seawater values, the possibility that such strontium isotopic composition is also a result of some influence by terrestrial material cannot be completely excluded. The Sr isotope compositions of the Hyangsanni Dolomite in previous studies are within the range of values obtained in this study (Park and Cheong, 1998; Shin and Lee, 2005). However, the lowest value obtained before (0.70828) is somewhat higher than the lowest value in this study (0.70740). In general, mixing of terrestrial materials or alteration by terrestrial strontium after sedimentation tends to increase the $^{87}Sr/^{86}Sr$ ratios of carbonate rocks from the original seawater value (e.g., Jacobsen and Kaufman, 1999). Because of this, we consider that the lowest Sr isotopic composition obtained in this study is closer to the seawater composition at the time of the deposition of the Hyangsanni Dolomite. Therefore, the lowest value of $^{87}Sr/^{86}Sr$ ratio of 0.70740 from the measured values so far, is the value that most closely represents the seawater composition at the time of sedimentation of the Hyangsanni Dolomite.

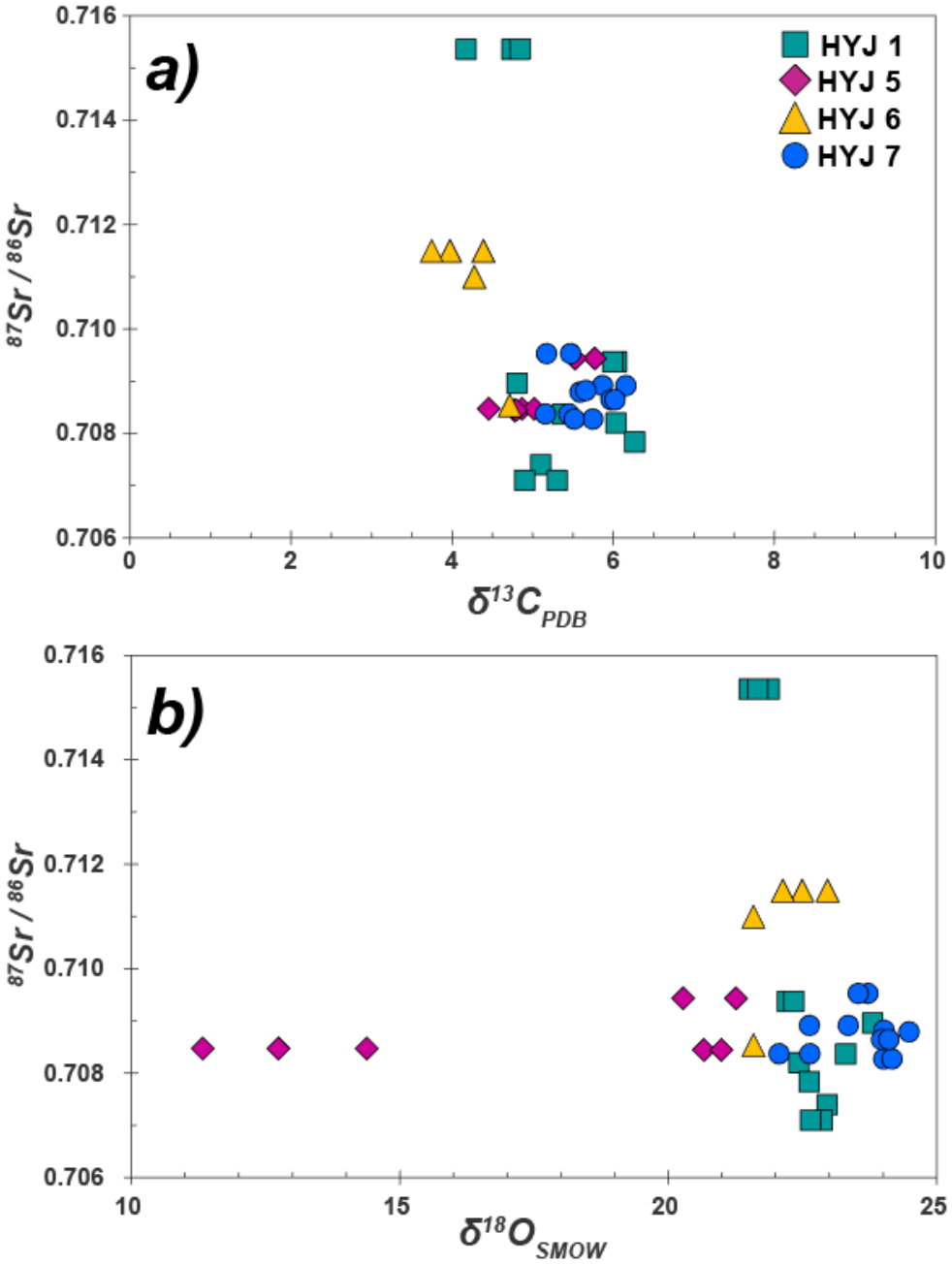

Figure 4-12. a) Carbon vs strontium b) Oxygen vs strontium isotopic compositions of the Hyangsanni Dolomite.

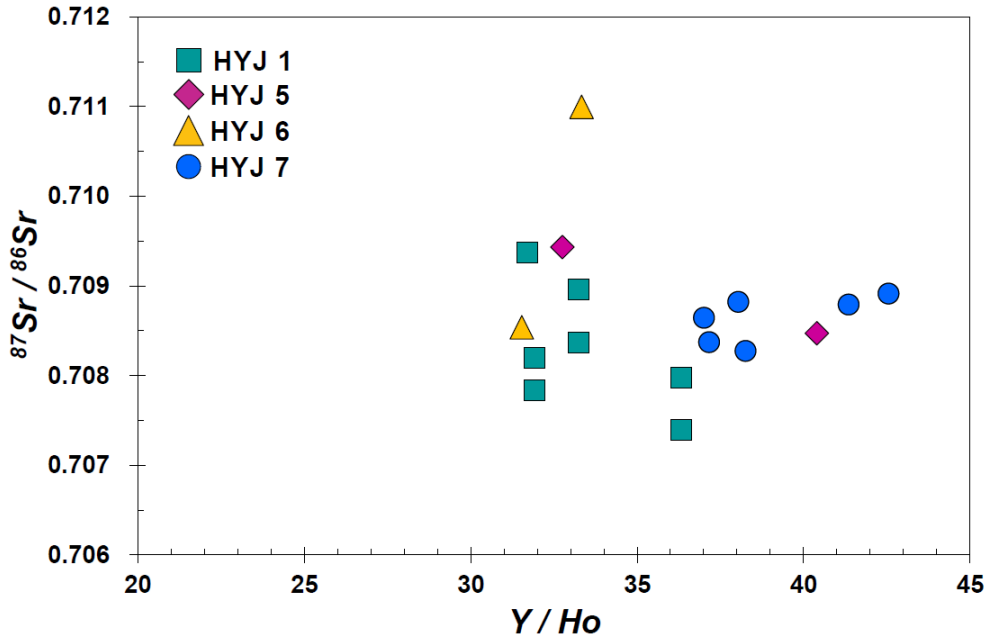

Figure 4-13. Y/Ho vs Strontium isotopic composition of the Hyangsanni Dolomite.

CHAPTER 5

Discussion

5.1 Tectonic environment of the depositional basin

The Hyangsanni Dolomite is composed of pure dolomite, and no fossils indicating the environment have been found. Therefore, geochemistry is an important tool to find out the depositional environment. Zhang et al. (2017) compiled the geochemical data of global carbonates and suggested that the magnitude of Ce anomalies $(Ce/Ce^*)_N$ of the carbonate rocks exhibits a distinct increase from the lowest (~0.29 ± 0.14) in the spreading ridge-influenced regime (open ocean floor) to successively higher values (~1.1) in the continental coastal sea. They also suggested that the carbonate rocks on active margins (~1.1–1) have apparently larger $(Ce/Ce^*)_N$ values than those on passive margins (~0.79), indicating a greater influence by the terrigenous materials. However, with $(Ce/Ce^*)_N$ values, active margins can hardly be distinguished from inland freshwater basins. Meanwhile, large ion lithophile elements such as Sr, Ba, and Rb can also provide useful information on the sedimentary environment in which carbonate rocks are deposited.

According to Zhang et al. (2017), the inland freshwater limestones, based on their low Sr/Ba and Sr/Rb ratios, are distinguished from the continental margin seawater limestones in the Sr/Ba vs. Sr/Rb diagram. In this study, we tried to constrain the tectonic environment in which the Hyangsanni Dolomite was deposited using several trace element discrimination diagrams presented by Zhang et al. (2017).

The Hyangsanni Dolomite samples have relatively high Sr/Ba and Sr/Rb ratios (Figure 5-1a and 5-1b) and therefore inland freshwater environments can be excluded. In both $(Ce/Ce^*)_N$ vs $(La/Yb)_N$ (Figure 5-1c) and $(Ce/Ce^*)_N$ vs $(La/Yb)_N$ (Figure 5-1d) diagrams, the Hyangsanni Dolomite samples are plotted in the inland + margins field rather than the open ocean field.

Taken together, we suggest that the Hyangsanni Dolomite was deposited in an oceanic environment of continental margins, not inland freshwater or open oceans. However, the fact that some samples of the Hyangsanni Dolomite were plotted in the inland field of Figure 5-1 suggests that the influence of terrigenous materials was somewhat larger than the general passive margin. Therefore, considering that the Okcheon Metamorphic Belt is claimed to be a rift basin based on the A-1 type magmatism in the Gyemyeongsan and Munjuri formations (e.g., Kim et al., 2020; Ko et al., 2005), it is suggested that it is more likely to be a rift basin connected to the open ocean rather than a passive continental margin.

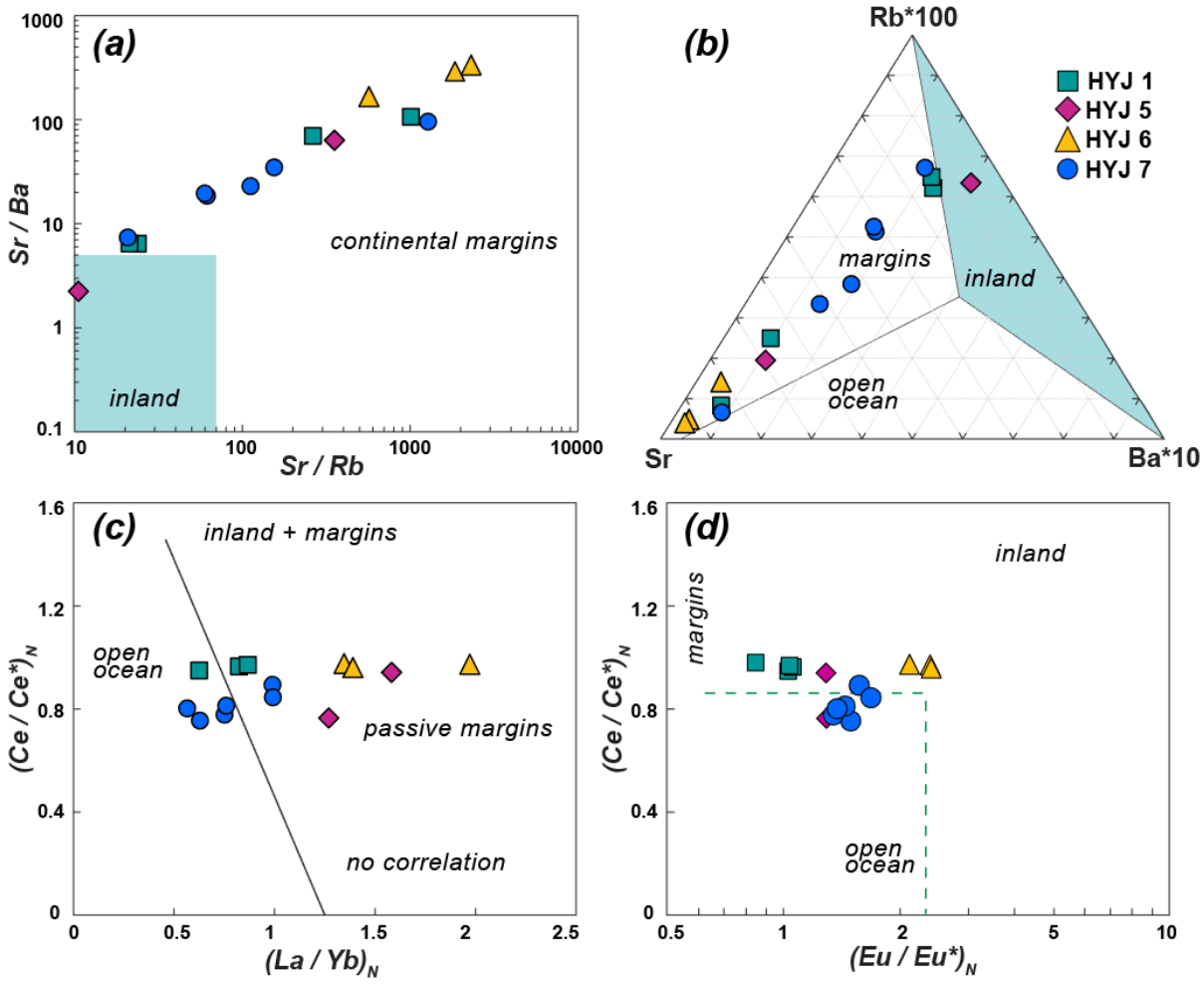

Figure 5-1. Geochemical discrimination diagrams to distinguish various depositional environments of the carbonate rocks. (a) Sr/Ba vs. Sr/Rb, (b) Rb–Sr–Ba triangular, (c) $(Ce/Ce^*)_N$ vs. $(La/Yb)_N$ and (d) $(Eu/Eu^*)_N$ vs. $(Ce/Ce^*)_N$ diagrams. REE abundances were normalized to PAAS (Taylor and McLennan, 1985).

5.2 Estimation of sedimentation timing by Carbon isotope composition

When estimating the age by chemostratigraphy, the carbon isotope composition is very useful, especially when determining whether it is Early Paleozoic or Neoproterozoic. Except for HYJ 5–3, which is suspected to have been altered, the analyzed $\delta^{13}C$ values of the Hyangsanni Dolomite ranged from 3.7‰ to 6.2‰.

Archaeocyatha has been well known to be a highly useful index fossil for Lower Cambrian worldwide due to its abundance, broad geographical distribution, detailed anatomy, and well-defined categorization. Based on the discovery of a fossil claiming to be Archaeocyatha, Lee et al. (1972) suggested that the Hyangsanni Dolomite was Early to Middle Cambrian. However, the carbon isotope composition of the Hyangsanni Dolomite is distinctly different from the Cambro-Ordovician carbonates of the adjacent Taebaeksan Basin. For example, the carbon isotopic values of the Jeongseon Formation fluctuate between −3‰ and + 1‰ (Hong and Lee, 2007). Globally, most of the marine carbonates during the Cambro-Ordovician have $\delta^{13}C$ values in the range of −3‰ to +1‰ (Veizer et al., 1999). It does not match the Hyangsanni Dolomite, which has a significantly higher value.

During Neoproterozoic, the $\delta^{13}C$ value of carbonate rocks remained relatively high between about +2 and +6, except for severe negative excursions during several glaciation periods (Halverson et al., 2005, 2018; Hoffman et al., 2017; Zhou et al., 2020). The $\delta^{13}C$ value of the Hyangsanni Dolomite agrees with the values found in the 850–580Ma interval globally, excluding several $\delta^{13}C$ negative excursions (Figure 5-2). However, a period of existence of Archaeocyatha have much lower carbon value than Neoproterozoic (Figure 5-3). In summary, Hyangsanni Dolomite is not Cambrian but Neoproterozoic strata.

5.3 Estimation of depositional age by Strontium isotope composition

The $^{87}Sr/^{86}Sr$ evolution curve of seawater can be used as a precise dating tool for Phanerozoic marine sediments (Jenkyns et al., 2002; Veizer et al., 1999), if an unaltered precise Sr isotope composition can be obtained. In recent years, a number of studies have been reported on isotopic evolution of seawater Sr during the middle and late Neoproterozoic (Halverson et al., 2007; Jacobsen and Kaufman, 1999; Melezhik et al., 2008; Zhang et al., 2020), extending the possible age estimation range of marine sediments using Sr-isotope chemostratigraphy to this period.

In order to accurately determine sedimentation time using Sr isotope composition of carbonate rocks, the analyzed Sr isotope composition should accurately indicate the seawater value at the time of deposition. However, many carbonate rocks often do not retain the initial seawater Sr isotopic composition at the time of deposition due to influence by terrestrial materials or post-depositional alteration. The alteration effect usually changes the Sr isotope value of the carbonate rock higher than the original value, because the average value of the $^{87}Sr/^{86}Sr$ ratio of continental materials is higher than that of seawater. Even if the Sr content of the mixed terrestrial materials at the time of sedimentation was sufficiently low, post depositional alterations can cause deviations from the original seawater value through the geological age (e.g. Otsuji et al., 2013; Zhou et al., 2020). This is because the growth of radiogenic strontium occurs through the geological age due to the enhanced Rb/Sr ratio of the mixed terrestrial materials. Although it is preferable to find carbonate rocks having low Rb/Sr ratios, it may be inevitable to use least altered rocks or to apply some corrections using Rb/Sr ratios and potential age of formation.

In fact, from the analyzed Hyangsanni Dolomite, we were unable to find a sample that perfectly met the aforementioned criteria, so we chose the next best option. First, we select the samples with the lowest level of the current $^{87}Sr/^{86}Sr$, and use their Rb/Sr ratio to estimate and discuss the $^{87}Sr/^{86}Sr$ initial values. Figure 5-2 shows the time evolution of the $^{87}Sr/^{86}Sr$ values corrected with the Rb/Sr ratios of the samples of the Hyangsanni Dolomite, superimposed with the published seawater $^{87}Sr/^{86}Sr$ evolution curve during Neoproterozoic and Cambrian from Zhou et al. (2020). In this figure, carbonate rocks with a lower Rb/Sr ratio show a flatter $^{87}Sr/^{86}Sr$ change, while those with a higher Rb/Sr ratio show more steep changes. To find out at which age the values intersect each other, HYJ 1–5a, which has the lowest present $^{87}Sr/^{86}Sr$ value, is similar to the Neoproterozoic seawater value in the range of about 660–640

Ma. HYJ 1–2a, which has a slightly higher slope, is roughly equivalent to the value of Neoproterozoic seawater in the 800–640 Ma range. All other estimates were calculated to have higher values of $^{87}Sr/^{86}Sr$ during the Neoproterozoic, and the effects of terrestrial materials appear to be relatively large.

Taken together, the discussion of the $^{87}Sr/^{86}Sr$ value suggests the possibility that Hyangsanni Dolomite was deposited during the Neoproterozoic period, as early as 800 Ma. In other words, the Hyangsanni Dolomite apparently has a lower $^{87}Sr/^{86}Sr$ value than Ediacaran seawaters, suggesting that it may be late Tonian or Cryogenian. Except for the interval with low carbon isotope values during the Sturtian glaciation, this is also consistent with the results of discussions based on carbon isotope values. Combined with inferences from carbon isotopic composition, the Hyangsanni Dolomite appears to have formed between about 800 Ma and about 720 Ma just before Sturtian Glaciation, or between about 660 Ma and about 640 Ma just before Marinoan Glaciation. However, in order to distinguish between these two sections or to define the age more precisely, it would be necessary to find synsedimentary volcanic layers or to refine the ages using carbonate chemostratigraphy.

As stated before, the Hyangsanni Dolomite has been suggested early to middle Cambrian strata based on occurrence of the Archaeocyatha fossil. However, our data does not match with those of Cambrian. According to the Phanerozoic strontium evolution curve, about 0.7074 value imply Permian-Triassic and Cretaceous (Figure 5-4).

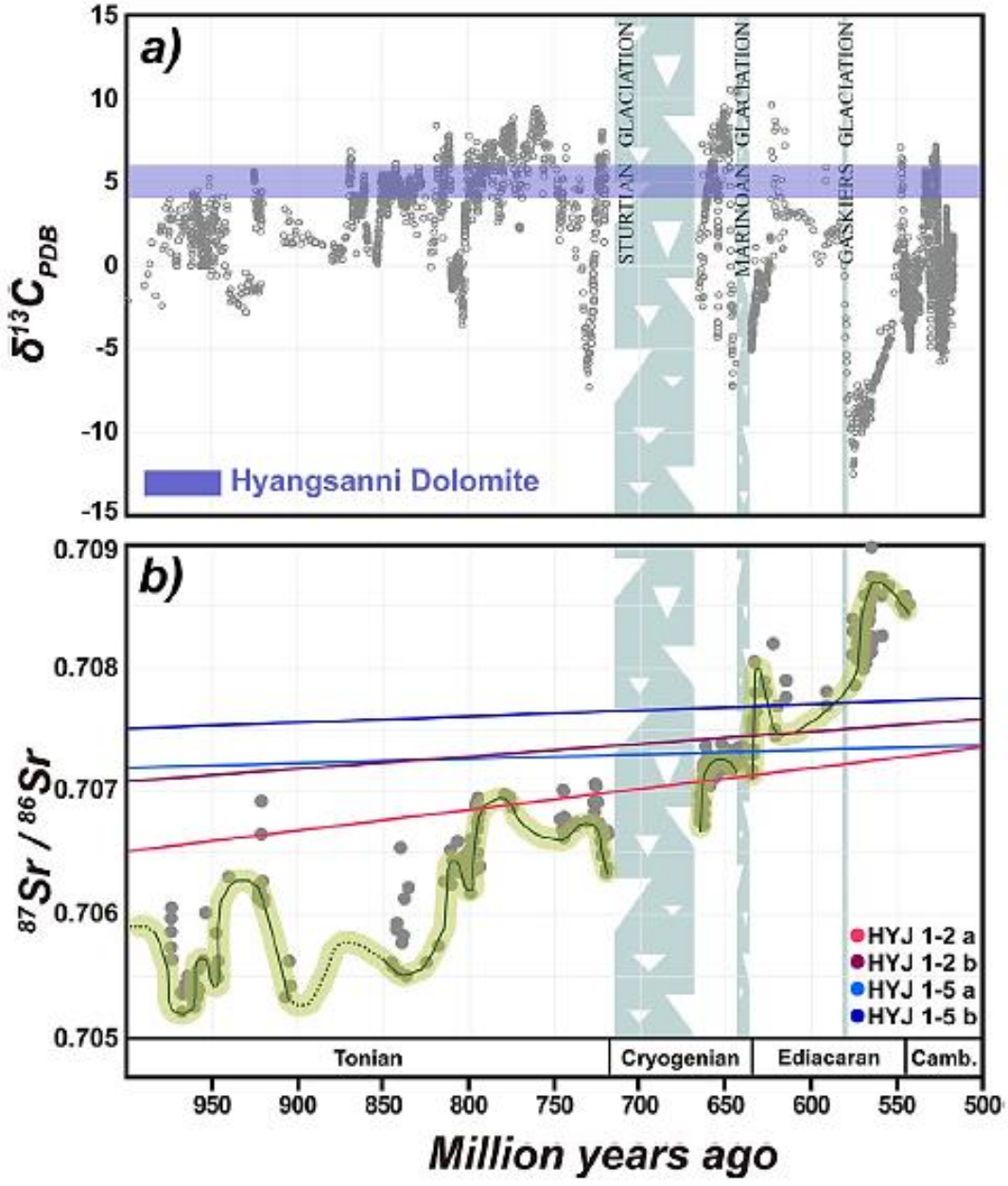

Figure. 5-2 Composite (a) carbon and (b) strontium isotope records for the Neoproterozoic from marine carbonates (modified from Zhou et al., 2020). In the top plot, the range of carbon isotope values determined in the Hyangsanni Dolomite is also shown as a purple colored band. The lines in the bottom plot show the corrected initial $^{87}Sr/^{86}Sr$ ratios according to the age based on their Rb/Sr ratios from the samples HYJ 1–2 and HYJ 1–5 with the lowest present $^{87}Sr/^{86}Sr$ ratios among the analyzed values from the Hyangsanni Dolomite. Three lines with lower $^{87}Sr/^{86}Sr$ ratios show that they are similar to seawater values prior to Ediacaran.

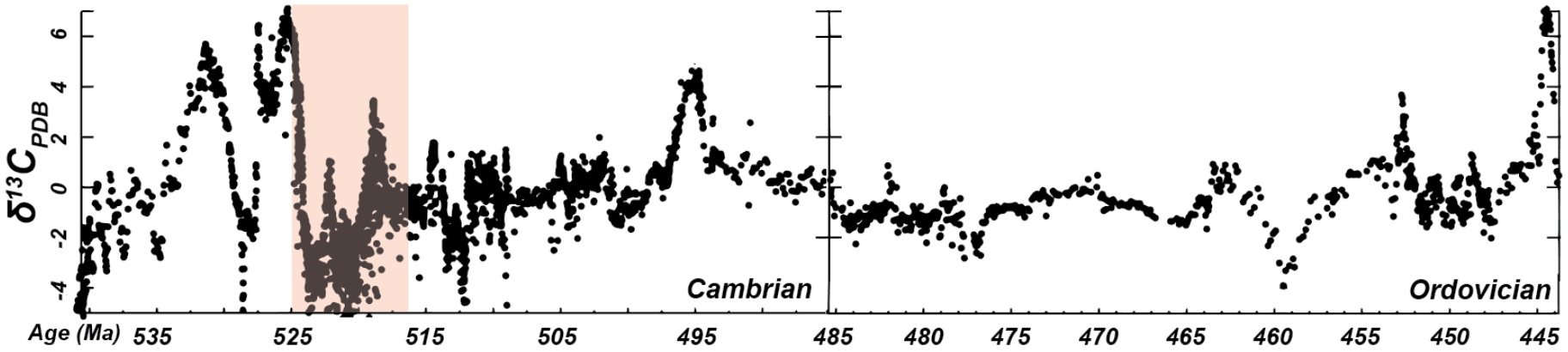

Figure 5-3. Variation of $\delta^{13}C$ through the Cambrian and Ordovician (modified from Saltzman and Thomas, 2012). Red rectangles represent the period during which the Archaeocyatha fossils existed.

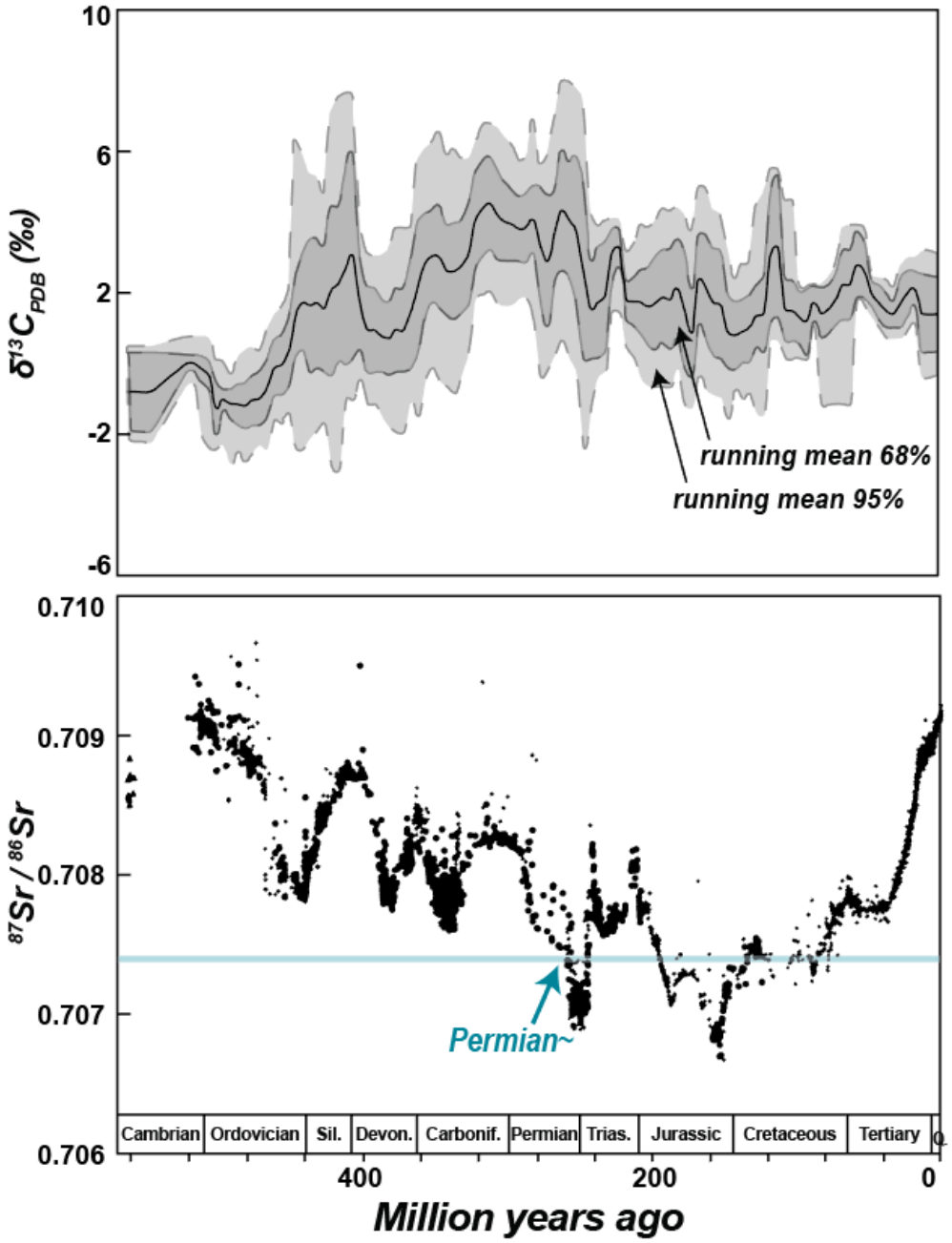

Figure 5-4. Composite $\delta^{13}C$ and $^{87}Sr/^{86}Sr$ records for the Phanerozoic seawater (modified after Veizer et al., 1999)

5.4 Evolution of the Okcheon Metamorphic Belt

Studies on Neoproterozoic periods have also been reported from several parts of North Korea (Peng et al., 2011; Hu et al., 2012), which appear to have evolved in connection with North China Craton since at least Paleoproterozoic. Consequentially, the northern part of the Korean Peninsula is known to have evolved with the adjoining North China Craton, at least since the Paleoproterozoic (Zhai et al., 2019).

However, various contrasting hypotheses have been proposed regarding the structural evolution of the southern part of the Korean Peninsula. In the case of South Korea, Neoproterozoic ages have been reported from the western part of the Gyeonggi massif and various regions of the Okcheon Metamorphic Belt (Lee et al., 1998a; Kim et al., 2006; Kee et al., 2019).

These results suggest that the traditional view of crustal evolution on the Korean Peninsula must be greatly modified in many ways. Among these, the Okcheon Metamorphic Belt, which has been recognized as a key part in understanding the crustal evolution of the Korean Peninsula, still needs studies to identify the timing of its formation and the tectonic environment.

The traditional view is that both the Gyeonggi and Yeongnam Massifs are part of a Sino-Korean Craton connected to the North China Craton. In this case, the Okcheon Metamorphic Belt is also part of the Sino-Korean Craton. However, there is a suggestion that the boundary between the Gyeonggi and Yeongnam Massifs, respectively correlated to South China Craton and North China Craton, passes along the southern margin of the Okcheon Metamorphic Belt (Chough et al., 2000; Kim et al., 2017).

The Okcheon Metamorphic Belt is a key for understanding the tectonic environment during Neoproterozoic because they show the A1-type intra-plate magmatism of about 860 Ma and 760 Ma (Lee et al., 1998a; Park et al., 2005; Kim et al., 2006, 2011), possibly associated with the break-up of Neoproterozoic supercontinent Rodinia. We need to think about the implications that Hyangsanni Dolomite is located near Neoproterozoic Gyemyeongsan and Munjuri metavolcanics. These metavolcanics with eruption times of 860 Ma and 760 Ma, respectively, have A-1 type magma characteristics, suggesting the development of within-plate rift. Perhaps the sedimentation in the basin created by these rifting led to the formation of glacial-related sediments, such as Hyangsanni Dolomite and Hwanggangni Formation consisting of diamictite.

The claim that the nearby Hwanggangni Formation consists of a diamictite, a glacial deposit (Reedman and Fletcher, 1976; Lee et al., 1998; Choi et al., 2012), also increases the likelihood that Hyangsanni Dolomite was deposited during the Neoproterozoic period, when there were well-known glaciations. In addition to the claim that Hwanggangni and Bugnori Formations are glacial deposits and the possibility that Geumgang Limestone is post-glacial cover carbonates (Choi et al., 2012; Ryu and Ahn, 2016; Ha, 2021), the possibility that Hyangsanni Dolomite is also a sedimentary layer near Neoproterozoic ice ages suggests that the research on Neoproterozoic glaciation in Korea could be activated.

The fact that Hyangsanni Dolomite is Neoproterozoic suggests that metasedimentary rocks in the surrounding northeastern Okcheon Metamorphic Belt were also deposited in Neoproterozoic. As mentioned above, recent geochronology data bear out it as well. In addition, this study reports the zircon U-Pb data of other constituents, metasedimentary sequences, of the Okcheon Metamorphic Belt as well. Which are the Daehyangsan Quartzite, Bugnori Formation, Hwanggangni Formation, Seochangni Formation, and Changni Formation.

5.4.1 Zircon U-Pb ages from the metasedimentary rocks in the Okcheon Metamorphic Belt

Daehyangsan Quartzite

The Daehyangsan Quartzite was considered that has been deposited in a normal marine setting between two rifting stages (ca. 860 Ma and 760 Ma) with Hyangsanni Dolomite (Choi et al., 2012). However, the results of zircon U-Pb age (Park et al., 2011) dating overturned previous theories. To confirm this, fieldwork and zircon age dating were conducted, and the result, youngest age belongs to Paleozoic, were consistent with the previous study. This study yields younger minimum age (~ ca. 328) than previous work (~ ca. 423, Park et al., 2011) (Figure 5-5).

The stratigraphic relationship between Hyangsanni Dolomite and Daehyangsan Quartzite is traditionally thought to be conformable, but no one knows the exact relationship between both. Besides, I could not find the zircons from the Daehyangsan Quartzite sample which is in direct contact with Hyangsanni Dolomite. All zircon U-Pb age dating including this study was conducted more south than the sampling location of the Hyangsanni Dolomite. What was interesting, the Hyangsanni Dolomite outcrop is nowhere to be seen in several fieldworks where was sampling the Daehyangsan Quartzite.

Daehyangsan Quartzite is currently marked on the same layers, but it needs to be separated into different layers. In addition, the Hyangsanni Dolomite seems to be not existed in the area where was sampling the Daehyangsan Quartzite. In other words, it means that a geological map needs to be modified (Figure 5-6).

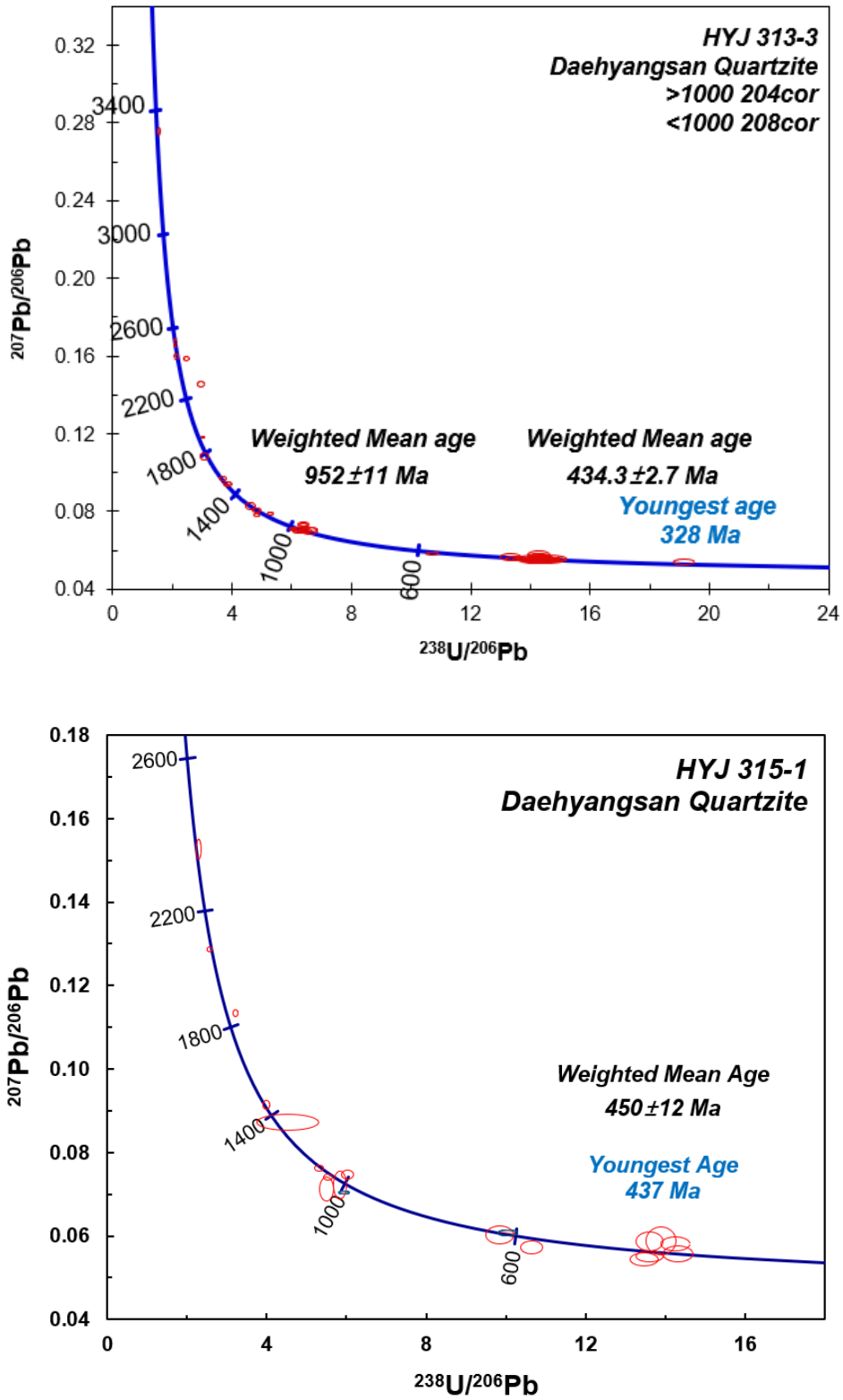

Figure 5-5. Terra-Wasserburg diagrams for the analyzed detrital zircons of the Daehyangsan Quartzite.

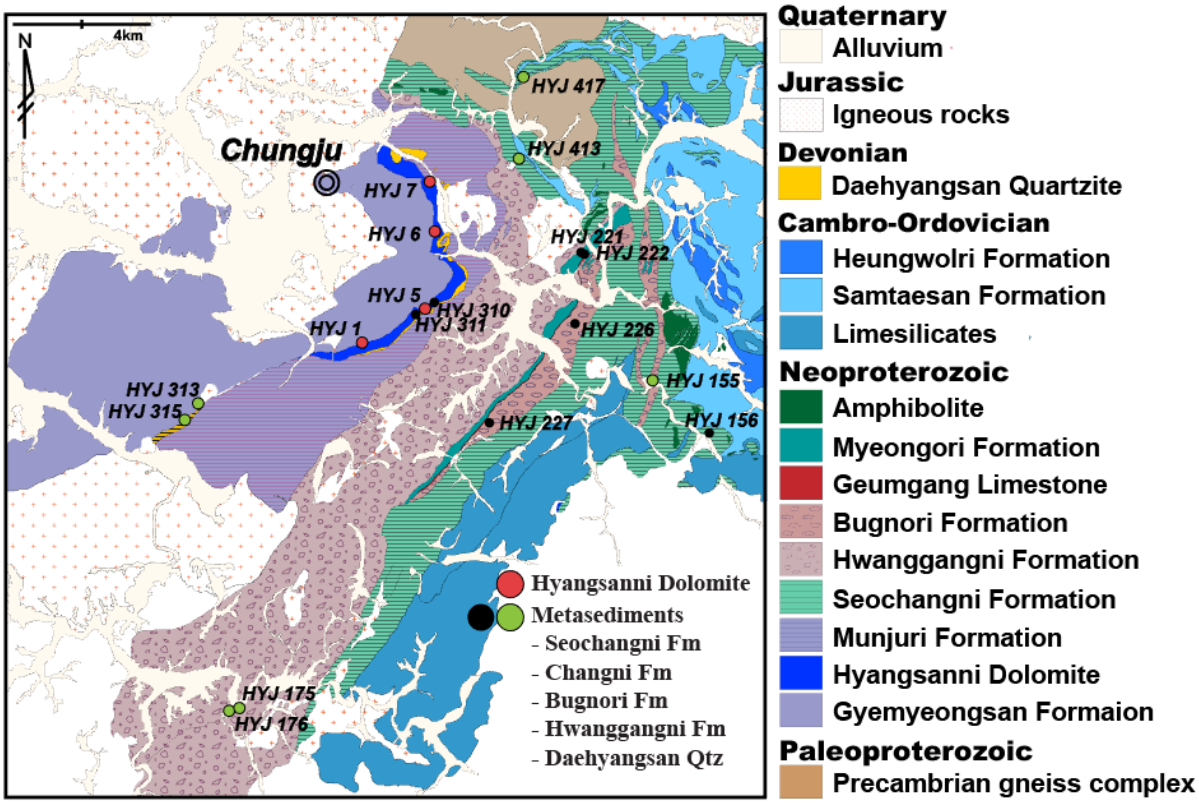

Figure 5-6. A newly proposed geological map of near the Chungju area based on this study.

Bugnori Formation and Hwanggangi Formation

The Hwangganggni and Bugnori Formations feature pebble-bearing phyllitic rocks. The pebbles are different sizes and shapes of limestone, granite, gneiss, and quartzite and such. These Formations were originally considered to be distinct from each other by Lee and Park (1965), so these formations are compartmentalized at the Hwanggangni quadrangle (Lee and Park, 1965). However, in the Okcheon (Kim et al., 1978) and Boeun (Kim et al., 1977) quadrangles, these two formations were treated as a single formation, named Hwanggangni Formation.

Lee et al. (1998b) suggested the sedimentation time of the Hwanggangni Formation as Late Paleozoic for the following reasons. First, Lee et al. (1989) claimed the discovery of Cambro-Ordovician conodont fossils from limestone clasts of the Hwanggangni Formation. However, the discovery of conodonts from the Hwanggangni Formation has not been confirmed since then and needs to be verified. Second, the CHIME age of granite clasts from the Hwanggangni Formation was determined to be 367 Ma (Cho et al., 1996). Research published later (Suzuki et al., 2006) suggested that Paleoproterozoic granitic gneiss clasts in the Hwanggangni Formation had xenotime grains with a metamorphic rim of about 370 Ma, suggesting that sedimentation of the Hwanggangni Formation was thereafter. In contrast, Choi et al. (2012) suggest that this formation is glaciogenic diamictite deposited during the Neoproterozoic Snowball Earth event based on correlation with the stratigraphy of Nanhua Basin in South China Craton, but did not provide definitive evidence.

As stated before, these two formations do not come into direct contact, and the phyllitic layers exist between the two. There is a relatively thin and continuous carbonate layer with a thickness of about 15-20 meters occur between the pebble-bearing phyllitic layers and the phyllitic layers. Such thin carbonate layer is suggested to post-glaciation sediments, cap-carbonate (Choi et al., 2012; Ryu and Ahn, 2016; Ha, 2021). The pebble-bearing phyllitic layers named Hwanggangni or Bugnori Formations, and phyllitic layers named Myeongori, Munjuri or Changni Formations depending on quadrangles.

Hwanggangni Formation is considered to be a glacial deposit later than Munjuri Formation because it contains about 750 Ma of zircons, which is the time of creation of Munjuri Formation (Lee et al., 1998; Cho et al., 2004; Kim et al., 2006). Both Sturtian glaciation and Marinoan glaciation fall under this category, which requires further study. Regarding the previous studies, the detrital zircon age of Hwanggangni Formation it is dominant by ca. 1870 Ma and 750 Ma even though differs from region

to region. Bugnori Formation is also considered as glaciogenic sedimentary sequence together with Hwanggangni Formation based on similarity to lithology with Hwanggnani Formation. The detrital zircon age of Bugnori Formation is predominant Mesoproterozoic component.

In this study, the U-Pb ages of the detrital zircons of the Bugnori and Hwanggangni Formations are quite similar (Figure 5-7 and 5-8). Instead, Bugnori Formation yield the Neoproterozoic component, ca. 748 Ma. Perhaps Bugnori and Hwanggangni Formations were created during each glaciation period. Therefore, it is necessary to clearly identify whether the two formations are separate formations with different sedimentation periods, or the same formation repeated by fold as suggested by Choi et al (2012).

Recently, Ha (2021) confirmed the possibility that the Geumgang Formation is a Neoproterozoic cap carbonate, and based on this, proposed a new stratigraphy of the surrounding layers of the Okcheon Metamorphic Belt. For consistency of naming, Ha (2021) suggest that the diamictite deposit with the limestone layer developed at the boundary is called Bugnori Formation, otherwise it is called Hwanggangni Formation.

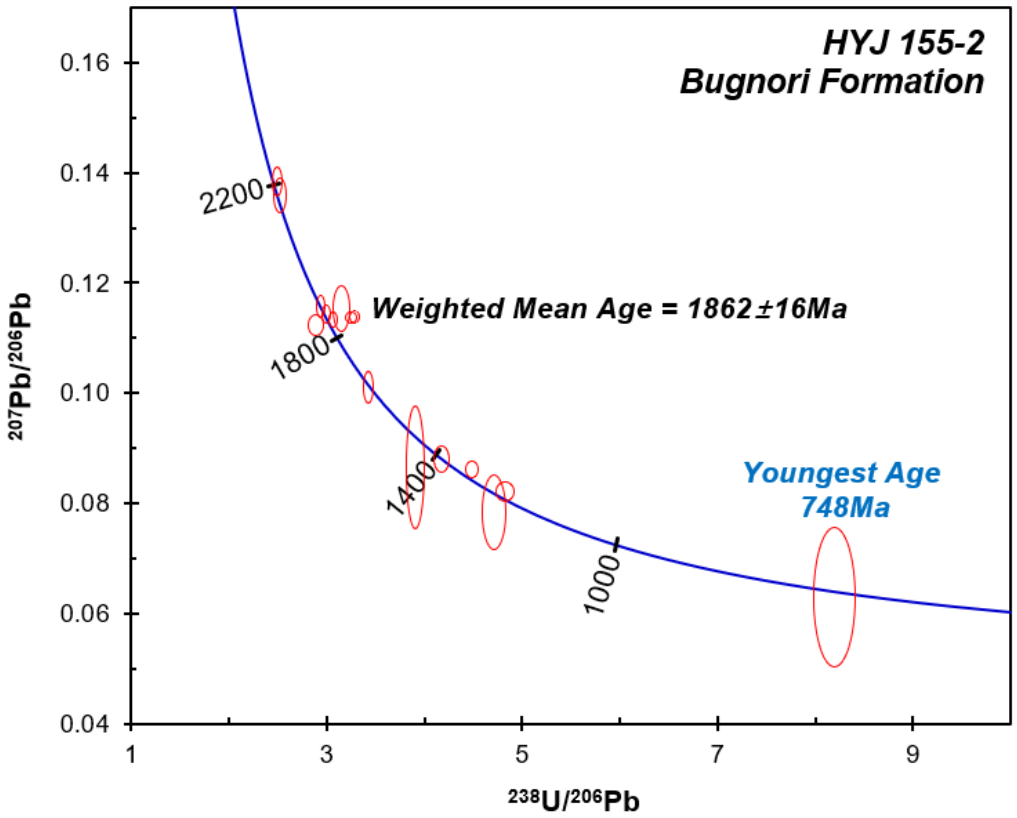

Figure 5-7. Terra-Wasserburg diagrams for the analyzed detrital zircons of the Bugnori Formation.

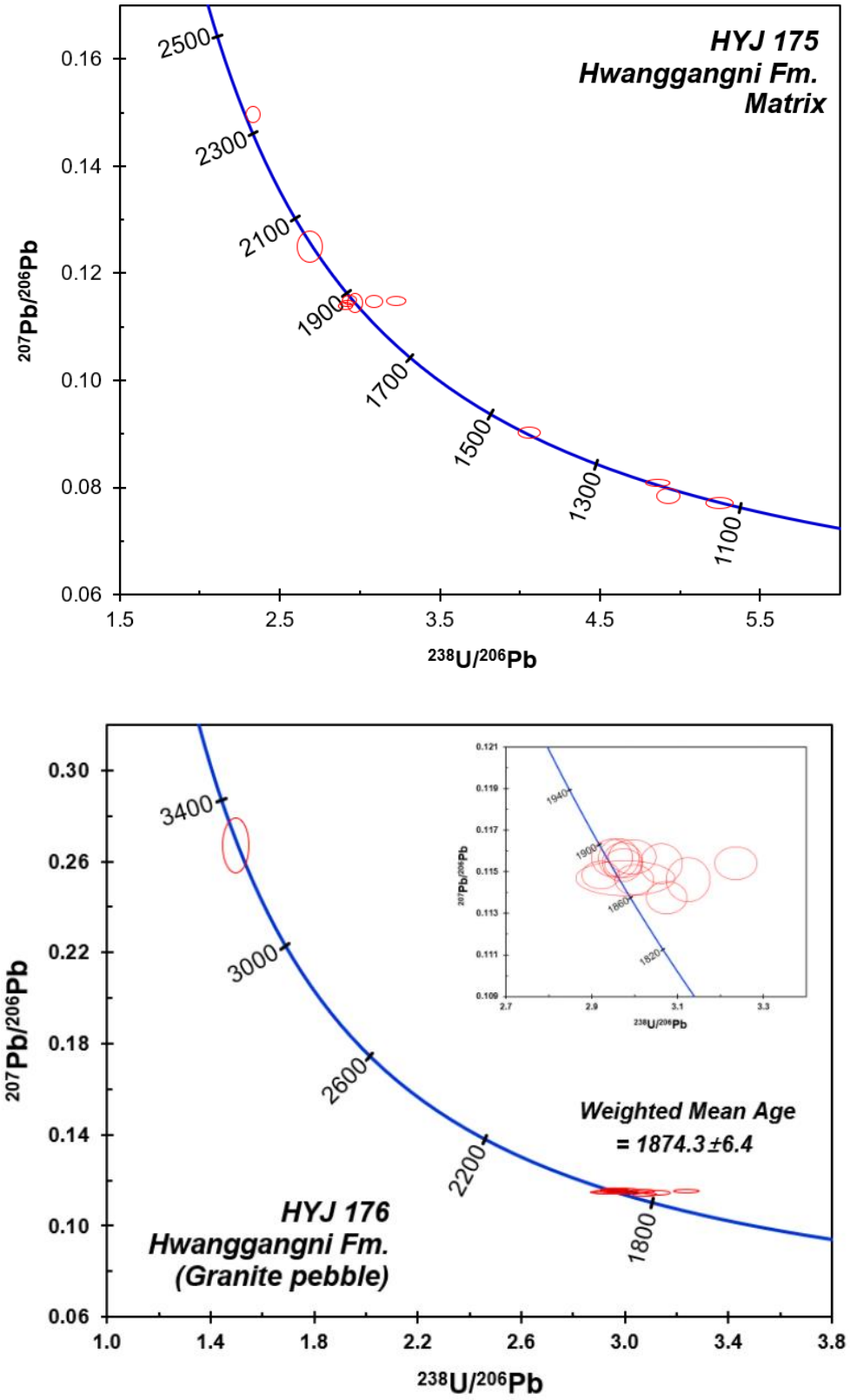

Figure 5-8. Terra-Wasserburg diagrams for the analyzed detrital zircons of the Hwanggangni Formation. HYJ 175 is matrix and HYJ 176 is granite pebble of the Hwanggangni Formation, respectively.

Seochangni Formation and Changni Formation

The U-Pb ages of the detrital zircons of the Changni Formation (Figure 5-9) are quite similar to those of the Seochangni Formation (Figure 5-10) distributed in the northeast of the Okcheon Metamorphic Belt. First of all, it is an important common feature that the U-Pb age is concentrated in the range from late Paleoproterozoic to Mesoproterozoic. It is also noteworthy that the age of about 750 Ma appears together. The similarity of the U-Pb ages of the detrital zircons of the Changni Formation and the Seochangni Formation suggests that they are correlated.

Other additional evidence also supports their correlation. One of these additional pieces of evidence is that these are all easternmost layers of the Okcheon Metamorphic Belt, the Seochangni Formation in the north and the Changni Formation in the south. Both formations are intruded with significant volumes of amphibolite. A U-Pb age of about 750 Ma was reported from the amphibolite that intruded the Changni Formation (Cheong et al., 2014). The fact that these two formations are correlated helps to unravel the enigmatic stratigraphy of the Okcheon Metamorphic Belt.

Recently, Ha (2021) confirmed the possibility that the Geumgang Formation is a Neoproterozoic cap carbonate, and based on this, proposed a new stratigraphy of the surrounding layers of the Okcheon Metamorphic Belt (Figure 5-11). Currently, the diamictite layer and the pelitic layer located on both sides of the Geumgang Formation in Boeun and Okcheon regions are called the Hwanggangni Formation and Munjuri Formation (some of them the Changni Formation), respectively. Ha (2021) suggested that it is more reasonable to call them the Bugnori Formation and the Myeongori Formation, respectively, compared with the formation names initially investigated. For the stratigraphy of the Okcheon Metamorphic Belt in the Okcheon-Boeun region, Ha (2021)'s proposal based on the carbon isotopic composition of carbonate rocks and the proposal based on the detrital zircon U-Pb ages of the Changni Formation in this study are generally harmonious.

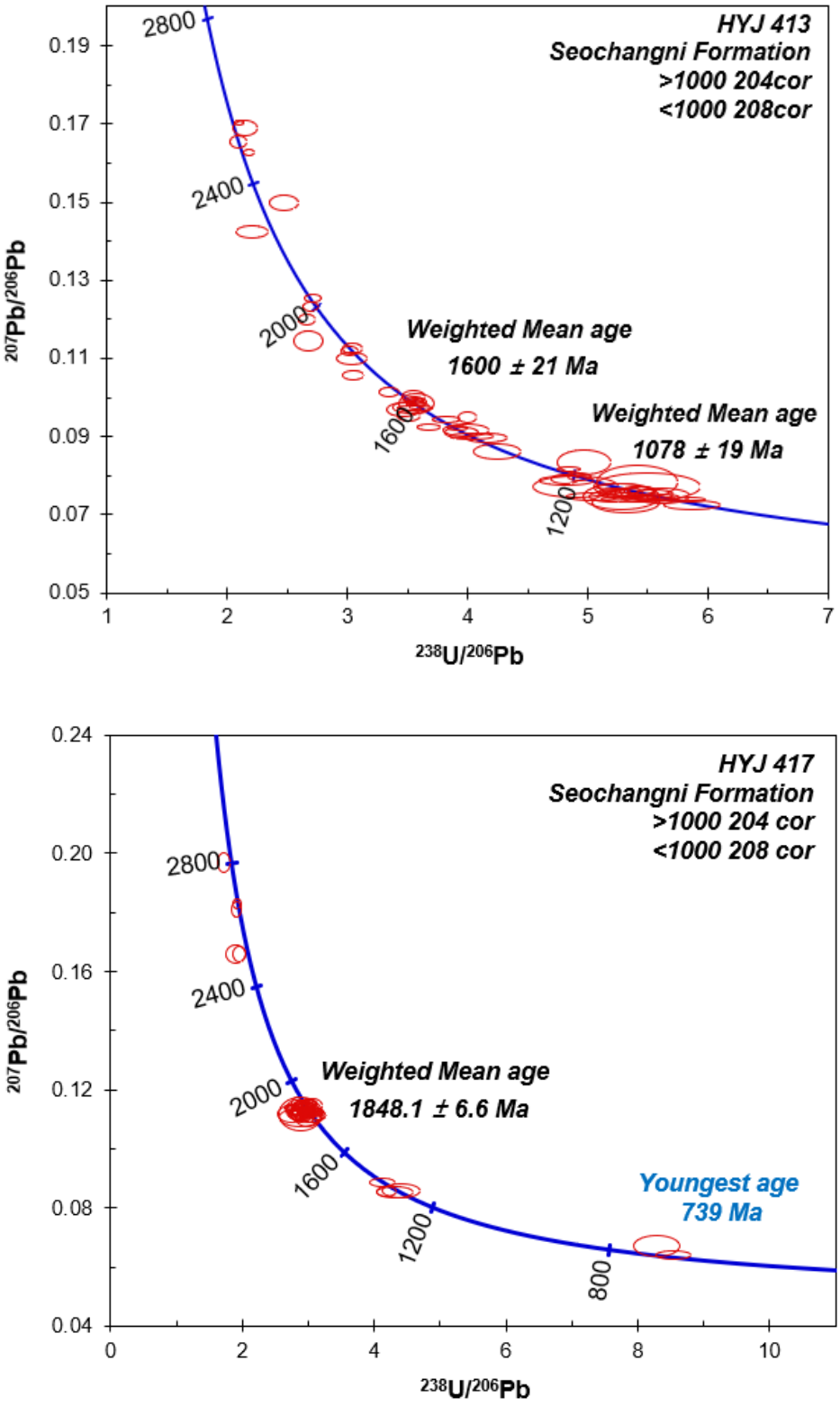

Figure 5-9. Terra-Wasserburg diagrams for the analyzed detrital zircons of the Seochangni Formation.

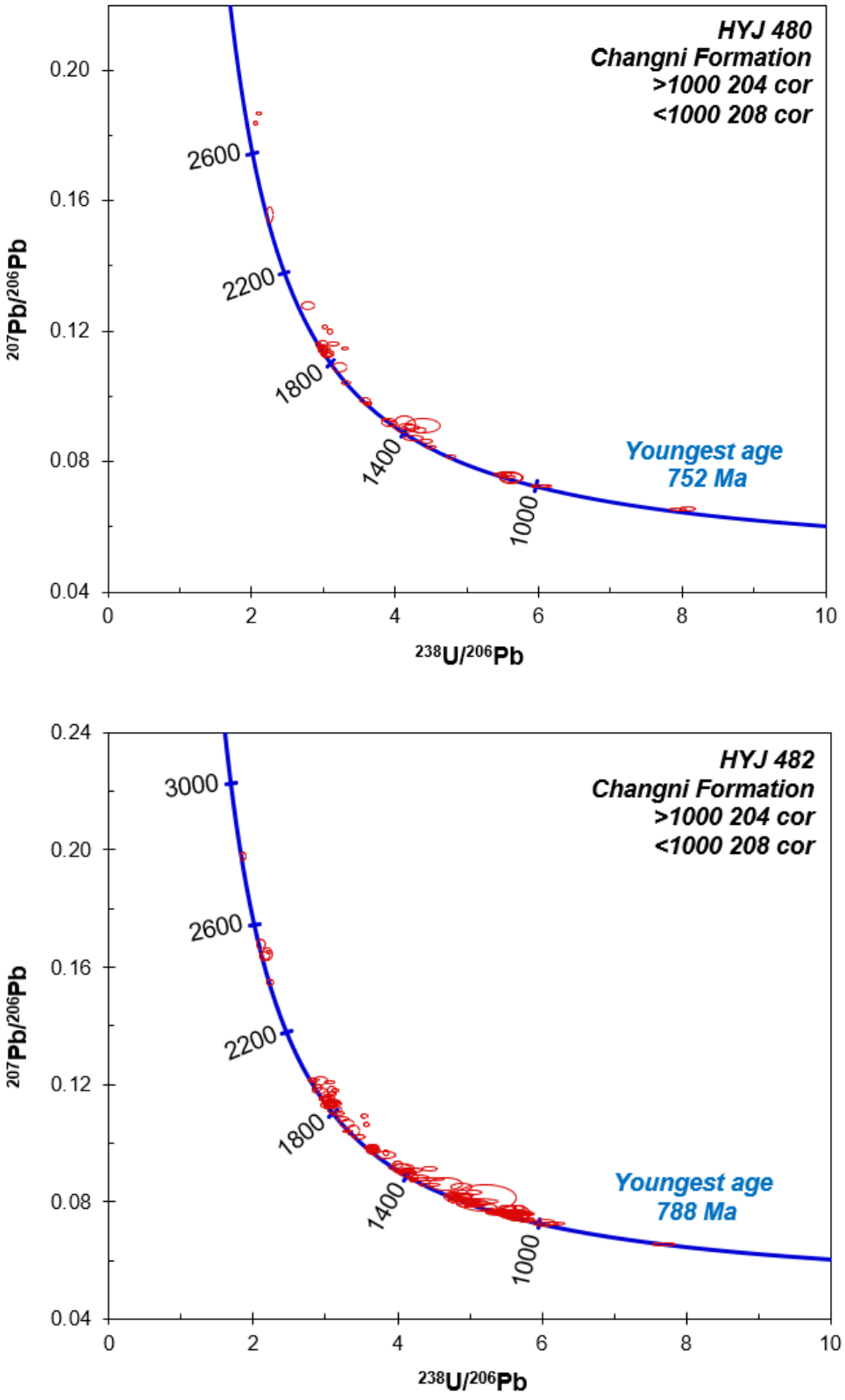

Figure 5-10. Terra-Wasserburg diagrams for the analyzed detrital zircons of the Changni Formation.

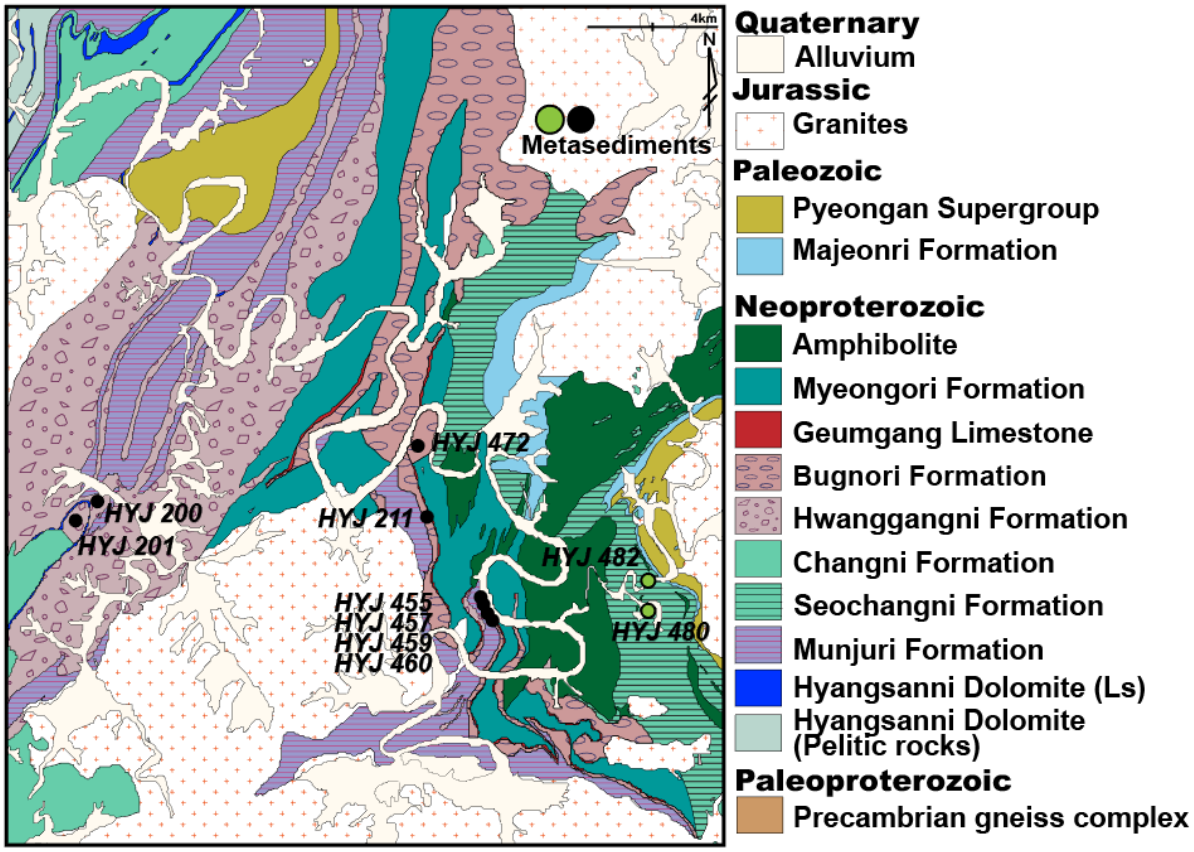

Figure 5-11. A newly proposed geological map of Okcheon-Boeun area based on this study.

5.5 Comparison with other carbonates distributed in the Okcheon Metamorphic Belt

5.5.1 Geumgang Limestone

Widespread glaciation were unusual events in Earth history and glaciogenic sequence is occurrence. Korean peninsula and Cratons in China record a series of significant geological events related to Rodinia supercontinent such as Neoproterozoic glaciations and continental rifting. It should be noted that although Neoproterozoic diamictites are widespread, their glacial affinity in Korean peninsula has been doubtful. The existence of the glaciogenic sequence may enable constraint on age of Okcheon Metamorphic Belt by deducing stratigraphic relationship with adjacent strata.

Because of this reason, the rare evidence of glaciation in Okcheon Metamorphic Belt would be the important key to understand link between Korean peninsula and Chinese Cratons. Furthermore, it could provide clear advantage insights into the tectonic evolution of East Asia.

The age-unknown limestone distributed throughout in the Okcheon Metamorphic Belt has been longstanding conundrum. Among the rest, the Geumgang Limestone is suggested as a cap carbonates based on the occurrence sharply overlie Hwanggangni Formation considered as Neoproterozoic diamictite (Choi et al., 2012). However as of yet, it is controversial issue since no distinct glacial sedimentological feature has been found in both the formations.

In the case that the Okcheon Metamorphic Belt had experienced glaciation in Neoproterozoic Era, some age-unknown limestone including Geumgang Limestone should have recorded its signal. In order to verify the imprinted evidence of a glaciation event in the Okcheon Metamorphic Belt, Ha (2021) carried out a series of geochemical analyses for the Geumgang Limestone formation occurred in Okcheon, Chungju and Jecheon area (Figure 5-12).

Most $\delta^{13}C$ and $\delta^{18}O$ values of samples show more depleted with respect to general cap carbonates. Besides, $^{87}Sr/^{86}Sr$ ratio also display more radiogenic value than that of Neoproterozoic Era. Therefore, it is difficult to simple and direct comparison between being well preserved cap carbonates and Geumgang Limestone because the Okcheon Metamorphic Belt had undergone greenschist to amphibolite facies metamorphism. In this sense, the isotopic data cannot dovetail those of general cap

carbonates. Thus, these exceptional isotopic values can be interpreted by alteration during metamorphism. Nevertheless, it possibly corresponding to the glaciation events in Neoproterozoic based on a comparison of negative carbon isotope composition with the global trend.

Cap carbonates define the pronounced notable negative excursions in Neoproterozoic successions. The negative carbon isotope excursion of Geumgang Limestone is analogous that of Neoproterozoic cap carbonates in worldwide though it has more depleted $\delta^{13}C$ value.

Ha (2021) provides new insights for the formation of the Okcheon Metamorphic Belt. Integrating her data and previous studies for adjacent formations, she suggests the Geumgang Limestone was deposited after Neoproterozoic glaciation even though we cannot pinpoint when. This perspective has important stratigraphic implications for that the Okcheon Metamorphic Belt is correlatable with not South China Craton but North China Craton.

Available geochronological data require age-unknown carbonates as the geochronology only for the siliciclastic rocks has demonstrably been known. The $\delta^{13}C$ values of this cap carbonate, Geumgang Limestone, are quite valuable. By correlation, the Hwanggangni, Bugnori, and Geumgang Limestone may include glaciogenic strata, thus these units could also be interpreted as Neoproterozoic in age.

Negative $\delta^{13}C$ values down to -12‰ typify the cap carbonates, and it is definitely peculiarity respect to Paleozoic carbonate. Integrating our geochemical data and stratigraphic correlation among periphery strata, and based on a comparison of the carbon isotope variations with global trend, it verifies that the Geumgang Limestone has strong correlation with post-glacial environment.

Although thus no reliable age is available at present, the pebble bearing phyllitic rocks, Hwanggangni, Bugnori, and Iwonri Formations, have been suggested to be correlated with the diamictite of the global snowball Earth event.

Therefore, the inference that Geumgang Limestone is cap carbonate seems to be completely clear. The finding of the Neoproterozoic glaciation related Geumgang Limestone from Okcheon Metamorphic Belt will untangle obscure tectonic evolution Connection between North and South China Craton and Korean Peninsula.

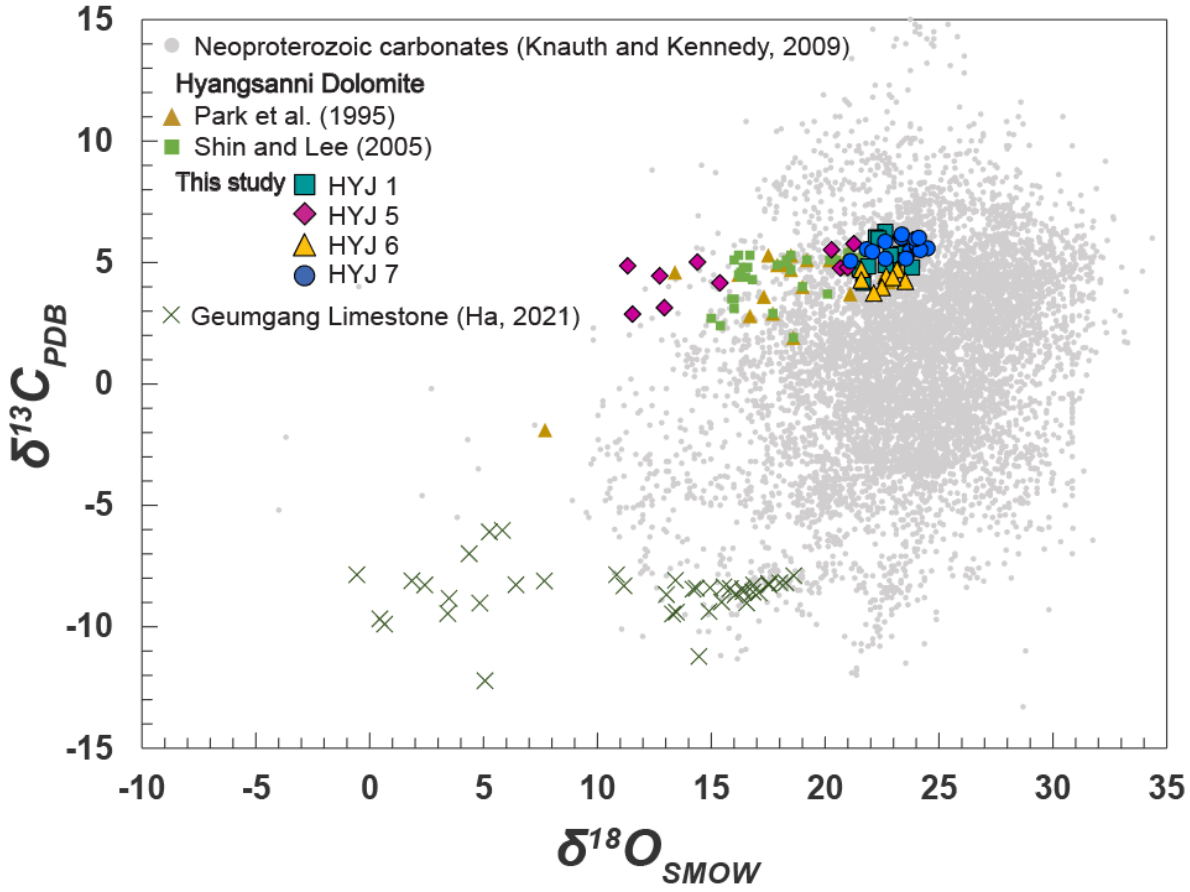

Figure 5-12. Carbon versus oxygen cross-plot for the Geumgang Limestone (Ha, 2021). Cross symbols represent data from the Geumgang Limestone. The others are from Hyangsanni Dolomite for this study and same with those of Figure 4-11.

5.5.2 Seochangni, Samtaesan and Heungwolri Formations

In terms of tectonic unit division, the northeastern Okcheon Metamorphic Belt is tectonically highly important because this area is contiguous with the western margin of Taebaeksan Basin and consists of various lithofacies including metavolcanics and carbonates. Lithologies in the study area, Jecheon-si in Chungcheongbuk-do Province, can be subdivided into four major groups: they are the Paleoproterozoic metamorphic rocks, Neoproterozoic Okcheon Supergroup, lower Paleozoic Joseon Supergroup, and Mesozoic granitoids (Choi et al., 2012) (Figure 2-1).

The Seochangni Formation has been considered as age-unknown stratum in the Okcheon Metamorphic Belt. Considering the proposals that the nearby Hwanggangni Formation, a diamictite deposit, is Neoproterozoic (Choi et al., 2012; Lee et al., 1998; Reedman and Fletcher, 1976; this study) and the Seochangni Formation (Kim et al., 2020; Kim et al., 2021) and Hyangsanni Dolomite (Ha et al., 2021; this study) are also Neoproterozoic. Geochronological information constrained by this study is also in accordance with detrital zircon U-Pb age from Seochangni Formation (Choi, 2013; Kim et al., 2021; this study).

The Samtaesan and Heungwolri Formations commonly referred to as the upper part of the lower Paleozoic strata. Because the Samtaesan and Heungwolri Formations from the Okcheon Metamorphic Belt are also identically named based on the lithostratigraphic similarity with those in the Taebaeksan Basin. This study for these formations makes reconsider South Korea Tectonic Line (SKTL) suggested boundary between Okcheon Metamorphic Belt and Taebaeksan Basin.

Carbon isotope data from the Seochangni, Samtaesan, and Heungwolri Formations can help to estimate their depositional age roughly. This study on the carbonate rocks from the study area manifests different results from conventional view. Given that the high carbon isotopic composition commonly suggesting Neoproterozoic, some parts of the Samtaesan Formation and Heungwolri Formation in the study area could not be regarded as Paleozoic strata. In addition, less than -6‰ of $\delta^{13}C$ values were obtained as well. As stated in Chapter 5.5, an identifiable negative $\delta^{13}C$ values of about -6‰ is common characteristic of cap carbonate.

However, referring to the evolution curves of Phanerozoic seawater carbon isotopes, there are highly fluctuating periods in the early Cambrian, not only Neoproterozoic. (Figure 5-13), and at this

time, a significantly greater variation of $\delta^{13}C$ value was investigated from the significant negative value below -6‰ to a significantly higher value approaching 8‰. However, these changes occur over a very short period (Figure 5-13). Therefore, it cannot rule out the possibility that the carbonate rocks in the study area may have been deposited in such a short period of time. On the other hand, it is well known that the carbon isotope composition of carbonates during the entire Neoproterozoic is generally much higher than that of Cambro-Ordovician, but there are several large negative excursions, and these periods coincide with the glaciation periods. Consequently, the carbonate rocks in the study area were mainly deposited earlier than the Cambro-Ordovician carbonate rocks distributed in the Taebaeksan Basin. Namely, it is thought that the latter is more likely to be deposited in Neoproterozoic rather than Cambro-Ordovician.

Taken together, this study suggests that a significant portion of the carbonate rocks, previously classified as a lower Paleozoic Joseon Supergroup, were deposited during the earliest Cambrian of or Neoproterozoic. It means that some parts of the Samtaesan and Heungwolri Formations distributed in the study area might have different ancestry from representative those of the Joseon Supergroup, and a new stratigraphic name may have to be given that distinguishes it from the existing one. In addition, it is also necessary to redefine the boundary between the Okcheon Metamorphic Belt and the Taebaeksan Basin. But further intensive multilateral studies are required for specifying their depositional timing.

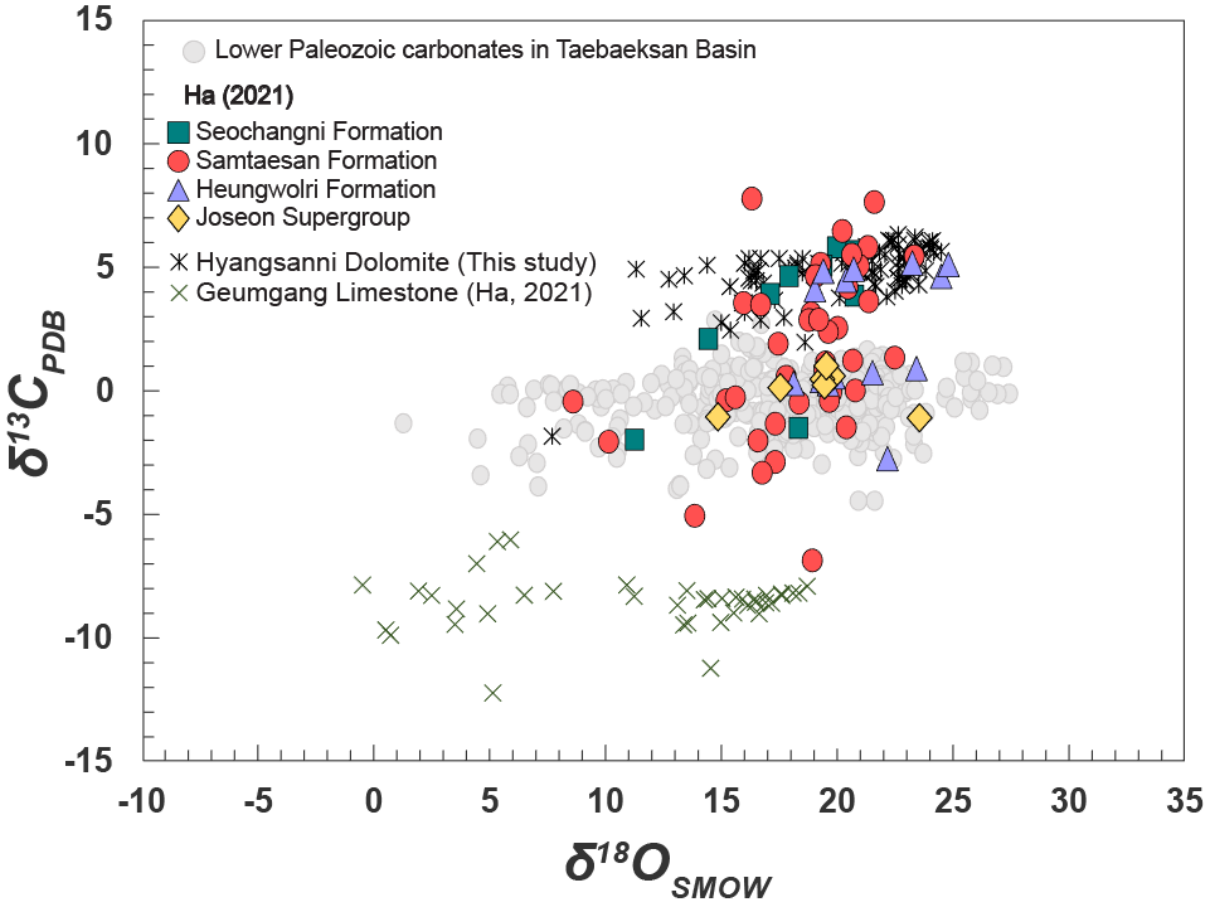

Figure 5-13. Carbon versus oxygen cross-plot for the Seochangni, Samtaesan and Heungwolri Formations and the Joseon Supergroup from the border between the Okcheon Metamorphic Belt and Taebaeksan Basin. Carbon and oxygen isotopic composition of the Lower Paleozoic carbonate rocks in Taebaeksan Basin (Kim, 1980; Park and Woo, 1986; Lim and Woo, 1995; Yoon and Woo, 2006; Hong and Lee, 2007; Lim et al., 2015) and Geumgang Limestone (Ha, 2021) are shown together. Asterisks are from carbonates from the Hyangsanni Dolomite and cross symbols are from the Geumgang Limestone (Ha, 2021).

5.6 Correlation with North China Craton

It has been suggested several times that the Gyeonggi Massif and the Okcheon Metamorphic Belt may be an extension of the South China Craton (Choi and Woo, 2012; Chough et al., 2000; Ree et al., 1996). The geological ages and tectonic settings of the Neoproterozoic rocks that occur in the southwestern Gyeonggi Massif (Figure 5-14) were similar to the arc to intra-continental rift tectonic setting at the margin of the Yangtze Craton (Kee et al., 2019; Oh et al., 2009) and support this argument.

Scholars who proposed Hwanggangni Formation as a glacial deposit of Neoproterozoic (Choi et al., 2012) argued for correlation with South China. Although the sedimentary rocks deposited during the glaciation of Late Neoproterozoic are widely distributed in South China, it is necessary to consider the possibility of correlation with North China. Because Neoproterozoic glaciation-related sediments have also been reported in the southern margin of craton in northern China

The recent studies on the age of detrital zircons from the western Gyeonggi Massif (Kim et al., 2019) and the northeastern Okcheon Metamorphic Belt (Cho et al., 2013; S.W. Kim et al., 2020; M.J. Kim et al., 2021) support the correlation with North China Craton. Lee et al. (2020) suggested that the Neoproterozoic igneous rocks in the northern Gyeonggi Massif (Figure 5-14) can be correlated with those formed in the within-plate tectonic setting in the southern and southeastern margins of the North China Craton during the period 830–930 Ma. Thus, during the Neoproterozoic of this period, the northeast and southwest of the Gyeonggi Massif were in different tectonic settings, and appear to have been correlated to the North China Craton and the South China Craton, respectively. In addition, the presence of Mesoproterozoic detrital zircons found in the Seochangni Formation of the Okcheon Metamorphic Belt (Kim et al., 2020; Kim et al., 2021; this study) is also the same as the Neoproterozoic sedimentary rocks in the southern margin of North China Craton.

These similarities suggest that Hyangsanni Dolomite, along with several other sedimentary formations in the Okcheon Metamorphic Belt, may correlate to the southern margin of North China Craton. The correlation of the Okcheon Metamorphic Belt, at least in part, with the southern margin of the North China Craton, provides important clues in interpreting crustal evolution and tectonics on the Korean Peninsula. This means that both Gyeonggi and Yeongnam Massifs, including at least part of the Okcheon Metamorphic Belt, have evolved as the same block since Paleoproterozoic with North China

Craton. This also means that the Early Triassic continental collision belt, which exists between the South and North China blocks, did not cross the Korean Peninsula.

In other words, the possibility that the southwestern part of Gyeonggi Massif might be correlated to South China Craton cannot be ruled out, but there is no continental collision belt that crosses the central region of the Korean peninsula from east to west. The presence of Gyemyeongsan Formation of about 860 Ma and Munjuri Formation of about 760 Ma, which consists of metavolcanics with the characteristic of A-1 type magma indicating continental rifting, suggests that the Okcheon Metamorphic Belt may have been produced in a failed rift. The Pirangdong Formation in North Korea and Hyangsanni Dolomite and Geumgang Limestone in South Korea are located in the eastern extension of the southern margin of North China Craton and show widespread traces of Neoproterozoic glaciation (Kim et al., 2016).

Taken together, during the Neoproterozoic, the northeastern part of the Okcheon metamorphic belt, including the Hyangsanni Dolomite, and the western part of the Gyeonggi Massif may also have been part of the Sino-Korean Craton along with the northeastern part of the Gyeonggi massif and the North China Craton. Therefore, such an occurrence of Neoproterozoic glaciation related sequence will unravel abstruse tectonic linkage between North and South China Craton and Korean Peninsula (Figure 5-14).

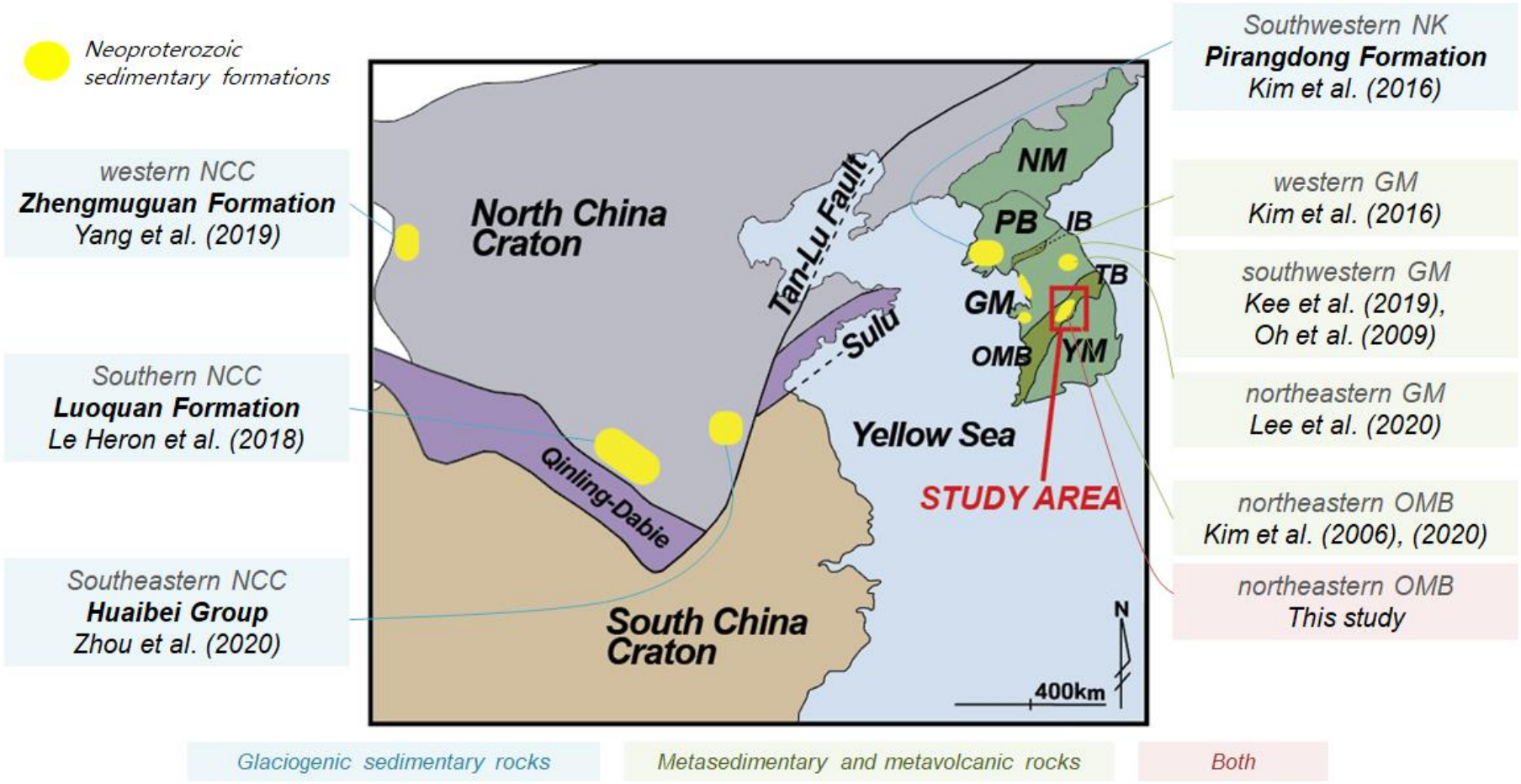

Figure 5-14. Schematic tectonic map of the northeast Asia. The areas marked in yellow are rough representations of areas where Neoproterozoic sedimentary formations are distributed in South Korea, North Korea, and North China Craton. From left, western (Zhengmuguan Formation; Yang et al., 2019), southern (Luoquan Formation; Le Heron et al., 2018), and southeastern (Huaibei Group; Zhou et al., 2020) North China Craton; southwestern (Pirangdong Formation; Kim et al., 2016) North Korea; western (Kim et al., 2016), southwestern (Kee et al., 2019; Oh et al., 2009), and northeastern Gyeonggi massif (Lee et al., 2020); and northeastern Okcheon metamorphic belt (Kim et al., 2006, 2020).

CHAPTER 6

Conclusion

In terms of the composition of trace and rare earth elements, the tectonic environment of the deposition of the Hyangsanni Dolomite is more similar to the continental margin than the open ocean. However, considering that some values span the range of inland freshwater, the influence of continental input seems to be greater than the general passive margin environment. In combination with the existing evidence of A-1 type magmatism in the Gyemyeongsan Formation suggesting a continental rifting (Ko et al., 2005), the Hyangsanni Dolomite was likely deposited in the rift basin when it was connected to the open ocean.

Based on fairly positive carbon isotope values (+2.9 to +6.2) and low $^{87}Sr/^{86}Sr$ initial ratios (minimum measured value is 0.7074), I suggest that the Hyangsanni Dolomite is a Neoproterozoic carbonate deposit, not Cambro-Ordovician as previously thought of. Therefore, the nearby Hwanggangni Formation, a diamictite deposit, is also likely a glacial deposit of Neoproterozoic. Considering the proposals that the nearby Hwanggangni Formation, a diamictite deposit (Choi and Woo, 2012; Kim et al., 2020; Reedman and Flecher, 1976) and the Seochangni Formation (Kim et al., 2020; Kim et al., 2021) are both of Neoproterozoic age, I suggest that the entire northeast Okcheon Metamorphic Belt excluding the Daehyangsan Quartzite is a Neoproterozoic sedimentary sequence deposited in a single rift basin. They may have been deposited in sedimentary basins created during rifting events indicated by A-type volcanics distributed in the Gyemyeongsan Formation and Munjuri Formation.

A-type magmatism of about 860 Ma, the occurrence of Mesoproterozoic detrital zircons, and the geographical distribution of Neoproterozoic sediments in contact with the Paleozoic sediments suggest that at least the northeastern region of the Okcheon Metamorphic Belt may correlate to the southern margin of North China Craton

In terms of carbon, oxygen and Sr isotope values, the Hyangsanni Dolomite is younger than the Early Tonian carbonate rocks but seems to be older than the Ediacaran ones occurring in the several basins in the North China Craton and North Korea. Therefore, further studies on the Hyangsanni Dolomite may play an important role in the studies related to carbonate rocks during the entire Neoproterozoic of the Sino- Korean Craton.

. This supports the possibility that at least the northeastern part of the Okcheon Metamorphic Belt

has evolved with the North as a single block of Sino-Korean Craton, suggesting the possibility that the so-called SKTL does not exist or is located west of the proposed current location.

Therefore, it can be another clue to untangling the Neoproterozoic tectonic connection between North and South China Cratons and Korean Peninsula. The redefinition of boundary between the Okcheon Metamorphic Belt and the Taebaeksan Basin will help understand the evolution of the integrated basin combining the Okcheon Metamorphic Belt and the Taebaeksan Basin from the Neoproterozoic to the Cambro-Ordovician and its correlation with the Pyeongnam Basin in North Korea.

REFERENCES

Bau, M. (1999). Scavenging of dissolved yttrium and rare earths by precipitating iron oxyhydroxide: experimental evidence for Ce oxidation, Y-Ho fractionation, and lanthanide tetrad effect. Geochimica et Cosmochimica Acta, 63(1), 67-77.

Bau, M., & Dulski, P. (1996). Distribution of yttrium and rare-earth elements in the Penge and Kuruman iron-formations, Transvaal Supergroup, South Africa. Precambrian Research 79, 37-55.

Cheong, C. H., Lee, D. Y., Ryu, Y. S., & Kang, K. W., (1979). Explanatory text of the geological map of Yeongwol Sheet, Sheet 6826-II, Scale 1:50,000. Geological Survey of Korea.

Cheong, C. S., Kee, W. S., Jeong, Y. J., & Jeong, G. Y. (2006). Multiple deformations along the Honam shear zone in southwestern Korea constrained by Rb–Sr dating of synkinematic fabrics: implications for the Mesozoic tectonic evolution of northeastern Asia. Lithos, 87(3-4), 289-299.

Cheong, W., Cho, M., Yi, K., Lee, M. S., & Kim, Y. (2016). Jurassic (~170Ma) Zircon U-Pb Age of a "Granite Boulder" in the Geumgang Limestone, Ogcheon Metamorphic Belt, Korea : Reinterpretation of its Origin 25, 29-37.

Cho, D. L., Suzuki, K., Adachi, M., & Chwae, U. (1996). A preliminary CHIME age determination of monazite from metamorphic and granitic rocks in the Gyeonggi massif, Korea. Journal of Earth and Planetary Sciences, Nagoya University, 43, 49-65.

Cho, M., Kim, T., & Kim, H. (2004). SHRIMP U-Pb zircon Age of a Felsic Meta-tuff in the Ogcheon Metamorhpic Belt, Korea: Neoproterozoic (ca. 750 Ma) Volcanism, Journal of the Petrological Society of Korea 13, 119-125. (in Korean with English abstract)

Cho, M., Cheong, W., Ernst, W.G., Yi, K., & Kim, J. (2013). SHRIMP U-Pb ages of detrital zircons in metasedimentary rocks of the central Ogcheon fold-thrust belt, Korea: Evidence for tectonic assembly of Paleozoic sedimentary protoliths. Journal of Asian Earth Sciences 63, 234-249.

Cho, M., Lee, Y., Kim, T., Cheong, W., Kim, Y., & Lee, S.R. (2017). Tectonic evolution of Precambrian basement massifs and an adjoining fold-and-thrust belt (Gyeonggi Marginal Belt), Korea: An overview. Geosciences Journal 21, 845-865.

Choi, D.K., & Chough, S.K. (2005). The Cambrian-Ordovician stratigraphy of the Taebaeksan Basin, Korea: a review. Geosciences Journal 9, 187-214.

Choi, D. K., Lee, J. G., Kim, D. H., Lee, S. B., Park, T. Y., & Hong, P. S. (2014). Early Paleozoic trilobite biostratigraphy of the Joseon Supergroup, Taebaeksan Basin, Korea: A synthesis. Journal of the Geological Society, 106-106.

Choi, D.K., Woo, J., & Park, T. (2012). The Okcheon Supergroup in the Lake Chungju area, Korea: Neoproterozoic volcanic and glaciogenic sedimentary successions in a rift basin. Geosciences Journal 16, 229-252.

Choi, J., E. (2013). SHRIMP U-Pb zircon ages of the Suchangri formation in Okcheon. MSc Thesis, Pukyong National University, Busan, Korea.

Chough, S., Kwon, S., Ree, J., & Choi, D. (2000). Tectonic and sedimentary evolution of the Korean peninsula: a review and new view. Earth-Science Reviews 52, 175-235.

Cluzel, D., Cadet, J. P., & Lapierre, H. (1990). Geodynamics of the Ogcheon belt (South Korea). Tectonophysics, 183(1-4), 41-56.

Cluzel, D. (1992). Late Paleozoic to early Mesozoic geodynamic evolution of the Circum-Pacific orogenic belt in South Korea and Southwest Japan. Earth and Planetary Science Letters 108, 289-305.

Cluzel, D., Jolivet, L., & Cadet, J. P. (1991). Early middle Paleozoic intraplate orogeny in the Ogcheon belt (South Korea): a new insight on the Paleozoic buildup of East Asia. Tectonics, 10(6), 1130-1151.

Cox, G.M., Halverson, G.P., Stevenson, R.K., Vokaty, M., Poirier, A., Kunzmann, M., Li, Z., Denyszyn, S.W., Strauss, J.V., & Macdonald, F.A. (2016). Continental flood basalt weathering as a trigger for Neoproterozoic Snowball Earth. Earth and Planetary Science Letters 446, 89-99.

Craig, H. (1953). The geochemistry of the stable carbon isotopes. Geochimica et cosmochimica acta, 3(2-3), 53-92.

Derry, L. A., & Jacobsen, S. B. (1990). The chemical evolution of Precambrian seawater: evidence from REEs in banded iron formations. Geochimica et Cosmochimica Acta, 54(11), 2965-2977.

Du, Q., Qin, Z., Wang, J., Wang, Z., Deng, Q., & Yang, F. (2020). The Cryogenian Nanhuan System (South China) during the interglacial-glacial transition: geochemistry, sedimentary provenance, and tectonic setting. International Geology Review, 1-19.

Elderfield, H., & Greaves, M.J. (1982). The rare earth elements in seawater. Nature 296, 214.

Ernst, W. G., & Liou, J. G. (1995). Contrasting plate-tectonic styles of the Qinling-Dabie-Sulu and Franciscan metamorphic belts. Geology, 23(4), 353-356.

Fairchild, I.J., & Kennedy, M.J. (2007). Neoproterozoic glaciation in the Earth System. Journal of the Geological Society 164, 895-921.

Fairchild, I.J., Spiro, B., Herrington, P.M., & Song, T. (2000). Controls on Sr and C isotope compositions of Neoproterozoic Sr-rich limestones of East Greenland and North China.

Frimmel, H.E. (2010). On the reliability of stable carbon isotopes for Neoproterozoic chemostratigraphic correlation. Precambrian Research 182, 239-253.

Geological Investigation Corps of Taebaeksan Region (1962) Report on the geology and mineral resources of the Taebaeksan Region. Geological Society of Korea, Seoul, 89 p. (in

Ha, Y., Satish-Kumar, M., Park, K. H., Song, Y. S., & Liu, S. (2021). Carbon, oxygen and strontium isotope geochemistry of the late Neoproterozoic carbonate platform deposit Hyangsanni Dolomite of the Okcheon metamorphic belt, Korea. Lithos, 396, 106219.

Halverson, G.P., Dudás, F.Ö., Maloof, A.C., & Bowring, S.A. (2007). Evolution of the $^{87}Sr/^{86}Sr$ composition of Neoproterozoic seawater. Palaeogeography, Palaeoclimatology, Palaeoecology 256, 103-129.

Halverson, G.P., Hoffman, P.F., Schrag, D.P., Maloof, A.C., & Rice, A.H.N. (2005). Toward a Neoproterozoic composite carbon-isotope record. GSA Bulletin 117, 1181-1207.

Halverson, G.P., Maloof, A.C., & Hoffman, P.F. (2004). The Marinoan glaciation (Neoproterozoic) in northeast Svalbard. Basin Research 16, 297-324.

Halverson, G.P., Porter, S.M., & Gibson, T.M. (2018). Dating the late Proterozoic stratigraphic record. Emerging topics in life sciences 2, 137-147.

Halverson, G.P., & Shields-Zhou, G. (2011). Chemostratigraphy and the Neoproterozoic glaciations. Geological Society, London, Memoirs 36, 51-66.

Halverson, G.P., Wade, B.P., Hurtgen, M.T., & Barovich, K.M. (2010). Neoproterozoic chemostratigraphy. Precambrian Research 182, 337-350.

Halverson, G.P., Hoffman, P.F., Schrag, D.P., & Kaufman, A.J. (2002). A major perturbation of the carbon cycle before the Ghaub glaciation (Neoproterozoic) in Namibia: Prelude to snowball Earth?. Geochemistry, Geophysics, Geosystems 3, 1-24.

Higgins, J. A., Blättler, C. L., Lundstrom, E. A., Santiago-Ramos, D. P., Akhtar, A. A., Ahm, A. C., & Swart, P. K. (2018). Mineralogy, early marine diagenesis, and the chemistry of shallow-water carbonate sediments. Geochimica et Cosmochimica Acta, 220, 512-534.

Hoffman, P.F., Kaufman, A.J., Halverson, G.P., & Schrag, D.P. (1998). A Neoproterozoic snowball earth. Science (New York, N.Y.) 281, 1342-1346.

Hohl, S.V., Becker, H., Jiang, S., Ling, H., Guo, Q., & Struck, U. (2017). Geochemistry of Ediacaran cap dolostones across the Yangtze Platform, South China: implications for diagenetic modification and seawater chemistry in the aftermath of the Marinoan glaciation. Journal of the Geological Society 174, 893-912.

Hu, B., Zhai, M., Li, T., Li, Z., Peng, P., Guo, J., & Kusky, T.M. (2012). Mesoproterozoic magmatic events in the eastern North China Craton and their tectonic implications: Geochronological evidence from detrital zircons in the Shandong Peninsula and North Korea. Gondwana Research 22, 828-842.

Hudson, J. D., & Anderson, T. F. (1989). Ocean temperatures and isotopic compositions through time. Earth and Environmental Science Transactions of the Royal Society of Edinburgh, 80(3-4), 183-192.

Jacobsen, S.B., & Kaufman, A.J. (1999). The Sr, C and O isotopic evolution of Neoproterozoic seawater. Chemical Geology 161, 37-57.

Jiang, G., Kaufman, A.J., Christie-Blick, N., Zhang, S., & Wu, H. (2007). Carbon isotope variability across the Ediacaran Yangtze platform in South China: implications for a large surface-to-deep ocean $\delta^{13}C$ gradient. Earth and Planetary Science Letters 261, 303-320.

Jiang, G., Kennedy, M.J., & Christie-Blick, N. (2003). Stable isotopic evidence for methane seeps in Neoproterozoic postglacial cap carbonates. Nature 426, 822.

Jones, C. E., & Jenkyns, H. C. (2001). Seawater strontium isotopes, oceanic anoxic events, and seafloor hydrothermal activity in the Jurassic and Cretaceous. American Journal of Science, 301(2), 112-149.

Kaufman, A.J., Hayes, J., Knoll, A.H., & Germs, G.J. (1991). Isotopic compositions of carbonates and organic carbon from upper Proterozoic successions in Namibia: stratigraphic variation and the effects of diagenesis and metamorphism. Precambrian Research 49, 301-327.

Kaufman, A. J., Jacobsen, S. B., & Knoll, A. H. (1993). The Vendian record of Sr and C isotopic variations in seawater: implications for tectonics and paleoclimate. Earth and Planetary Science Letters, 120(3-4), 409-430.

Kaufman, A.J., & Knoll, A.H. (1995). Neoproterozoic variations in the C-isotopic composition of seawater: stratigraphic and biogeochemical implications. Precambrian Research 73, 27-49.

Kaufman, A. J., Knoll, A. H., & Narbonne, G. M. (1997). Isotopes, ice ages, and terminal Proterozoic earth history. Proceedings of the National Academy of Sciences, 94(13), 6600-6605.

Kaufman, A. J., Sial, A. N., Frimmel, H. E., & Misi, A. (2009). Neoproterozoic to Cambrian palaeoclimatic events in southwestern Gondwana. Developments in Precambrian Geology, 16, 369-388.

Kang, J. H. (1994). Geological structure and tectonics of the Ogcheon zone in the Chungju-Jangseonri area, South Korea. Journal of Science (Hiroshima University) C, 10, 11-23.

Kang, J., Lee, D., Noh, S., Jeong, J., & Koh, S. (2017). Geology and constituent rocks of the Chungju-Goesan area in the northwestern part of Ogcheon metamorphic zone, Korea: Considering on the history of igneous activities accompanying formation and evolution processes of the Ogcheon rift basin. Journal of the geological society of korea 53, 51-77. (in Korean with English abstract)

Kamber, B. S., Greig, A., & Collerson, K. D. (2005). A new estimate for the composition of weathered young upper continental crust from alluvial sediments, Queensland, Australia. Geochimica et Cosmochimica Acta, 69(4), 1041-1058.

Kamber, B. S., & Webb, G. E. (2001). The geochemistry of late Archaean microbial carbonate: implications for ocean chemistry and continental erosion history. Geochimica et Cosmochimica Acta, 65(15), 2509-2525.

Kee, W., Kim, S.W., Kwon, S., Santosh, M., Ko, K., & Jeong, Y. (2019). Early Neoproterozoic (ca. 913–895 Ma) arc magmatism along the central–western Korean Peninsula: Implications for the amalgamation of Rodinia supercontinent. Precambrian Research 335, 105498.

Kennedy, M. J. (1996). Stratigraphy, sedimentology, and isotopic geochemistry of Australian Neoproterozoic postglacial cap dolostones; deglaciation, delta ^{13}C excursions, and carbonate precipitation. Journal of sedimentary Research, 66(6), 1050-1064.

Kennedy, M.J., & Christie-Blick, N. (2011). Condensation origin for Neoproterozoic cap carbonates during deglaciation. Geology 39, 319-322.

Kennedy, M.J., Christie-Blick, N., & Prave, A.R. (2001). Carbon isotopic composition of Neoproterozoic glacial carbonates as a test of paleoceanographic models for snowball Earth phenomena. Geology 29, 1135-1138.

Kennedy, M.J., Runnegar, B., Prave, A.R., Hoffmann, K., & Arthur, M.A. (1998). Two or four Neoproterozoic glaciations?. Geology 26, 1059-1063.

Kihm, Y. H., Kim, J. H., & Lee, J. U. (1999). Geological structures of the Choseon and Ogcheon Supergroups in the Deoksan-Cheongpung area, Jecheon-gun, Chungcheongbuk-do. Korea. Journal of the Geological Society of Korea, 35, 233-252. (in Korean with English abstract)

Kihm, Y., H., Kim, J., H., & Koh, H., J. (1996). Geology of the Deogsan-myeon area, Jecheon-gun, Chungcheongbuk-do, Korea: contact between the Choseon and Ogcheon supergroups 32, 483-499. (in Korean with English abstract)

Kim, D.H., Chang, T.W., Kim, W.Y., & Hwang, J.H., (1978). Geologicmap of Korea, Okcheon Sheet (1:50,000). Korea Research Institute of Geoscience and Mineral Resources.

Kim, D.H., & Choi, D.K. (2000). Lithostratigraphy and biostratigraphy of the Mungok Formation (Lower Ordovician), Youngwol, Korea. Geosciences Journal, 4(4), 301-311.

Kim, H. S. (1971). Metamorphic facies and regional metamorphism of Ogcheon metamorphic belt. Geological Society of Korea 3, 7(4), 221-256. (in Korean with English abstract)

Kim, J.,N., Han., R.,Y., Zhao, L., Li., Q.,L., & Kim, S.,S (2016). Study on the petrographic and SIMS zircon U-Pb geochronological characteristics of the magmatic rocks associated with the Jongju and Cholsan REE deposits in northern Korean Peninsula. (in Chinese with English abstract)

Kim, K.,H. (1980). Carbon and Oxygen Isotope Studies of the Paleozoic Limestones from the Taebaegsan Region, South Korea 13, 21-27. (in Korean with English abstract)

Kim, K.W., & Lee, H.,K. (1965). Geological Report of the Chungju Sheet (1:50,000). Geological Survey of Korea, 35p. (in Korean)

Kim, K.W., Park, B.S., & Lee, H.K., (1967). Explanatory text of the geological map of Jecheon Sheet, Sheet 6825-III, Scale 1:50,000. Geological Survey of Korea, 46p.

Kim, M.G., & Lee, Y.I., (2018). The Pyeongan Supergroup (upper Paleozoic–Lower Triassic) in the Okcheon Belt, Korea: A review of stratigraphy and detrital zircon provenance, and its implications for the tectonic setting of the eastern Sino-Korean Block. Earth-Science Reviews 185, 1170-1186.

Kim, M. J., Park, K. H., Yi, K., & Koh, S. M. (2013). Timing of metamorphism of the metavoclanics within the Gyemyeongsan Formation. The Journal of the Petrological Society of Korea, 22(4), 291-298. (in Korean with English abstract)

Kim, M. J., Ha, Y., Choi, J. E., Park, K. H., Song, Y. S., & Liu, S. (2021). U-Pb ages and Hf isotopic compositions of detrital zircons from the Seochangni Formation of the northeastern Okcheon Metamorphic Belt: Implications to the crustal evolution of the Sino-Korean craton since Paleoproterozoic. Lithos, 106340.

Kim, O. J. (1968). Stratigraphy and tectonics of Okcheon System in the area between Chungju and Munkyeong. Economic and Environmental Geology, 1(1), 35-46. (in Korean with English abstract)

Kim, O.J., Lee, H.Y., Lee, D.S., & Yun, S. (1973). The Stratigraphy and Geologic Structure of the Great Limestone Series in South Korea. Journal of the Korean Institute of Mining Geology, 6(2), 81-114. (in Korean with English abstract)

Kim, O. J., Min, K. D., & Kim, K. H. (1986). Geology and Mineral Resources of the Okchŏn Zone-The Boundary between the Okchŏn and Chosŏn Systems in the South of Jechŏn, and the Geology in its Vicinity. Economic and Environmental Geology, 19(3), 225-230. (in Korean with English abstract)

Kim, S.W., Cho, D., Lee, S., Kwon, S., Park, S., Santosh, M., & Kee, W. (2018). Mesoproterozoic magmatic suites from the central-western Korean Peninsula: Imprints of Columbia disruption in East Asia. Precambrian Research 306, 155-173.

Kim, S.W., Kee, W.S., Santosh, M., Cho, D., Hong, P.S., Ko, K., Lee, B.C., Byun, U.H., & Jang, Y. (2020). Tracing the Precambrian tectonic history of East Asia from Neoproterozoic sedimentation and magmatism in the Korean Peninsula. Earth-Science Reviews, 103311.

Kim, S.W., Kee, W., Lee, S.R., Santosh, M., & Kwon, S. (2013b). Neoproterozoic plutonic rocks from the western Gyeonggi massif, South Korea: implications for the amalgamation and break-up of the Rodinia supercontinent. Precambrian Research 227, 349-367.

Kim, S.W., Kwon, S., Koh, H.J., Yi, K., Jeong, Y., & Santosh, M., (2011). Geotectonic framework of Permo–Triassic magmatism within the Korean Peninsula. Gondwana Research. 20, 865–889.

Kim, S. W., Kwon, S., Santosh, M., Cho, D. L., Kee, W. S., Lee, S. B., & Jeong, Y. J. (2019). Detrital zircon U-Pb and Hf isotope characteristics of the Early Neoproterozoic successions in the central-western Korean Peninsula: Implication for the Precambrian tectonic history of East Asia. Precambrian Research, 322, 24-41.

Kim, S.W., Oh, C.W., Ryu, I., Williams, I., Sajeev, K., Santosh, M., & Rajesh, V. (2006). Neoproterozoic bimodal volcanism in the Okcheon Belt, South Korea, and its comparison with the Nanhua Rift, South China: implications for rifting in Rodinia. The Journal of geology 114, 717-733.

Kim, S.W., Park, S., Jang, Y., Kwon, S., Kim, S.J., & Santosh, M. (2017). Tracking Paleozoic evolution of the South Korean Peninsula from detrital zircon records: Implications for the tectonic history of East Asia. Gondwana Research 50, 195-215.

Kim, S. W., Williams, I. S., Kwon, S., & Oh, C. W. (2008). SHRIMP zircon geochronology, and geochemical characteristics of metaplutonic rocks from the south-western Gyeonggi Block, Korea: Implications for Paleoproterozoic to Mesozoic tectonic links between the Korean Peninsula and eastern China. Precambrian Research, 162(3-4), 475-497.

Ryu, I. C., & Kim, T. H. (2009). Stratigraphy and geological structure of the northwestern Okcheon metamorphic belt near the Chungju area. Economic and Environmental Geology, 42(1), 9-25. (in Korean with English abstract)

Kirschvink, J.L. (1992). Late Proterozoic low-latitude global glaciation: the snowball Earth.

Knauth, L.P., & Kennedy, M.J. (2009). The late Precambrian greening of the Earth. Nature 460, 728-732.

Knoll, A. H., & Walter, M. R. (1992). Latest Proterozoic stratigraphy and Earth history. Nature, 356(6371), 673-678.

Kobayashi, T. (1966). The Cambro-Ordovician formations and faunas of South Korea. Part X. stratigraphy of Chosen Group in Korea and South Manchuria and its relation to the Cambro-Ordovician formations of other areas. Sect. A. The Chose Group of South Korea. Journal of the Faculty of Science, University of Tokyo, Section II, 16, 1-84.

Kobayashi, T., Yosimura, I., Iwaya, Y., & Hukasawa, T. (1942). 115. The Yokusen Geosyncline in the Chosen Period Brief Notes on the Geologic History of the Yokusen Orogenic Zone, 1. Proceedings of the Imperial Academy, 18(9), 579-584.

Koh, S. M., Kim, J. H., & Park, K. H. (2005). Neoproterozoic A-type volcanic activity within the Okcheon Metamorphic Belt. The Journal of the Petrological Society of Korea, 14(3), 157-168. (in Korean with English abstract)

Kuznetsov, A. B., Gorokhov, I. M., Melezhik, V. A., Mel'nikov, N. N., Konstantinova, G. V., & Turchenko, T. L. (2012). Strontium isotope composition of the lower proterozoic carbonate concretions: The Zaonega Formation, Southeast Karelia. Lithology and Mineral Resources, 47(4), 319-333.

Kroopnick, P. M. (1985). The distribution of 13C of ΣCO2 in the world oceans. Deep Sea Research Part A. Oceanographic Research Papers, 32(1), 57-84.

Kwon, S.-T., Sajeev, K., Mitra, G., Park, Y., Kim, S.W., & Ryu, I. (2009). Evidence for Permo-Triassic collision in far east Asia: the Korean collisional orogen. Earth and Planetary Science Letters 279, 340-349.

Kwon, Y. K., Chough, S. K., Choi, D. K., & Lee, D. J. (2006). Sequence stratigraphy of the Taebaek Group (Cambrian–Ordovician), mideast Korea. Sedimentary Geology, 192(1-2), 19-55.

Kwon, Y. K., Kwon, Y. J., Yeo, J. M., & Lee, C. Y. (2019). Basin Evolution of the Taebaeksan Basin during the Early Paleozoic. Economic and Environmental Geology, 52(5), 427-448. (in Korean with English abstract)

Lawrence, M.G., Greig, A., Collerson, K.D., & Kamber, B.S. (2006a). Rare earth element and yttrium variability in South East Queensland waterways. Aquatic Geochemistry 12, 39-72.

Lawrence, M.G., & Kamber, B.S. (2006b). The behaviour of the rare earth elements during estuarine mixing-revisited. Marine Chemistry 100, 147-161.

Le Heron, D.P., Eyles, N., & Busfield, M.E. (2020). The Laurentian Neoproterozoic Glacial Interval: reappraising the extent and timing of glaciation. Austrian Journal of Earth Sciences 113, 59-70.

Le Heron, D.P., Vandyk, T.M., Kuang, H., Liu, Y., Chen, X., Wang, Y., Yang, Z., Scharfenberg, L., Davies, B., & Shields, G. (2019). Bird's-eye view of an Ediacaran subglacial landscape. Geology 47, 705-709.

Le Heron, D.P., Vandyk, T.M., Wu, G., & Li, M. (2018). New perspectives on the Luoquan Glaciation (Ediacaran-Cambrian) of North China. The Depositional Record 4, 274-292.

Lee, C.H., & Kim, J.H., 1972, Geologic map of Korea, Goesan Sheet (1:50,000). Geological Survey of Korea (in Korean).

Lee, H., M., (2013). Geochemical and isotopic characteristics of the Pirrit Hills granite in West Antarctica (Ph.D. Thesis). Kongju National University, Chungcheongnamdo, Korea.

Lee, J.G. (1995). Late Cambrian Trilobites from the Machari Formation, Yeongweol, Korea: (Ph.D. Thesis). Seoul National University, Seoul, Korea.

Lee, B. Y., Oh, C. W., Lee, S. H., Seo, J., & Yi, K. (2020). Ages and tectonic settings of the Neoproterozoic igneous rocks in the Gyeonggi Massif of the southern Korean Peninsula and the correlation with the Neoproterozoic igneous rocks in China. Lithos, 370, 105625.

Lee, C. H., Lee, M. S., & Park, B., S., (1980). Explanatory notice of the 1:50,000 geologic map of Korea, Miweon sheet. Korea Research Institute of Geoscience and Mineral Resource, Seoul. 29p. (in Korean with English summary)

Lee, H., G., Yu, E. G., & Hong, S. H., (1971). Explanatory notice of the 1:50,000 geologic map of Korea, Yongyuri sheet. Korea Research Institute of Geoscience and Mineral Resource, Seoul. 29p. (in Korean with English summary)

Lee, H.S., & Chough, S.K. (2006). Sequence stratigraphy of Pyeongan Supergroup (Carboniferous-Permian), Taebaek area, mideast Korea. Geosciences Journal 10, 369.

Lee, M. S., Yeo, J. P., Lee, J. I., Jwa, Y. J., Yoshida, S., & Lee, H. Y. (1998). Glaciogenic diamictite of Ogcheon System and its geologic age, and paleogeography of Korean Peninsula in Late Paleozoic. Journal of the Geological Society of Korea, 34, 343-370. (in Korean with English abstract)

Lee, K. S., Chang, H. W., & Park, K. H. (1998). Neoproterozoic bimodal volcanism in the central Ogcheon belt, Korea: age and tectonic implication. Precambrian Research, 89(1-2), 47-57.

Lee, K., Chang, H., & Park, K. (1998). Neoproterozoic bimodal volcanism in the central Ogcheon belt, Korea: age and tectonic implication. Precambrian Research 89, 47-57.

Lee, M.S., & Park, B.S. (1965) Explanatory text of the geological map of Hwanggang-ni Sheet, Sheet 6825-III, Scale 1:50,000. Geological Survey of Korea, 43p.

Lee, M., Yeo, J., Lee, J., Jwa, Y., Yoshida, S., & Lee, H. (1998). Glaciogenic diamictite of Ogcheon System and its geologic age, and paleogeography of Korean Peninsula in Late Paleozoic. Journal of the Geological Society of Korea 34, 343-370.

Lee, W.K. (1983) Sedimentary Petrological Study on the Heungwolri Formation. Journal of the Geological Society of Korea, 19, 190-202.

Li, L., Yun, H., & Zhang, X. (2018). Precambrian-Cambrian transition in the southern margin of North China.

Li, Z., Evans, D.A., & Halverson, G.P. (2013). Neoproterozoic glaciations in a revised global palaeogeography from the breakup of Rodinia to the assembly of Gondwanaland. Sedimentary Geology 294, 219-232.

Li, Z. X., Zhang, L., & Powell, C. M. (1996). Positions of the East Asian cratons in the Neoproterozoic supercontinent Rodinia. Australian Journal of Earth Sciences, 43(6), 593-604.

Ling, H., Chen, X., Li, D., Wang, D., Shields-Zhou, G.A., & Zhu, M. (2013). Cerium anomaly variations in Ediacaran–earliest Cambrian carbonates from the Yangtze Gorges area, South China: implications for oxygenation of coeval shallow seawater. Precambrian Research 225, 110-127.

Lim, J. N., Chung, G. S., Park, T. Y. S., & Lee, K. S. (2015). Lithofacies and stable carbon isotope stratigraphy of the Cambrian Sesong Formation in the Taebaeksan Basin, Korea. Journal of the Korean earth science society, 36(7), 617-631. (in Korean with English abstract)

Lim, S. B., Chun, H. Y., Kim, Y. B., Kim, B. C., & Cho, D. L. (2005). Geologic ages, stratigraphy and geological structures of the metasedimentary strata in Bibong similar to Yeonmu area, NW

Okcheon belt, Korea. Journal of the Geological Society of Korea, 41(3), 335-368. (in Korean with English abstract)

Lim, S.-B., Chun, H.-Y., Kim, Y.B., Kim, B.C., & Song, K.-Y. (2006). Stratigraphy and geological ages of the metasedimentary strata in Jinsan~Boksu area, Chungcheongnam-do, NW Okcheon belt. Journal of the Geological Society of Korea, 42, 149-174. (in Korean with English abstract)

Lim, S.-B., Chun, H.-Y., Kim, Y.B., Lee, S.R., & Kee, W.-S. (2007). Geological ages and stratigraphy of the metasedimentary strata in Hoenam~Miwon area, NW Okcheon belt. Journal of the Geological Society of Korea, 43, 125-150. (in Korean with English abstract)

Lim, S. W., & Woo, K. S. (1995). The origin of the dolomite of the Pungchon Formation near Taebaeg City, Kangwondo, Korea. The Korean Journal of Petroleum Geology, 3(1), 28-39. (in Korean with English abstract)

Liu, S., Zhang, J., Li, Q., Zhang, L., Wang, W., & Yang, P. (2012). Geochemistry and U–Pb zircon ages of metamorphic volcanic rocks of the Paleoproterozoic Lüliang Complex and constraints on the evolution of the Trans-North China Orogen, North China Craton. Precambrian Research, 222, 173-190.

Macdonald, F.A., Jones, D.S., & Schrag, D.P. (2009). Stratigraphic and tectonic implications of a newly discovered glacial diamictite–cap carbonate couplet in southwestern Mongolia. Geology 37, 123-126.

Macdonald, F. A., Smith, E. F., Strauss, J. V., Cox, G. M., Halverson, G. P., Roots, C. F., & Relf, C. (2010). Neoproterozoic and early Paleozoic correlations in the western Ogilvie Mountains, Yukon. Yukon Exploration and Geology, 161-182.

McLennan, S.M. (1989) Rare Earth Elements in Sedimentary Rocks. Influence of Provenance and Sedimentary Processes. Reviews in Mineralogy, 21, 169-200.

McLennan, S.M., Nance, W.B., & Taylor, S.R., (1980). Rare earth element-thorium correlations in sedimentary rocks, and the composition of the continental crust. Geochim. Cosmochim. Acta, 44: 833-1840.

McArthur, J. M., Howarth, R. J., & Shields, G. A. (2012). Strontium isotope stratigraphy. The geologic time scale, 1, 127-144.

McFadden, K.A., Huang, J., Chu, X., Jiang, G., Kaufman, A.J., Zhou, C., Yuan, X., & Xiao, S. (2008). Pulsed oxidation and biological evolution in the Ediacaran Doushantuo Formation. Proceedings of the National Academy of Sciences of the United States of America 105, 3197-3202.

McKenzie, J.A. (1981). Holocene dolomitization of calcium carbonate sediments from the coastal sabkhas of Abu Dhabi, UAE: a stable isotope study. The Journal of geology 89, 185-198.

Meert, J.G., & Torsvik, T.H. (2004). Paleomagnetic constraints on Neoproterozoic ‘Snowball Earth’ continental reconstructions. The extreme Proterozoic: geology, geochemistry, and climate. AGU Geophysical Monograph Series 146, 5-11.

Melezhik, V., Bingen, B., Fallick, A., Gorokhov, I., Kuznetsov, A., Sandstad, J., Solli, A., Bjerkgård, T., Henderson, I., & Boyd, R. (2008). Isotope chemostratigraphy of marbles in northeastern Mozambique: apparent depositional ages and tectonostratigraphic implications. Precambrian Research 162, 540-558.

Melezhik, V. A., Gorokhov, I. M., Fallick, A. E., & Gjelle, S. (2001). Strontium and carbon isotope geochemistry applied to dating of carbonate sedimentation: an example from high-grade rocks of the Norwegian Caledonides. Precambrian Research, 108(3-4), 267-292.

Melezhik, V. A., Gorokhov, I. M., Kuznetsov, A. B., & Fallick, A. E. (2001). Chemostratigraphy of Neoproterozoic carbonates: implications for 'blind dating'. Terra Nova, 13(1), 1-11.

Melezhik, V., Roberts, D., Fallick, A., Gorokhov, I., & Kusnetzov, A. (2005). Geochemical preservation potential of high-grade calcite marble versus dolomite marble: implication for isotope chemostratigraphy. Chemical Geology 216, 203-224.

Meng, E., Liu, F. L., Liu, P. H., Liu, C. H., Yang, H., Wang, F., & Cai, J. (2014). Petrogenesis and tectonic significance of Paleoproterozoic meta-mafic rocks from central Liaodong Peninsula, northeast China: evidence from zircon U–Pb dating and in situ Lu–Hf isotopes, and whole-rock geochemistry. Precambrian Research, 247, 92-109.

Min, K., & Cho, M. (1998). Metamorphic evolution of the northwestern Ogcheon metamorphic belt, South Korea. Lithos 43, 31-51.

Miyazaki, T., & Shuto, K. (1998). Sr and Nd isotope ratios of twelve GSJ rock reference samples. Geochemical Journal 32, 345-350.

Montañez, I.P., Osleger, D.A., Banner, J.L., Mack, L.E., & Musgrove, M. (2000). Evolution of the Sr and C isotope composition of Cambrian oceans. GSA today 10, 1-7.

Neo, N., Takazawa, E., & Shuto, K. (2006). Quantitative analysis of trace elements in basaltic and peridotitic rocks by quadruple inductively–coupled plasma mass spectrometry. Report of Grant–in–Aid for Scientific Research (C), (16540413), 79-94.

Nogueira, A.C., Riccomini, C., Sial, A.N., Moura, C.A., Trindade, R.I., & Fairchild, T.R. (2007). Carbon and strontium isotope fluctuations and paleoceanographic changes in the late Neoproterozoic Araras carbonate platform, southern Amazon craton, Brazil. Chemical Geology 237, 168-190.

Nozaki, Y., Zhang, J., & Amakawa, H. (1997). The fractionation between Y and Ho in the marine environment. Earth and Planetary Science Letters 148, 329-340.

Oh, C.W., Choi, S.-G., Seo, J., Rajesh, V.J., Lee, J.H., Zhai, M., & Peng, P., (2009). The tectonic evolution of the Gogunsan Islands in the southwestern margin of the Gyeonggi Massif and its implication for the Neoproterozoic tectonic evolution relating to the Rodinia in the Northeast Asia. Gondwana Research. 16, 272–284.

Oh, C. W., Lee, B. C., Yi, S. B., & Ryu, H. I. (2019). Correlation of Paleoproterozoic igneous and metamorphic events of the Korean Peninsula and China; Its implication to the tectonics of Northeast Asia. Precambrian Research, 326, 344-362.

Oh, C.W. (2006). A new concept on tectonic correlation between Korea, China and Japan: histories from the late Proterozoic to Cretaceous. Gondwana Research 9, 47-61.

Oh, C.W., & Kusky, T. (2007). The Late Permian to Triassic Hongseong-Odesan collision belt in South Korea, and its tectonic correlation with China and Japan. International Geology Review 49, 636-657.

Otsuji, N. (2013). Late-Tonian to early-Cryogenian apparent depositional ages for metacarbonate rocks from the Sør Rondane Mountains, East Antarctica, 413.

Park, B. K., & Woo, K. S. (1986). Carbon and oxygen isotope composition of the Middle Cambrian Pungchon Limestone Formation. Korea. Journal of the Geological Society of Korea, 22, 40-52. (in Korean with English abstract)

Park, B. S., & Yeo, S. C. (1971). Explanatory text of the geological map of Moggye sheet. Geological Survey of Korea, 40. (in Korean)

Park, K., Choi, D.K., & Kim, J.H. (1994). The Mungog Formation (Lower Ordovician) in the northern part of Yeongweol area: lithostratigraphic subdivision and trilobite faunal assemblages. Journal of the Geological Society of Korea, 30(2), 168-181. (in Korean with English abstract)

Park, S., Kim, S.W., Kwon, S., Santosh, M., Ko, K., & Kee, W. (2017). Nature of Late Mesoproterozoic to Early Neoproterozoic magmatism in the western Gyeonggi massif, Korean Peninsula and its tectonic significance. Gondwana Research 47, 291-307.

Park, K. H. (2011). SHRIMP U-Pb ages of detrital zircons in the Daehyangsan Quartzite of the Okcheon Metamorphic Belt. Journal of the Geological Society of Korea, 47, 423-431. (in Korean with English abstract)

Peng, P., Zhai, M., Li, Q., Wu, F., Hou, Q., Li, Z., Li, T., & Zhang, Y. (2011). Neoproterozoic (~ 900 Ma) Sariwon sills in North Korea: Geochronology, geochemistry and implications for the evolution of the south-eastern margin of the North China Craton. Gondwana Research 20, 243-254.

Ramkumar, M. (2015). Toward standardization of terminologies and recognition of chemostratigraphy as a formal stratigraphic method. In *Chemostratigraphy* (pp. 1-21). Elsevier.

Ree, J. H., Cho, M., Kwon, S. T., & Nakamura, E. (1996). Possible eastward extension of Chinese collision belt in South Korea: the Imjingang belt. Geology, 24(12), 1071-1074.

Ree, J.-H., Kwon, S.-H., Park, Y., Kwon, S.-T., & Park, S.-H. (2001). Pretectonic and posttectonic emplacements of the granitoids in the south central Okchon belt, South Korea: Implications for the timing of the strike-slip shearing and thrusting. Tectonics, 20, 850–867.

Reedman, A. J., Fletcher, C. J. N., Evans, R. B., Workman, D. R., Yoon, K. S., Rhyu, H. S., ... & Park, J. N. (1973). Geology of the Hwanggangri mining district, Republic of Korea. Anglo-Korean Mineral Exploration Group, 119p.

Reedman, A. J., & Fletcher, C. J. N. (1976). Tillites of the Ogcheon Group and their stratigraphic significance. Journal of the Geological Society of Korea, 12(3), 107-112.

Riccomini, C., Nogueira, A.C., & Sial, A.N. (2007). Carbon and oxygen isotope geochemistry of Ediacaran outer platform carbonates, Paraguay Belt, central Brazil. Anais da academia Brasileira de Ciências 79, 519-527.

Rooney, A.D., Strauss, J.V., Brandon, A.D., & Macdonald, F.A. (2015) A Cryogenian chronology: two long-lasting synchronous Neoproterozoic glaciations. Geology 43, 459–462

Ryu, Y., & Ahn, J. (2016). A test for Snowball Earth hypothesis in Korean peninsula by analyzing stable carbon isotopes of carbonates from the Okcheon Supergroup. Journal of the geological society of korea 52, 829-845. (in Korean with English abstract)

Saltzman, M., & Thomas, E. (2012). Carbon isotope stratigraphy. The geologic time scale 1, 207-232.

Sansjofre, P., Ader, M., Trindade, R., Elie, M., Lyons, J., Cartigny, P., & Nogueira, A. (2011). A carbon isotope challenge to the snowball Earth. Nature 478, 93-96.

Sawaki, Y., Ohno, T., Tahata, M., Komiya, T., Hirata, T., Maruyama, S., Windley, B.F., Han, J., Shu, D., & Li, Y. (2010). The Ediacaran radiogenic Sr isotope excursion in the Doushantuo Formation in the three Gorges area, South China. Precambrian Research 176, 46-64.

Schrag, D.P., Berner, R.A., Hoffman, P.F., & Halverson, G.P. (2002). On the initiation of a snowball Earth. Geochemistry, Geophysics, Geosystems 3, 1-21.

Shen, B., Xiao, S., Kaufman, A.J., Bao, H., Zhou, C., & Wang, H. (2008). Stratification and mixing of a post-glacial Neoproterozoic ocean: evidence from carbon and sulfur isotopes in a cap dolostone from northwest China. Earth and Planetary Science Letters 265, 209-228.

Shen, B., Xiao, S., Zhou, C., Kaufman, A.J., & Yuan, X. (2010). Carbon and sulfur isotope chemostratigraphy of the Neoproterozoic Quanji Group of the Chaidam Basin, NW China: Basin stratification in the aftermath of an Ediacaran glaciation postdating the Shuram event?. Precambrian Research 177, 241-252.

Shen, Y., Zhang, T., & Chu, X. (2005). C-isotopic stratification in a Neoproterozoic postglacial ocean. Precambrian Research 137, 243-251.

Shields, G.A. (2007). A normalised seawater strontium isotope curve: possible implications for Neoproterozoic-Cambrian weathering rates and the further oxygenation of the Earth. EEarth 2, 35-42.

Shields, G.A., & Veizer, J. (2002). Precambrian marine carbonate isotope database: Version 1.1.

Shin, W. J., Choi, S. H., Ryu, J. S., Song, B. Y., Song, J. H., Park, S., & Min, J. S. (2018). Discrimination of the geographic origin of pork using multi-isotopes and statistical analysis. Rapid Communications in Mass Spectrometry, 32(21), 1843-1850.

Sial, A. N., Campos, M. S., Gaucher, C., Frei, R., Ferreira, V. P., Nascimento, R. C., & Rodler, A. (2015). Algoma-type Neoproterozoic BIFs and related marbles in the Seridó Belt (NE Brazil): REE, C, O, Cr and Sr isotope evidence. Journal of South American Earth Sciences, 61, 33-52.

Slack, J. F., Grenne, T., Bekker, A., Rouxel, O. J., & Lindberg, P. A. (2007). Suboxic deep seawater in the late Paleoproterozoic: evidence from hematitic chert and iron formation related to seafloor-hydrothermal sulfide deposits, central Arizona, USA. Earth and Planetary Science Letters, 255(1-2), 243-256.

Son, J. W., & Choi, D. K. (2005). Revision of the upper Cambrian trilobite biostratigraphy of the Sesong and Hwajeol formations, Taebaek group, Korea. Journal of Paleothological society of Korea, 21(2), 195. (in Korean with English abstract)

Son, J.W., Kim, D.H., & Choi, D.K. (2001). Stratigraphy of the Cambro-Ordovician Strata in the Mt. Samtae area, Danyang, Korea. Journal of the Paleontological Society of Korea, 17, 23-34. (in Korean with English abstract)

Suzuki, K., Dunkley, D., Adachi, M., & Chwae, U. (2006). Discovery of a c. 370 Ma granitic gneiss clast from the Hwanggangri pebble-bearing phyllite in the Okcheon metamorphic belt, Korea. Gondwana Research, 9(1-2), 85-94.

Tahata, M., Ueno, Y., Ishikawa, T., Sawaki, Y., Murakami, K., Han, J., Shu, D., Li, Y., Guo, J., & Yoshida, N. (2013). Carbon and oxygen isotope chemostratigraphies of the Yangtze platform, South China: decoding temperature and environmental changes through the Ediacaran. Gondwana Research 23, 333-353.

Takahashi, T., Hirahara, Y., Miyazaki, T., Vaglarov, B. S., Chang, Q., Kimura, J. I., & Tatsumi, Y. (2009). Precise determination of Sr isotope ratios in igneous rock samples and application to micro-analysis of plagioclase phenocrysts. JAMSTEC Report of Research and Development, 2009, 59-64.

Tam, P. Y., Zhao, G., Zhou, X., Sun, M., Guo, J., Li, S., & He, Y. (2012). Metamorphic P–T path and implications of high-pressure pelitic granulites from the Jiaobei massif in the Jiao-Liao-Ji Belt, North China Craton. Gondwana Research, 22(1), 104-117.

Tang, H., Chen, Y., Santosh, M., Zhong, H., Wu, G., & Lai, Y. (2013). C–O isotope geochemistry of the Dashiqiao magnesite belt, North China Craton: implications for the Great Oxidation Event and ore genesis. Geological Journal 48, 467-483.

Valley, J. W. (2001). Stable isotope thermometry at high temperatures. Reviews in mineralogy and geochemistry, 43(1), 365-413.

Veizer, J., Ala, D., Azmy, K., Bruckschen, P., Buhl, D., Bruhn, F., Carden, G.A., Diener, A., Ebneth, S., & Godderis, Y. (1999). 87Sr/86Sr, δ13C and δ18O evolution of Phanerozoic seawater. Chemical Geology 161, 59-88.

Veizer, J., Godderis, Y., & Francois, L. M. (2000). Evidence for decoupling of atmospheric CO 2 and global climate during the Phanerozoic eon. Nature, 408(6813), 698-701.

Wada, H., & Suzuki, K. (1983). Carbon isotopic thermometry calibrated by dolomite-calcite solvus temperatures. Geochimica et Cosmochimica Acta, 47(4), 697-706.

Wang, P., Du, Y., Yu, W., Algeo, T.J., Zhou, Q., Xu, Y., Qi, L., Yuan, L., & Pan, W. (2020). The chemical index of alteration (CIA) as a proxy for climate change during glacial-interglacial transitions in Earth history. Earth-Science Reviews 201, 103032.

Wissert, M., Kern, M., Radbruch, L., Graf, G., Mütter, M., & Voltz, R. (2008). Case Management in palliative care in Germany: Presenting author Lukas Radbruch. Palliative Medicine, 22.

Won, C. G., & Lee, H.Y., (1967), Explanatory text of the geological map of Danyeong Sheet, Sheet 6824-I, Scale 1:50,000. Geological Survey of Korea.

Wu, F. Y., Han, R. H., Yang, J. H., Wilde, S. A., Zhai, M. G., & Park, S. C. (2007). Initial constraints on the timing of granitic magmatism in North Korea using U–Pb zircon geochronology. Chemical Geology, 238(3-4), 232-248.

Wu, F. Y., Yang, J. H., Wilde, S. A., Liu, X. M., Guo, J. H., & Zhai, M. G. (2007). Detrital zircon U–Pb and Hf isotopic constraints on the crustal evolution of North Korea. Precambrian Research, 159(3-4), 155-177.

Yang, J., Lyons, T.W., Zeng, Z., Odigie, K.O., Bates, S., & Hu, L. (2019). Geochemical constraints on the origin of Neoproterozoic cap carbonate in the Helan Mountains, North China: Implications for mid-late Ediacaran glaciation?. Precambrian Research 331, 105361.

Yi, J. M., Kim, K. H., Tanaka, T., & Kawabe, L. (2000). REE and Sr isotopic compositions of carbonate pebbles in the phyllitic rocks of the Hwanggangni Formation, Okcheon zone. Journal of the Geological Society of Korea, 36, 257-278. (in Korean with English abstract)

Yin, A., Nie, S. (1993). An indentation model for the North and South China collision and the development of the Tan-Lu and Honam fault systems, eastern Asia. Tectonics 12, 801-813.

Yosimura, I. (1940) Geology of the Neietsu District, Kogendo, Tyosen. Journal of the Geological Society of Japan 40, 112-122.

Yoon, K. H., & Woo, K. S. (2006). Textural and geochemical characteristics of crystalline limestone (high-purity, limestone) in the Daegi Formation. Korea. Journal of the geological society of Korea, 42, 561-576. (in Korean with English abstract)

Young, G.M. (2013). Precambrian supercontinents, glaciations, atmospheric oxygenation, metazoan evolution and an impact that may have changed the second half of Earth history. Geoscience Frontiers 4, 247-261.

Yu, W.C., Algeo, T.J., Du, Y.S., Zhou, Q., Wang, P., Xu, Y., Yuan, L.J., & Pan, W., (2017). Newly discovered Sturtian cap carbonate in the Nanhua Basin, South China. Precambrian Res. 293, 112–130.

Zhai, M., Zhang, X., Zhang, Y., Wu, F., Peng, P., Li, Q., Li, Z., Guo, J., Li, T., Zhao, L., Zhou, L., & Zhu, X. (2019). The geology of North Korea: An overview. Earth-Science Reviews 194, 57-96.

Zhang, S., Jiang, G., Zhang, J., Song, B., Kennedy, M. J., & Christie-Blick, N. (2005). U-Pb sensitive high-resolution ion microprobe ages from the Doushantuo Formation in south China: Constraints on late Neoproterozoic glaciations. Geology, 33(6), 473-476.

Zhao, G., & Cawood, P. A. (2012). Precambrian geology of China. Precambrian Research, 222, 13-54.

Zhao, G., Cao, L., Wilde, S. A., Sun, M., Choe, W. J., & Li, S. (2006). Implications based on the first SHRIMP U–Pb zircon dating on Precambrian granitoid rocks in North Korea. Earth and Planetary Science Letters, 251(3-4), 365-379.

Zhao, G., Cawood, P.A., Li, S., Wilde, S.A., Sun, M., Zhang, J., He, Y., & Yin, C. (2012). Amalgamation of the North China Craton: key issues and discussion. Precambrian Research 222, 55-76.

Zhao, G., Sun, M., Wilde, S. A., & Li, S. (2003). Assembly, accretion and breakup of the Paleo-Mesoproterozoic Columbia Supercontinent: records in the North China Craton. Gondwana Research, 6(3), 417-434.

Zhou, G., Luo, T., Zhou, M., Xing, L., & Gan, T. (2017). A ubiquitous hydrothermal episode recorded in the sheet-crack cements of a Marinoan cap dolostone of South China: implication for the origin of the extremely 13C-depleted calcite cement. Journal of Asian Earth Sciences, 134, 63-71.

Zhou, Y., von Strandmann, Philip AE Pogge, Zhu, M., Ling, H., Manning, C., Li, D., He, T., & Shields, G.A. (2020). Reconstructing Tonian seawater 87Sr/86Sr using calcite microspar. Geology 48, 462-467.

APPENDIXES

Appendix 1. HYJ 155-2, Bugnori Formation.

Spot number	Common ^{206}Pb (%)	U (ppm)	Th (ppm)	Th/U	Discor-dancy (%)	$^{206}Pb/^{238}U$	% error	$^{207}Pb/^{206}Pb$	% error	Date (Ma)	
1.1	1.01	367	208	0.57	8	0.3085	1.14	0.1138	0.6	1860.7	11.5
1.2	-0.57	575	122	0.21	-6	0.3483	1.85	0.1123	1.2	1837.3	21.0
2.1	0.14	246	65	0.27	0	0.3352	1.02	0.1144	0.9	1870.8	15.7
2.2	2.23	380	190	0.50	17	0.2744	2.16	0.1127	1.0	1843.2	18.1
3.1	-0.12	89	87	0.98	-8	0.2128	1.66	0.0784	5.7	1157.2	112.7
4.1	0.24	196	80	0.41	-1	0.2931	1.06	0.1012	1.8	1645.6	33.9
5.1	2.18	319	96	0.30	15	0.2833	1.14	0.1139	1.0	1862.4	17.5
6.1	0.15	130	64	0.49	-5	0.1222	1.76	0.0631	13.1	710.7	278.7
6.2	1.20	457	219	0.48	46	0.0620	3.53	0.0626	5.2	696.3	111
7.1	3.86	194	203	1.05	15	0.4036	1.36	0.1639	0.7	2496.5	11.1
8.1	0.26	173	85	0.49	2	0.4020	1.33	0.1384	1.3	2207.8	22.2
9.1	1.17	371	86	0.23	9	0.3058	0.97	0.1138	0.6	1860.9	11.7
10.1	0.30	107	101	0.95	1	0.3988	1.56	0.1360	1.5	2176.9	26.0
11.1	-0.02	194	104	0.54	0	0.3417	1.03	0.1157	1.1	1890.8	19.5
12.1	0.02	307	141	0.46	3	0.2077	1.22	0.0823	1.4	1251.8	27.5
13.1	0.30	240	89	0.37	2	0.3271	1.00	0.1134	0.8	1854.1	14.6

Appendix 2. HYJ 175, Hwanggangni Formation matrix.

Spot number	Common ^{206}Pb (%)	U (ppm)	Th (ppm)	Th/U	Discor-dancy (%)	$^{206}Pb/^{238}U$	% error	$^{207}Pb/^{206}Pb$	% error	Date (Ma)	
1.1	0.01	207	71	0.34	0	0.2401	1.22	0.0880	1.78	1382.6	34.1
1.2	0.43	418	122	0.29	4	0.2235	0.97	0.0862	1.06	1342.8	20.4
2.1	0.11	79	28	0.35	6	0.3186	1.81	0.1153	2.35	1885.3	42.4
3.1	-0.38	40	37	0.94	-10	0.2566	1.60	0.0866	8.53	1351.7	164.6
4.1	0.53	123	75	0.61	4	0.3241	1.08	0.1143	0.85	1869.6	15.2
5.1	0.06	112	56	0.50	0	0.2464	1.10	0.0899	1.50	1423.6	28.6
6.1	-0.37	347	271	0.78	-3	0.3441	1.00	0.1137	0.44	1860.0	7.9
7.1	0.07	328	201	0.61	0	0.2058	0.98	0.0805	0.86	1209.0	17.0
8.1	-0.23	373	99	0.27	-2	0.3425	0.98	0.1143	0.42	1869.6	7.6
9.1	-0.13	16	9	0.52	-2	0.3719	1.95	0.1228	4.29	1997.5	76.3
10.1	0.47	81	38	0.47	2	0.4294	1.18	0.1500	0.91	2345.6	15.5
11.1	1.06	272	90	0.33	7	0.3099	1.22	0.1137	0.64	1859.3	11.5
12.1	-0.02	193	56	0.29	0	0.3375	1.03	0.1147	1.12	1875.5	20.3
13.1	0.00	158	328	2.08	0	0.1907	1.08	0.0770	1.81	1122.3	36.0
13.2	-0.17	347	458	1.32	-4	0.2031	1.00	0.0782	1.41	1150.8	28.1
14.1	-0.09	219	38	0.18	-1	0.3412	1.02	0.1151	0.61	1880.7	11.1

Appendix 3. HYJ 176, Hwanggangni Formation granite pebble.

Spot number	Common ^{206}Pb (%)	U (ppm)	Th (ppm)	Th/U	Discor-dancy (%)	$^{206}Pb/^{238}U$	% error	$^{207}Pb/^{206}Pb$	% error	Date (Ma)	
1.1	0.06	187	86	0.46	0	0.3390	1.08	0.1148	0.73	1876.7	13.2
2.1	1.41	402	37	0.09	11	0.3032	1.69	0.1154	0.49	1886.4	8.9
2.2	0.27	251	123	0.49	1	0.3337	1.22	0.1148	0.66	1876.2	11.9
3.1	1.17	260	134	0.51	9	0.3090	1.01	0.1150	0.59	1880.5	10.6
4.1	2.69	293	183	0.62	22	0.2609	1.03	0.1139	0.79	1862.2	14.3
5.1	0.14	193	100	0.52	1	0.3365	1.05	0.1152	0.73	1882.3	13.2
6.1	0.13	185	74	0.40	0	0.3370	1.05	0.1141	0.80	1866.4	14.5
7.1	0.15	314	150	0.48	1	0.3335	1.00	0.1145	0.52	1872.0	9.4
8.1	1.39	330	159	0.48	11	0.3002	0.99	0.1147	0.56	1875.4	10.1
9.1	0.52	173	77	0.45	4	0.3265	1.06	0.1152	0.76	1883.0	13.7
10.1	0.07	211	95	0.45	0	0.3358	2.58	0.1147	0.63	1874.6	11.3
11.1	-0.17	322	140	0.43	-2	0.3423	0.99	0.1145	0.47	1872.1	8.5
12.1	0.36	286	122	0.43	2	0.3252	1.01	0.1134	0.58	1854.4	10.5
13.1	3.64	601	257	0.43	41	0.1701	1.61	0.1005	0.73	1633.5	13.6
14.1	0.67	137	66	0.48	5	0.3200	1.09	0.1143	0.92	1868.7	16.5
15.1	-0.74	72	49	0.68	-1	0.6696	2.32	0.2666	2.99	3286.0	47.0
15.2	0.14	358	167	0.47	1	0.3363	0.99	0.1153	0.51	1884.1	9.1

Appendix 4. HYJ 313-3, Daehyangsan Quartzite.

Spot number	U (ppm)	Th (ppm)	Th/U	Discor-dancy (%)	$^{206}Pb/^{238}U$	% error	$^{207}Pb/^{206}Pb$	% error	Date (Ma)	
1	1120	820	0.73	5	3.0276	0.0440	0.1181	0.0004	1927.3	3.6
2	374	11	0.03	3	6.5876	0.2040	0.0709	0.0010	910.0	26.0
3	197	190	0.96	1	2.1088	0.0414	0.1669	0.0018	2526.0	10.0
4	1224	385	0.31	-4	13.6612	0.2053	0.0557	0.0006	455.4	6.8
5	927	440	0.47	-3	6.0606	0.0955	0.0711	0.0004	984.0	14.0
6	193	247	1.28	-4	6.2617	0.1804	0.0704	0.0013	954.0	26.0
7	252	396	1.57	-1	4.8123	0.1204	0.0807	0.0010	1211.0	14.0
8	140	192	1.37	-5	6.1920	0.1495	0.0701	0.0012	964.0	22.0
9	708	314	0.44	-2	6.2228	0.1046	0.0710	0.0005	960.0	15.0
10	1951	1667	0.85	2	14.5138	0.2738	0.0558	0.0004	429.6	7.6
11	243	132	0.54	-11	14.3267	0.3489	0.0559	0.0019	435.0	10.0
12	355	191	0.54	-7	14.2450	0.3450	0.0550	0.0011	437.0	10.0
13	626	137	0.22	16	2.5840	0.0668	0.1636	0.0007	2494.8	4.9
14	18	-1	-0.05	21	7.6336	2.6222	0.0810	0.0160	770.0	240.0
15	1498	163	0.11	-6	10.7181	0.1723	0.0582	0.0005	576.1	9.4
16	305	164	0.54	2	6.5833	0.2080	0.0700	0.0014	911.0	27.0
17	150	107	0.72	-1	2.1322	0.0591	0.1599	0.0012	2460.6	8.3
18	405	322	0.79	-6	14.3678	0.4748	0.0550	0.0013	434.0	14.0
19	482	288	0.60	-6	14.2857	0.4694	0.0553	0.0014	436.0	14.0
20	1868	489	0.26	-11	14.1243	0.2593	0.0550	0.0005	440.9	7.6
21	690	475	0.69	-6	14.4718	0.5026	0.0546	0.0010	433.0	15.0
22	641	290	0.45	4	14.3885	0.6832	0.0557	0.0013	433.0	20.0
23	482	487	1.01	-9	14.2450	0.4870	0.0549	0.0011	437.0	14.0
24	1984	513	0.26	-6	14.5138	0.3581	0.0549	0.0005	430.0	10.0
25	388	180	0.46	2	3.6860	0.1019	0.0973	0.0009	1576.0	10.0
26	674	242	0.36	10	2.4691	0.0914	0.1586	0.0009	2442.6	4.5
27	2223	1839	0.83	-1	14.4092	0.4775	0.0556	0.0004	432.0	14.0
28	210	588	2.80	-41	14.2857	0.4490	0.0545	0.0016	436.0	13.0
29	147	330	2.24	7	14.2653	0.3052	0.0575	0.0019	436.7	8.7
30	128	72	0.56	-60	16.1290	0.4422	0.0533	0.0022	388.0	10.0
31	675	55	0.08	-6	4.8309	0.0770	0.0781	0.0005	1151.2	7.4
32	1183	544	0.46	8	6.3776	0.1464	0.0732	0.0011	939.0	20.0
33	1572	1084	0.69	-10	14.2857	0.4286	0.0546	0.0005	436.0	13.0
34	450	216	0.48	-9	14.5138	0.2317	0.0547	0.0007	430.2	6.5
35	92	140	1.52	1	4.6062	0.1379	0.0828	0.0012	1265.0	17.0
36	538	397	0.74	0	3.8241	0.0556	0.0934	0.0004	1498.6	5.2

Appendix 4. *(Continued)*

Spot number	U (ppm)	Th (ppm)	Th/U	Discor-dancy (%)	$^{206}Pb/^{238}U$	% error	$^{207}Pb/^{206}Pb$	% error	Date (Ma)	
37	682	502	0.74	-8	14.0845	0.2380	0.0549	0.0006	442.0	7.1
38	725	248	0.34	9	19.1534	0.2825	0.0541	0.0009	328.0	4.7
39	401	259	0.65	3	14.4425	0.2002	0.0562	0.0010	431.5	5.8
40	571	290	0.51	0	14.2653	0.2238	0.0558	0.0007	436.5	6.3
41	624	236	0.38	-1	6.2539	0.1643	0.0705	0.0009	960.0	24.0
42	(ppm)	(ppm)	0.08	2	6.4725	0.1424	0.0701	0.0007	926.0	
43	1054	289	0.27	-4	14.5773	0.3400	0.0552	0.0007	427.9	9.4
44	2750	599	0.22	-6	14.6628	0.2365	0.0548	0.0004	425.5	6.5
45	225	98	0.44	18	2.6316	0.0900	0.1657	0.0011	2512.9	8.7
46	166	35	0.21	-3	3.0581	0.1122	0.1083	0.0017	1772.0	21.0
47	968	43	0.04	7	6.3857	0.1060	0.0730	0.0007	938.0	15.0
48	432	434	1.00	-3	14.3431	0.1934	0.0556	0.0010	434.4	5.7
49	555	396	0.71	-4	14.7711	0.3491	0.0553	0.0009	424.0	10.0
50	453	315	0.70	-7	14.4509	0.2506	0.0552	0.0010	431.0	7.1
51	1280	632	0.49	-3	13.5135	0.2922	0.0555	0.0009	460.0	9.5
52	218	271	1.24	7	14.2450	0.2638	0.0565	0.0017	437.4	8.0
53	194	175	0.90	-6	13.3511	0.2852	0.0565	0.0015	465.2	9.8
54	378	283	0.75	18	2.9586	0.0875	0.1458	0.0011	2301.0	11.0
55	144	87	0.60	2	3.8521	0.1202	0.0941	0.0010	1511.0	12.0
56	226	231	1.03	4	1.5552	0.0363	0.2757	0.0012	3339.5	3.5
57	473	380	0.80	5	5.2882	0.0699	0.0791	0.0006	1174.1	8.4
58	341	195	0.57	5	6.4144	0.1152	0.0713	0.0011	934.0	16.0
59	65	66	1.00	19	2.6525	0.1618	0.1634	0.0027	2503.0	20.0
60	72	24	0.33	64	10.0604	0.4959	0.1042	0.0038	610.0	28.0

Appendix 5. HYJ 315-1, Daehyangsan Quartzite.

Spot number	Common ^{206}Pb (%)	U (ppm)	Th (ppm)	Th/U	Discor-dancy (%)	$^{206}Pb/^{238}U$	% error	$^{207}Pb/^{206}Pb$	% error	Date (Ma)	
1.2	0.18	140	77	0.55	-2	0.1019	2.45	0.0604	2.30	625.7	14.6
2.2	0.02	296	181	0.61	-17	0.0942	1.68	0.0574	1.74	580.4	9.3
3.2	0.44	82	44	0.54	6	0.2220	11.30	0.0873	1.45	1366.4	27.8
4.2	0.07	1410	6	0.00	0	0.0998	1.59	0.0608	0.67	613.0	9.3
5.2	-0.32	1840	77	0.04	-9	0.1689	1.49	0.0700	0.39	927.7	8.0
6.2	0.02	174	73	0.42	-13	0.0701	1.72	0.0557	2.21	436.7	7.3
7.1	0.03	992	435	0.44	0	0.1665	1.57	0.0749	1.03	992.9	14.4
8.1	-0.42	42	21	0.49	-10	0.1825	2.11	0.0714	2.70	1080.7	21.0
9.2	0.81	317	123	0.39	6	0.3122	1.59	0.1118	0.66	1751.6	24.3
10.2	-0.09	436	319	0.73	-3	0.1816	1.48	0.0742	0.64	1046.5	12.9
11.1	-0.06	639	257	0.40	-1	0.1895	1.58	0.0782	1.67	1118.7	16.2
12.2	-0.21	87	81	0.94	-3	0.1720	1.97	0.0723	3.19	1023.2	18.7
13.2	0.04	271	154	0.57	-4	0.0703	1.66	0.0582	1.86	438.2	7.0
14.1	0.54	43	34	0.80	2	0.4420	2.06	0.1582	1.29	2359.4	40.7
15.2	-0.08	468	215	0.46	-14	0.0736	1.61	0.0553	1.54	457.9	7.1
16.2	0.25	110	71	0.65	11	0.0722	1.83	0.0590	3.70	449.3	7.9
17.1	0.10	208	180	0.86	1	0.2530	1.72	0.0942	1.29	1453.8	22.4
18.1	-0.13	565	407	0.72	-17	0.0737	1.64	0.0589	2.64	458.4	7.3
19.1	-0.59	655	248	0.38	-3	0.3938	1.52	0.1295	0.45	2140.3	27.7
20.2	0.12	435	239	0.55	-99	0.0744	1.74	0.0546	1.93	462.7	7.8

Appendix 6. HYJ 413, Seochangni Formation (intercalated Quartzite)

Spot number	U (ppm)	Th (ppm)	Th/U	Discor-dancy (%)	$^{206}Pb/^{238}U$	% error	$^{207}Pb/^{206}Pb$	% error	Date (Ma)	
1	519	266	0.51	0	2.7137	0.0538	0.1253	0.0008	2035.4	5.9
2	221	169	0.76	0	3.0377	0.0674	0.1124	0.0011	1851.0	12.0
3	309	376	1.22	2	2.1763	0.0365	0.1626	0.0006	2482.2	3.5
4	147	90	0.61	0	2.0877	0.0567	0.1653	0.0013	2521.5	8.7
5	276	116	0.42	0	5.4407	0.1066	0.0760	0.0010	1096.0	15.0
6	530	238	0.45	1	3.9124	0.0673	0.0922	0.0006	1468.7	7.1
7	414	160	0.39	1	5.4466	0.0920	0.0763	0.0007	1099.0	11.0
8	569	274	0.48	2	4.8450	0.0775	0.0817	0.0005	1236.0	7.8
9	119	52	0.44	10	4.9677	0.1802	0.0834	0.0026	1304.0	45.0
10	658	145	0.22	0	5.6243	0.1076	0.0745	0.0006	1060.0	10.0
11	129	92	0.71	2	3.5499	0.0794	0.1003	0.0012	1624.0	12.0
12	725	15	0.02	6	3.9952	0.0623	0.0950	0.0011	1527.0	19.0
13	571	10	0.02	2	2.0960	0.0312	0.1703	0.0005	2561.5	3.0
14	262	274	1.05	0	3.5511	0.0618	0.0992	0.0008	1608.9	9.0
15	581	17	0.03	0	5.8548	0.0994	0.0739	0.0005	1042.4	8.1
16	94	64	0.68	7	2.4752	0.0980	0.1499	0.0015	2347.0	11.0
17	93	59	0.63	4	2.1459	0.0829	0.1689	0.0016	2549.2	9.4
18	63	50	0.79	0	3.5765	0.1164	0.0985	0.0021	1596.0	22.0
19	188	70	0.37	-1	5.8720	0.1931	0.0726	0.0010	1003.0	16.0
20	75	40	0.54	-8	4.9020	0.2884	0.0772	0.0022	1118.0	27.0
21	51	32	0.62	2	5.4113	0.2782	0.0783	0.0036	1137.0	50.0
22	267	526	1.97	1	5.5463	0.1292	0.0751	0.0010	1078.0	18.0
23	152	112	0.74	2	4.1580	0.1435	0.0898	0.0010	1422.0	13.0
24	791	291	0.37	1	4.0306	0.1543	0.0901	0.0007	1431.3	8.1
25	639	483	0.76	0	3.5651	0.1195	0.0972	0.0006	1574.9	6.4
26	90	71	0.79	0	3.9841	0.1524	0.0918	0.0013	1462.0	18.0
27	180	124	0.69	0	3.9448	0.1136	0.0910	0.0011	1449.0	14.0
28	1020	296	0.29	-5	5.4230	0.2500	0.0739	0.0006	1046.0	13.0
29	251	321	1.28	0	3.5663	0.0649	0.0983	0.0009	1590.0	10.0
30	83	149	1.80	-1	3.5336	0.1249	0.0975	0.0014	1577.0	16.0
31	144	178	1.23	-2	3.0395	0.1016	0.1100	0.0012	1791.0	14.0
32	225	138	0.61	-6	3.6751	0.0797	0.0925	0.0007	1476.9	9.1
33	172	144	0.84	-2	3.3456	0.0660	0.1014	0.0010	1651.7	9.2
34	147	84	0.57	-4	3.4686	0.1143	0.0969	0.0014	1571.0	16.0
35	406	116	0.29	-4	5.2219	0.1118	0.0758	0.0010	1084.0	14.0
36	260	208	0.80	-7	5.2002	0.1487	0.0747	0.0011	1061.0	18.0

Appendix 6. *(Continued)*

Spot number	U (ppm)	Th (ppm)	Th/U	Discor-dancy (%)	$^{206}Pb/^{238}U$	% error	$^{207}Pb/^{206}Pb$	% error	Date (Ma)	
37	271	168	0.62	1	3.5765	0.0691	0.0989	0.0009	1604.6	8.6
38	269	193	0.72	-1	4.9310	0.0802	0.0797	0.0008	1187.0	14.0
39	117	44	0.37	-1	4.2463	0.1587	0.0861	0.0016	1344.0	22.0
40	61	19	0.32	3	5.4945	0.3623	0.0772	0.0028	1144.0	44.0
41	275	204	0.74	-1	3.0157	0.0555	0.1118	0.0010	1831.9	8.5
42	364	97	0.27	1	3.8212	0.0949	0.0943	0.0006	1515.0	7.2
43	225	162	0.72	-9	2.6738	0.1001	0.1146	0.0021	1888.0	20.0
44	283	293	1.03	-5	3.0479	0.0715	0.1058	0.0010	1727.0	10.0
45	203	87	0.43	-2	5.4025	0.1138	0.0758	0.0010	1095.0	20.0
46	169	102	0.60	-4	3.5112	0.0727	0.0954	0.0011	1539.0	13.0
47	261	139	0.53	-1	2.6954	0.0523	0.1233	0.0009	2008.3	7.0
48	174	127	0.73	-1	4.8077	0.0901	0.0792	0.0010	1199.0	19.0
49	327	254	0.78	-2	5.3419	0.0942	0.0757	0.0008	1082.0	12.0
50	375	57	0.15	0	5.2438	0.1512	0.0772	0.0008	1131.0	10.0
51	94	37	0.40	14	5.6786	0.2451	0.0802	0.0021	1208.0	32.0
52	413	11	0.03	-4	4.8239	0.1862	0.0787	0.0009	1169.0	14.0
53	395	345	0.87	-6	2.2075	0.1121	0.1424	0.0013	2254.7	7.1
54	95	122	1.29	-9	5.3163	0.2318	0.0730	0.0021	1006.0	33.0
55	709	167	0.24	-10	5.0480	0.1835	0.0747	0.0007	1062.0	13.0
56	278	100	0.36	-5	2.6610	0.0588	0.1199	0.0011	1954.5	8.5
57	104	79	0.76	19	3.9920	0.1323	0.1078	0.0020	1760.0	21.0
58	233	114	0.49	-13	5.0761	0.2834	0.0733	0.0016	1043.0	21.0
59	54	28	0.51	-7	5.2826	0.2567	0.0745	0.0027	1067.0	45.0
60	83	33	0.40	-4	5.6148	0.1955	0.0748	0.0017	1046.0	29.0

Appendix 7. HYJ 417, Seochangni Formation.

Spot number	U (ppm)	Th (ppm)	Th/U	Discor-dancy (%)	$^{206}Pb/^{238}U$	% error	$^{207}Pb/^{206}Pb$	% error	Date (Ma)	
1	450	140	0.31	18	3.6765	0.1622	0.1129	0.0017	1867.0	29.0
2	442	91	0.21	13	3.4722	0.0965	0.1144	0.0007	1869.9	7.1
3	480	132	0.27	1	2.9949	0.0807	0.1147	0.0006	1874.7	5.2
4	147	124	0.84	4	4.4053	0.2329	0.0859	0.0020	1341.0	29.0
5	340	213	0.63	0	4.3103	0.2229	0.0852	0.0015	1335.0	24.0
6	199	130	0.65	3	3.1133	0.0960	0.1124	0.0010	1838.3	8.3
7	104	69	0.66	-1	2.9586	0.1050	0.1122	0.0015	1841.0	16.0
8	197	57	0.29	1	3.0572	0.0888	0.1131	0.0008	1854.1	7.8
9	295	145	0.49	11	3.4083	0.0860	0.1120	0.0010	1841.0	11.0
10	387	105	0.27	10	3.3818	0.0709	0.1123	0.0008	1842.0	7.8
11	203	246	1.21	-1	2.9603	0.0657	0.1118	0.0011	1826.0	11.0
12	202	93	0.46	0	3.0030	0.0992	0.1126	0.0010	1841.0	11.0
13	66	67	1.01	-10	2.7473	0.1660	0.1117	0.0022	1811.0	18.0
14	321	106	0.33	-3	2.9499	0.0957	0.1120	0.0010	1836.0	11.0
15	245	80	0.33	1	3.0303	0.1102	0.1125	0.0010	1838.9	9.4
16	112	81	0.72	-1	2.9940	0.1434	0.1105	0.0023	1813.0	21.0
17	181	56	0.31	-1	4.1288	0.1585	0.0886	0.0013	1406.0	17.0
18	145	125	0.86	0	3.0395	0.1293	0.1105	0.0013	1806.0	15.0
19	195	124	0.63	26	4.1288	0.1432	0.1167	0.0022	1906.0	27.0
20	291	99	0.34	0	2.9851	0.1158	0.1124	0.0012	1845.0	14.0
21	267	92	0.34	-2	1.9120	0.0512	0.1829	0.0012	2677.6	6.3
22	622	123	0.20	3	3.1348	0.1081	0.1114	0.0012	1824.0	10.0
23	43	29	0.68	-6	2.8818	0.2658	0.1117	0.0047	1856.0	44.0
24	191	57	0.30	2	3.1338	0.0933	0.1113	0.0013	1818.0	13.0
25	143	92	0.65	1	3.0769	0.1325	0.1108	0.0017	1809.0	16.0
26	294	215	0.73	-2	3.0139	0.0627	0.1106	0.0014	1812.0	11.0
27	81	74	0.91	-4	2.8736	0.2642	0.1107	0.0026	1806.0	31.0
28	156	106	0.68	-6	2.8409	0.0807	0.1116	0.0017	1825.0	14.0
29	128	115	0.90	-7	2.8329	0.1124	0.1119	0.0016	1823.0	22.0
30	144	203	1.41	-5	2.8902	0.1420	0.1123	0.0022	1846.0	21.0
31	451	71	0.16	-6	2.8305	0.0433	0.1120	0.0009	1841.1	8.7
32	67	79	1.17	-3	2.8986	0.1344	0.1118	0.0025	1850.0	26.0
33	273	81	0.30	0	3.0488	0.1394	0.1120	0.0010	1838.7	9.7
34	92	78	0.84	-5	2.8169	0.1349	0.1132	0.0026	1873.0	28.0
35	247	130	0.52	-6	2.7933	0.1014	0.1132	0.0012	1859.0	15.0
36	33	48	1.47	18	3.4602	0.5388	0.1220	0.0140	2020.0	180.0

Appendix 7. *(Continued)*

Spot number	U (ppm)	Th (ppm)	Th/U	Discor-dancy (%)	$^{206}Pb/^{238}U$	% error	$^{207}Pb/^{206}Pb$	% error	Date (Ma)	
37	110	67	0.60	-5	1.7182	0.0768	0.1968	0.0027	2797.0	12.0
38	228	68	0.30	-7	2.8011	0.0942	0.1124	0.0010	1840.9	8.5
39	215	78	0.36	1	3.0488	0.1394	0.1126	0.0014	1841.0	11.0
40	104	66	0.64	-2	2.8902	0.1169	0.1128	0.0023	1852.0	25.0
41	141	158	1.12	-3	2.8257	0.0655	0.1151	0.0021	1884.0	13.0
42	166	52	0.31	-3	1.9048	0.0653	0.1811	0.0020	2663.0	13.0
43	220	216	0.98	-3	2.8986	0.1176	0.1122	0.0014	1848.0	15.0
44	424	183	0.43	-7	4.1859	0.1191	0.0855	0.0012	1321.0	15.0
45	74	50	0.68	-5	1.9493	0.0836	0.1660	0.0022	2518.0	13.0
46	67	48	0.71	20	2.7322	0.1941	0.1597	0.0022	2460.0	14.0
47	389	51	0.13	-7	2.7473	0.0906	0.1139	0.0011	1863.0	11.0
48	98	50	0.51	-7	1.9011	0.1229	0.1658	0.0026	2518.0	14.0
49	388	80	0.20	-7	2.7465	0.0520	0.1137	0.0006	1862.5	5.2
50	149	28	0.19	-2	2.8986	0.1092	0.1142	0.0016	1864.0	15.0
51	168	134	0.79	-1	2.9735	0.0690	0.1136	0.0012	1860.0	13.0
52	130	115	0.89	1	3.0120	0.1089	0.1138	0.0016	1864.0	13.0
53	376	92	0.24	2	2.9851	0.0642	0.1161	0.0007	1895.9	6.3
54	327	299	0.91	2	8.5397	0.2188	0.0641	0.0012	739.0	25.0
55	86	57	0.66	4	3.0581	0.1216	0.1147	0.0019	1873.0	20.0
56	278	63	0.23	3	3.0340	0.0801	0.1152	0.0010	1886.7	8.1
57	123	88	0.72	-1	2.9326	0.1118	0.1146	0.0015	1873.0	14.0
58	114	50	0.44	6	8.2919	0.2819	0.0669	0.0029	809.0	52.0
59	301	68	0.22	1	2.9586	0.1138	0.1155	0.0010	1897.0	12.0
60	326	170	0.52	-1	2.9155	0.1190	0.1149	0.0009	1894.9	8.5

Appendix 8. HYJ 480, Changni Formation.

Spot number	U (ppm)	Th (ppm)	Th/U	Discor-dancy (%)	$^{206}Pb/^{238}U$	% error	$^{207}Pb/^{206}Pb$	% error	Date (Ma)	
1	163	58	0.36	8	4.3860	0.1924	0.0909	0.0018	1200.0	160.0
2	485	153	0.31	4	4.1719	0.0922	0.0907	0.0007	1389.0	20.0
3	181	137	0.76	1	3.0130	0.0554	0.1140	0.0006	1833.0	23.0
4	381	119	0.31	0	4.2608	0.1144	0.0872	0.0006	1338.0	19.0
5	174	62	0.36	6	4.3554	0.0683	0.0895	0.0007	1340.0	21.0
6	46	14	0.31	4	4.1288	0.1227	0.0914	0.0022	1373.0	31.0
7	70	46	0.67	1	5.6148	0.1198	0.0751	0.0015	1027.0	17.0
8	230	98	0.42	2	2.9931	0.0546	0.1161	0.0007	1861.0	23.0
9	359	151	0.42	1	5.5835	0.0748	0.0752	0.0004	1046.0	15.0
10	331	29	0.09	1	2.2609	0.0373	0.1558	0.0019	2339.0	31.0
11	1117	60	0.05	34	5.4407	0.0858	0.1018	0.0005	1087.0	16.0
12	636	153	0.24	31	4.7893	0.1193	0.1090	0.0005	1226.0	27.0
13	588	81	0.14	55	9.8328	0.2030	0.0883	0.0009	603.0	12.0
14	503	87	0.17	8	2.1008	0.0291	0.1866	0.0003	2530.0	32.0
15	120	86	0.71	0	3.0093	0.0643	0.1142	0.0010	1810.0	46.0
16	207	42	0.20	2	5.5249	0.0824	0.0760	0.0007	1063.0	24.0
17	384	80	0.21	38	4.4228	0.0880	0.1302	0.0006	1314.0	24.0
18	1026	60	0.06	6	3.1377	0.0709	0.1160	0.0005	1790.0	35.0
19	433	111	0.26	44	6.1350	0.0941	0.1061	0.0005	931.0	14.0
20	231	497	2.15	1	3.0460	0.0659	0.1130	0.0005	1788.0	40.0
21	73	57	0.78	2	3.0665	0.0724	0.1131	0.0010	1783.0	74.0
22	465	167	0.36	1	6.0132	0.1049	0.0725	0.0003	989.0	17.0
23	552	185	0.34	1	6.0533	0.0989	0.0723	0.0004	986.0	16.0
24	78	41	0.53	0	3.9185	0.0783	0.0918	0.0010	1428.0	20.0
25	683	83	0.12	34	5.0994	0.0650	0.1071	0.0003	1124.0	31.0
26	117	61	0.52	0	3.5817	0.0603	0.0987	0.0007	1579.0	16.0
27	482	117	0.24	0	3.3234	0.0475	0.1041	0.0003	1678.0	17.0
28	431	69	0.16	1	3.0003	0.0450	0.1141	0.0004	1822.0	16.0
29	190	98	0.51	0	2.9577	0.0341	0.1151	0.0005	1859.0	16.0
30	642	274	0.43	3	4.4425	0.0632	0.0862	0.0004	1371.0	32.0
31	330	71	0.21	7	3.0202	0.0292	0.1214	0.0004	1860.0	20.0
32	229	593	2.59	1	3.0202	0.0328	0.1132	0.0005	1842.0	11.0
33	325	24	0.07	12	3.5261	0.0584	0.1121	0.0005	1604.0	33.0
34	456	92	0.20	1	4.7847	0.0504	0.0815	0.0005	1219.0	11.0
35	896	603	0.67	3	7.9491	0.0948	0.0653	0.0003	761.6	9.3
36	472	95	0.20	9	3.2971	0.0370	0.1146	0.0004	1698.0	17.0

Appendix 8. *(Continued)*

Spot number	U (ppm)	Th (ppm)	Th/U	Discor-dancy (%)	$^{206}Pb/^{238}U$	% error	$^{207}Pb/^{206}Pb$	% error	Date (Ma)	
37	61	19	0.31	3	3.2321	0.0783	0.1090	0.0011	1720.0	30.0
38	181	71	0.39	5	2.7941	0.0726	0.1278	0.0010	1984.0	45.0
39	208	57	0.27	1	2.9851	0.0374	0.1150	0.0004	1858.0	14.0
40	1155	658	0.57	0	3.8730	0.0390	0.0930	0.0002	1485.0	4.7
41	107	78	0.73	1	3.0506	0.0465	0.1127	0.0006	1802.0	19.0
42	274	252	0.92	4	8.0775	0.0848	0.0655	0.0005	752.0	7.9
43	239	210	0.88	5	4.2212	0.0909	0.0904	0.0006	1302.0	60.0
44	101	61	0.60	1	3.9714	0.0536	0.0915	0.0008	1463.0	23.0
45	435	115	0.26	8	3.0960	0.0345	0.1198	0.0005	1821.0	24.0
46	379	99	0.26	27	8.0515	0.0778	0.0737	0.0003	745.0	7.2
47	75	15	0.19	3	5.6180	0.1294	0.0750	0.0012	1023.0	16.0
48	754	249	0.33	1	5.4555	0.0744	0.0759	0.0004	1073.0	9.2
49	113	63	0.56	0	2.9326	0.0335	0.1158	0.0006	1879.0	14.0
50	931	1177	1.26	1	4.5086	0.0569	0.0843	0.0003	1272.0	23.0
51	2910	268	0.09	56	10.7875	0.2560	0.0838	0.0007	551.0	12.0
52	84	53	0.63	1	2.9985	0.0477	0.1144	0.0012	1833.0	31.0
53	168	109	0.65	1	3.6166	0.0445	0.0976	0.0005	1564.0	15.0
54	399	191	0.48	1	3.6140	0.0431	0.0980	0.0003	1569.0	15.0
55	411	304	0.74	5	2.0542	0.0203	0.1838	0.0005	2545.0	62.0

Appendix 9. HYJ 482-1, Changni Formation.

Spot number	U (ppm)	Th (ppm)	Th/U	Discordancy (%)	$^{206}Pb/^{238}U$	% error	$^{207}Pb/^{206}Pb$	% error	Date (Ma)	
1	331	222	0.67	1	4.0634	0.0726	0.0905	0.0004	1437.8	3.8
2	96	93	0.97	2	5.5556	0.0741	0.0755	0.0005	1083.3	8.2
3	205	206	1.00	2	5.6085	0.1007	0.0753	0.0006	1068.0	8.2
4	67	28	0.42	4	5.0736	0.1339	0.0796	0.0008	1184.3	9.8
5	101	39	0.39	0	4.9334	0.0925	0.0794	0.0009	1188.0	14.0
6	90	33	0.37	1	4.0601	0.0989	0.0912	0.0012	1453.0	18.0
7	857	684	0.80	2	6.1237	0.1500	0.0724	0.0003	975.0	22.0
8	850	809	0.95	0	7.6923	0.1302	0.0656	0.0004	788.0	13.0
9	74	19	0.26	1	5.5928	0.1001	0.0753	0.0010	1079.0	14.0
10	292	63	0.21	3	4.8426	0.1665	0.0822	0.0004	1247.6	6.0
11	216	51	0.24	2	4.7596	0.0702	0.0826	0.0007	1255.3	5.8
12	29	11	0.38	-1	6.0277	0.1272	0.0726	0.0010	988.0	20.0
13	166	87	0.52	1	2.8893	0.0543	0.1187	0.0009	1941.0	6.7
14	157	86	0.55	3	5.5402	0.1197	0.0763	0.0008	1109.0	11.0
15	66	38	0.57	2	5.5556	0.1080	0.0752	0.0007	1086.0	11.0
16	255	46	0.18	1	3.0788	0.0768	0.1126	0.0008	1837.8	8.2
17	352	83	0.24	1	5.5556	0.1481	0.0759	0.0006	1089.5	6.0
18	266	106	0.40	1	5.5804	0.1028	0.0749	0.0005	1067.2	7.3
19	82	59	0.72	1	3.6550	0.0668	0.0977	0.0011	1586.0	11.0
20	102	53	0.52	34	5.4675	0.0747	0.1008	0.0010	1641.0	11.0
21	84	45	0.53	3	3.1270	0.0782	0.1113	0.0011	1818.9	9.9
22	348	105	0.30	2	5.4083	0.1550	0.0763	0.0006	1115.6	8.0
23	179	76	0.43	2	3.3852	0.0642	0.1043	0.0015	1702.0	15.0
24	155	46	0.30	1	2.8098	0.0458	0.1217	0.0006	1982.5	4.0
25	834	644	0.77	3	4.4053	0.1941	0.0877	0.0005	1376.5	4.1
26	534	45	0.08	3	5.5710	0.1893	0.0763	0.0007	1106.0	14.0
27	72	39	0.55	2	2.1552	0.0511	0.1637	0.0012	2493.0	9.1
28	163	86	0.53	3	2.1930	0.0577	0.1645	0.0017	2501.7	3.8
29	894	88	0.10	42	13.1926	0.4003	0.0665	0.0004	471.0	14.0
30	514	117	0.23	1	5.7537	0.1126	0.0740	0.0004	1043.0	6.4
31	321	103	0.32	5	3.0836	0.0456	0.1167	0.0005	1907.0	3.7
32	98	44	0.44	2	3.0488	0.0930	0.1131	0.0010	1851.0	11.0
33	116	51	0.44	1	5.6625	0.1315	0.0745	0.0009	1057.0	11.0
34	172	43	0.25	4	5.0505	0.2806	0.0802	0.0009	1207.0	11.0
35	484	129	0.27	4	2.9300	0.0833	0.1213	0.0011	1975.0	10.0

Appendix 9. *(Continued)*

Spot number	U (ppm)	Th (ppm)	Th/U	Discordancy (%)	$^{206}Pb/^{238}U$	% error	$^{207}Pb/^{206}Pb$	% error	Date (Ma)	
36	315	78	0.25	2	2.8490	0.0584	0.1216	0.0006	1978.3	5.3
37	429	176	0.41	7	3.0647	0.0545	0.1206	0.0004	1963.1	3.3
38	318	67	0.21	7	5.5279	0.0886	0.0780	0.0005	1144.5	6.0
39	406	298	0.73	10	5.0607	0.0845	0.0833	0.0005	1279.9	7.3
40	442	83	0.19	4	5.5928	0.2064	0.0761	0.0008	1097.8	8.1
41	520	72	0.14	4	5.6022	0.0942	0.0762	0.0005	1097.0	10.0
42	155	61	0.39	2	4.1220	0.0782	0.0906	0.0006	1437.2	5.4
43	127	62	0.49	1	3.0469	0.0650	0.1135	0.0009	1854.9	7.9
44	433	137	0.32	5	3.1506	0.0407	0.1139	0.0007	1866.9	7.1
45	98	33	0.34	1	5.5066	0.0940	0.0761	0.0008	1092.0	11.0
46	120	39	0.33	2	3.2971	0.0783	0.1066	0.0011	1739.2	9.3
47	64	131	2.06	2	3.0276	0.0752	0.1150	0.0012	1875.8	8.7
48	345	38	0.11	9	5.6850	0.0646	0.0779	0.0006	1145.0	10.0
49	506	236	0.47	5	4.2212	0.0944	0.0907	0.0007	1449.0	15.0
50	72	26	0.36	6	4.6577	0.1866	0.0859	0.0018	1338.0	22.0
51	776	102	0.13	1	2.9727	0.0477	0.1151	0.0003	1880.6	3.5
52	104	24	0.24	10	3.5348	0.0400	0.1091	0.0007	1782.7	6.3
53	94	40	0.42	6	3.0855	0.0486	0.1180	0.0011	1919.0	10.0
54	191	65	0.34	4	5.5096	0.1062	0.0770	0.0013	1118.0	15.0
55	127	26	0.21	2	5.6980	0.1201	0.0745	0.0007	1059.3	9.6
56	185	79	0.43	0	5.2743	0.0584	0.0770	0.0006	1126.0	11.0
57	19	0	0.01	10	5.2083	0.3526	0.0812	0.0037	1263.0	56.0
58	170	74	0.43	8	4.8828	0.1192	0.0851	0.0010	1310.3	8.7
59	202	56	0.28	0	5.0736	0.1081	0.0788	0.0007	1159.0	11.0
60	173	230	1.33	7	5.6211	0.1611	0.0768	0.0015	1123.0	24.0

Appendix 10. HYJ 482-4 Changni Formation.

Spot number	U (ppm)	Th (ppm)	Th/U	Discor-dancy (%)	$^{206}Pb/^{238}U$	% error	$^{207}Pb/^{206}Pb$	% error	Date (Ma)	
1	485	139	0.29	7	3.1368	0.0344	0.1178	0.0004	1919.7	3.6
2	190	20	0.11	3	5.2604	0.0996	0.0780	0.0008	1153.0	12.0
3	316	46	0.15	9	3.5714	0.0332	0.1063	0.0006	1740.9	5.5
4	127	49	0.38	2	4.2863	0.1194	0.0881	0.0008	1382.0	10.0
5	461	116	0.25	0	5.3735	0.0780	0.0761	0.0003	1100.6	3.9
6	159	81	0.51	2	3.0525	0.0848	0.1135	0.0008	1860.7	6.8
7	311	122	0.39	2	3.0817	0.0655	0.1130	0.0006	1844.1	5.0
8	102	56	0.55	2	2.1062	0.0395	0.1678	0.0012	2531.9	6.5
9	123	102	0.83	3	3.0826	0.0808	0.1140	0.0010	1860.4	7.2
10	124	54	0.44	3	3.8241	0.1170	0.0960	0.0010	1538.7	9.6
11	451	203	0.45	0	3.3157	0.0550	0.1040	0.0003	1693.7	3.2
12	85	33	0.39	1	2.2391	0.0381	0.1548	0.0008	2401.9	4.1
13	93	47	0.51	1	2.9129	0.0798	0.1180	0.0009	1923.6	7.9
14	289	67	0.23	2	5.8207	0.0542	0.0739	0.0006	1038.1	9.9
15	184	63	0.34	2	3.0057	0.0669	0.1151	0.0005	1879.2	4.9
16	289	102	0.35	2	3.6219	0.0748	0.0986	0.0005	1597.0	5.8
17	141	79	0.56	2	4.1999	0.0617	0.0886	0.0007	1398.0	10.0
18	171	124	0.73	1	4.2159	0.0480	0.0875	0.0006	1370.6	6.6
19	102	29	0.29	3	4.0552	0.1431	0.0917	0.0008	1461.2	8.0
20	113	61	0.54	2	3.6483	0.0732	0.0986	0.0006	1595.4	6.3
21	273	145	0.53	1	3.6456	0.0611	0.0979	0.0005	1587.2	6.3
22	204	64	0.31	1	5.7438	0.0462	0.0739	0.0006	1040.0	10.0
23	332	177	0.53	6	5.8005	0.0807	0.0759	0.0004	1090.9	6.2
24	380	124	0.33	5	5.7904	0.0704	0.0755	0.0003	1081.1	4.0
25	175	86	0.49	1	1.8636	0.0313	0.1978	0.0012	2806.0	6.9
26	134	49	0.36	1	3.6390	0.0649	0.0984	0.0009	1595.0	12.0
27	668	142	0.21	1	5.4496	0.0980	0.0765	0.0006	1103.6	9.2
28	192	135	0.70	1	4.8239	0.1001	0.0812	0.0006	1226.8	6.5
29	174	37	0.21	1	4.9554	0.0761	0.0802	0.0005	1198.1	8.4
30	295	127	0.43	4	4.8309	0.1540	0.0816	0.0011	1251.0	35.0
31	246	134	0.54	4	3.8344	0.0309	0.0967	0.0007	1556.4	8.5
32	98	89	0.91	1	5.4915	0.0965	0.0759	0.0008	1097.0	12.0
33	545	120	0.22	2	3.0003	0.0639	0.1153	0.0008	1882.4	5.5
34	382	122	0.32	4	4.9188	0.0871	0.0817	0.0007	1236.7	8.7
35	163	89	0.54	3	5.5188	0.0853	0.0758	0.0005	1093.4	6.3

Appendix 10. *(Continued)*

Spot number	U (ppm)	Th (ppm)	Th/U	Discor-dancy (%)	$^{206}Pb/^{238}U$	% error	$^{207}Pb/^{206}Pb$	% error	Date (Ma)	
36	148	41	0.27	1	5.4496	0.0861	0.0764	0.0007	1109.3	9.6
37	641	111	0.17	3	5.5218	0.2012	0.0763	0.0004	1105.5	8.3
38	859	212	0.25	3	5.0968	0.1481	0.0794	0.0004	1184.4	5.0
39	469	194	0.41	4	3.1309	0.0333	0.1138	0.0005	1861.2	4.1
40	478	380	0.80	3	6.1501	0.0567	0.0726	0.0005	1003.5	9.1
41	477	150	0.32	1	3.6630	0.0805	0.0976	0.0004	1575.4	4.5
42	282	103	0.36	4	2.2090	0.0234	0.1652	0.0005	2507.9	3.6
43	273	240	0.88	1	3.0202	0.0365	0.1132	0.0005	1853.0	4.5
44	355	71	0.20	1	5.5804	0.0903	0.0757	0.0006	1086.2	7.9
45	334	78	0.23	3	4.4346	0.1180	0.0859	0.0004	1341.5	4.7
46	79	23	0.29	3	4.1271	0.1039	0.0899	0.0009	1432.0	13.0
47	84	65	0.77	2	4.0032	0.0593	0.0925	0.0009	1471.0	12.0
48	347	345	0.99	2	3.4662	0.0697	0.1020	0.0005	1659.7	4.8
49	1157	8	0.01	9	4.4385	0.0906	0.0914	0.0006	1453.0	11.0
50	383	83	0.22	4	5.6022	0.1255	0.0764	0.0006	1110.4	9.7
51	369	317	0.86	3	3.1328	0.0726	0.1135	0.0005	1855.0	5.2
52	690	19	0.03	23	4.0145	0.0741	0.1144	0.0004	1870.3	4.2
53	410	72	0.18	13	5.5127	0.1064	0.0817	0.0008	1233.2	9.3
54	319	143	0.45	2	3.1716	0.0754	0.1101	0.0005	1802.2	4.5
55	495	117	0.24	3	5.5741	0.0777	0.0757	0.0006	1090.2	7.9
56	239	105	0.44	2	3.2415	0.0567	0.1083	0.0007	1771.1	8.8
57	99	44	0.44	1	3.0139	0.0454	0.1146	0.0008	1873.7	7.2
58	278	137	0.49	0	3.6456	0.0253	0.0973	0.0005	1570.3	6.7
59	135	56	0.42	2	4.7939	0.0666	0.0817	0.0006	1237.9	7.8
60	325	100	0.31	1	5.3562	0.0631	0.0766	0.0005	1115.3	6.8